A STOCHASTIC SHELL MODEL BASED ON EDQNM THEORY FOR TURBULENT MIXING AND REACTING FLOWS

A Dissertation

Presented to the Faculty of the Graduate School

of Cornell University

in Partial Fulfillment of the Requirements for the Degree of

Doctor of Philosophy

by

Yanjun Xia

January 2011

A STOCHASTIC SHELL MODEL BASED ON EDQNM THEORY FOR TURBULENT MIXING AND REACTING FLOWS

Yanjun Xia, Ph.D.

Cornell University 2011

The probability density function (PDF) method provides an elegant solution to the closure problems of the highly-nonlinear chemical source terms. The instantaneous velocity, temperature and species concentrations are replaced by a high-dimensional joint PDF. Higher-order moments can be computed from this joint PDF. However, since the PDF model lacks two-point information, the effects of molecular mixing have to be modeled. Since the qualitative shape of the PDF is sensitive to the mixing model, especially when molecular mixing plays an important role, an accurate description of mixing is critical to PDF methods. Because molecular mixing is a multi-scale process, a spectral model is most desirable for it can naturally introduce all the length and time scales. However, it has difficulties in closing the chemical source term. A new model aiming at exploiting the advantages of the PDF framework and the spectral representation in a complementary way is derived. The eddy damped quasi-normal Markovian (EDQNM) model is chosen to provide the spectral information, and the stochastic shell mixing model (SSMM) based on the EDQNM model is able to supply the fine-grained joint PDF of velocity and scalars. A Monte Carlo scheme is used to advance the notional particles in spectral space. The Lagrangian statistics predicted by SSMM are in good agreement with direct numerical simulation (DNS). However, violation of the scalar bounds poses a challenge to the SSMM. An effective modification, called “zeroth” mode, has been proposed for an isotropic homogeneous system. Comparisons of the bounded SSMM have been made with DNS and they are in overall good agreement. Another work done in this thesis is the development of the EDQNM model for turbulent reacting fields, its comparison with DNS data and its application to study effects of different critical dimensionless parameters such as Reynolds

number, Schmidt number and Damköhler number.

BIOGRAPHICAL SKETCH

Yanjun Xia was born in 1980 and grew up in a small, quiet and gorgeous village near Suizhou, Hubei Province, P. R. China. There she spent a happy childhood. At age of twelve Yanjun moved into Suizhou and went to Dongguan middle school and the No. one high school of Suizhou. She became very interested in physics and chemistry. However, due to the poor education environment in the small town, she did not have access to the fantastic world of science. In 1998 Yanjun was admitted to the University of Science and Technology of China (USTC) in Hefei, Anhui Province, China. There for the first time in her life she "touched" a computer and had the chance to do many experiments in physics and chemistry. The five-year undergraduate study in the department of thermal science and energy engineering made her more interested in scientific research. Yanjun graduated with honor from USTC with a Bachelor's degree of Engineering in 2003. Attracted by the famous and prestigious graduate programs, Yanjun decided to pursue her Ph.D in Mechanical and Aerospace Engineering at Cornell. She joined Professor Lance Collins' team in 2004 and worked with a friendly group. Her Ph.D dissertation is about the development and application of a stochastic spectral model to describe turbulent mixing process under PDF framework.

This document is dedicated to my parents and my husband, Hainan, for their patient and generous support.

ACKNOWLEDGEMENTS

I believe I would never have completed this work without the help and support from Professor Lance Collins, my advisor and committee chair. A simple “thank you” will never be enough to convey my gratitude for his insightful guidance, his warm encouragements, and even his criticisms. To merit his approval is a great honor for me. I owe a special thank you to the former group members, Mr. Yang Liu and Dr. Thirunavukkarasu Vaithianathan, who dedicated a considerable amount of time and patience explaining to me, discussing with me, and reviewing the work for me. It is a great honor to me to have Professor Stephen Pope, Professor Gennady Samorodnitskymany and Dr. Thirunavukkarasu Vaithianathan in my committee. Many thanks to them for spending their precious time reading this dissertation. I would also like to thank Professor Zellman Warhaft for his constructive suggestions. I feel very lucky to have Dr. Juan Isaza, Dr. Shi Jin, Dr. Sarma Rani, Kama Raju Kusumanchi, Dr. Juan Salazar, Ammar Abdilghanie and David Korda as colleagues and friends. They deserve a special thank you for their gracious and vital help along the way in completing this work. I would also like to thank Haifeng Wang, Renfeng Richard Cao, Zhuyin Ren and Lijian Tan for sharing research experiences and thoughts with me. I want to thank National Science Foundation for providing financial support through grant No. CTS-0121573. Meanwhile, under the same grant, the collaboration with Professor Michael Modest and Professor Dan Haworth gave me a better understanding of the big picture of this work. Last but not least, I would like to thank my parents, my brother and sister-in-law, my parents-in-law and my husband for their incredible sacrifices and support over all these years.

TABLE OF CONTENTS

[1] Originally published as: Y. Xia, Y. Liu, T. Vaithianathan and L. Collins, *Physics of Fluids*, 22, 045103, (2010). The format is adapted to meet the requirement of this thesis.

[2] Originally published as: Y. Xia, T. Vaithianathan and L. Collins, *Flow, turbulence and combustion*, (2010). The format is adapted to meet the requirement of this thesis.

LIST OF TABLES

LIST OF FIGURES

CHAPTER 1

INTRODUCTION

Turbulent transport and mixing play an important role in many disciplines such as chemical engineering, geosciences and biology. The classic Reynolds Averaged Navier-Stokes (RANS) modeling for turbulent flows can be extended to study turbulent mixing of scalars (e.g., temperature or chemical concentrations). Governing equations are usually derived in physical space over the domain of interest with proper boundary and initial conditions.[74] However, a closure problem is inevitable in this method. Usually a "gradient diffusion" hypothesis is employed to achieve the closure. For simple convection-diffusion problems, this method can yield satisfactory results.[75] However, when it comes to turbulent reacting flows, such as combustion in gas turbines, boilers, industrial furnaces, rocket engines, etc., the system becomes much more complicated due to the presence of chemical reactions. Chemical source terms are generally highly nonlinear functions of temperature and scalar concentrations, making the conventional moment closure extremely inapplicable.

An attractive alternative is the probability density function (PDF) method. It replaces a set of instantaneous variables which determines the thermochemical/hydrodynamic state of a reacting system (like velocity, temperature and/or compositions) with a joint probability density function, by means of which the reaction source terms and nonlinear convection terms are treated exactly.[64] The PDF method has received significant attention since its inception, especially in the form of the Lagrangian PDF method.[66] It has been widely used to study different turbulent reacting systems. Recent studies have demonstrated the effectiveness of the PDF method to calculate the complex non-linear interactions between turbulence and chemical reactions .[4,5,45–48,67,88] However, since the the joint PDF is usually a one-time, one-point function, its evolution equation needs a closure approximation

for molecular diffusive fluxes, which depend on the gradients of scalars that cannot be computed in terms of the joint PDF. Moreover, since chemical reactions require mixing to proceed down to molecular scales, for flames containing significant turbulence-chemistry interactions, the accuracy of PDF model calculations relies not only on an accurate representation of the chemistry, but also on the accuracy of the mixing model.[6]

The mixing of scalars is inherently a multi-scale process. It involves a large number of interactions among eddies of different sizes. According to the Obukhov[57] and Corrsin[10] theory, mixing proceeds in a manner analogous to the cascade of turbulent kinetic energy from large scales to small scales. Based on this idea, conventional mixing models assume the characteristic time scale of mixing is proportional to the integral time scale of turbulence, estimated to be K/ε, where K is turbulent kinetic energy and ε is is the energy dissipation rate. However, this does not account for the broad range of length and time scales of turbulence. Besides, reactions can steepen the spatial gradients of the scalars thus enhancing the mixing rate. Failure to represent this "local reaction rate" will lead to inaccurate predictions in many situations. Moreover, reaction intermediates are often formed in the thin reaction zones, thus the mechanism of mixing and reaction of these intermediates is substantially different from what mixes the stable fuel and air. The conventional single-point mixing models fail to adequately capture these more complex mixing scenarios.

Another important phenomenon that single-point mixing models cannot account for is differential diffusion, a process that decorrelates different scalars due to their distinct molecular diffusivities.[2] Differential diffusion originates from small scales and proceeds to large scales via an inverse cascade. Generally it is argued that at large Reynolds numbers, since large scales and small scales are widely separated, only small scales are affected by the effect of differential diffusion and large scales are insensitive to it. Therefore the

effect of differential diffusion is usually ignored by invoking the "unity Schmidt number" approximation. However both experiments[12,40,72] and direct numerical simulations (DNS)[43,89] have demonstrated that differential diffusion persists even at high Reynolds numbers.

Subramaniam and Pope[73] identified the following eight features of an idea mixing model:

1. mean scalar concentrations are not directly affected by mixing
2. mixing causes the monotonic decrease of the eigenvalues of the covariance matrix $\langle \phi'_\alpha \phi'_\beta \rangle$, where ϕ'_α is the fluctuation in the concentration of species α, and α, β run over the entire species domain
3. all scalars obey the bounds imposed by initial and boundary conditions
4. the model satisfies the invariant properties of linearity and independence
5. the joint composition PDF relax to a joint normal distribution eventually
6. the model should account for differential diffusion
7. the model should include the influence of the length scales of scalar fields
8. the model should account for the influence of reaction on mixing

The goal of this research is to develop a new mixing model that addresses as many of these criteria as we can. The model will be based on the PDF framework, but will incorporate aspects of the spectral representation of scalar mixing. In particular, the spectral model known as the eddy damped quasi-normal Markovian (EDQNM) model will be used to develop a new mixing model for the PDF equations. In the sections below we provide a review of PDF modeling (single-point and two-point) and the EDQNM model. There is also a simple and straightforward illustration of the criteria each model satisfies in Table 1.1.

Table 1.1: This table lists the models in the order they are discussed in Sections 1.1, 1.2 and 1.4. The diamond symbol indicates that the model satisfies the corresponding criterion proposed by Subramaniam and Pope.[73]

Model	1	2	3	4	5	6	7	8
IEM	◇	◇	◇	◇				
PSP	◇	◇	◇		◇			
Particle Interaction	◇	◇	◇	◇				
Langevin	◇	◇		◇	◇			
Binomial	◇	◇	◇	◇	◇			
Mapping Closure	◇	◇	◇		◇			
Joint PDF	◇	◇	◇	◇	◇			
LSR	◇	◇	◇	◇	◇		◇	
SSMM	◇	◇		◇	◇	◇	◇	◇

1.1 Single-Point PDF Mixing Models

The PDF framework is well known for its capability of formally closing the nonlinear chemical reaction source terms and those associated with radiative thermal emission. However, molecular mixing, which involves two-point statistics, must be modeled. Since the qualitative behavior of PDF is strongly affected by the mixing model, an inaccurate mixing model will cause the PDF to lose its major strength, i.e., the formally closed source terms may not be accurately predicted, especially when modeling diffusion-dominated flames such as flames near blow-out, where the reaction rate is profoundly affected by local fluctuations in the rate of mixing. A most simple example to illustrate the importance of mixing model is the scalar mixing in homogeneous turbulence, where the scalar's PDF

$P(\phi,t)$ is evolved by molecular mixing only and $P(\phi,t)$ is governed by:[64]

$$\frac{\partial P(\phi,t)}{\partial t} = -\frac{\partial}{\partial \phi}\left[\langle \mathcal{D}\,\nabla^2\psi \mid \phi\rangle P(\phi,t)\right] = -\frac{1}{2}\frac{\partial^2}{\partial \phi^2}\left[\chi(\phi,t)P(\phi,t)\right], \tag{1.1}$$

where $\langle \cdot \mid \phi\rangle$ indicates an expectation conditioned on $\psi=\phi$, $\chi(\phi,t)\equiv\langle 2\mathcal{D}\,\nabla\psi\cdot\nabla\psi \mid \phi\rangle$ is the expected conditional scalar dissipation, and $\mathcal{D}$ is the scalar diffusivity. The scalar PDF $P(\phi,t)$ lacks the information required to calculate the inherently two-point quantity on the right-hand side of Eq. (1.1), hence it must be modeled. The quality of the mixing model is critical to accurately describing this process.

Below is a brief review of the existing one-point mixing models:

1. **Interaction by Exchange with the Mean (IEM)** [83] IEM model (also known as the linear mean-square estimation (LMSE) model[13]) is based on the idea that molecular mixing reduces scalar fluctuations and in the phase space causes the instantaneous scalar values to approach their local mean. The model usually takes the form below

$$\langle \mathcal{D}\,\nabla^2\psi \mid \phi\rangle = -\frac{1}{2}\,C_\phi\,\frac{[\phi-\langle\psi\rangle]}{K/\varepsilon} \tag{1.2}$$

   where C_ϕ is the mechanical-to-scalar time scale ratio usually assumed as a constant with a value near 2. In fact the performance of IEM model depends on this specified value of C_ϕ.[6] The IEM model is the most widely used because it is simple to implement and it will not violate the scalar bounds set by the initial and boundary conditions. It also can be easily extended to multiple scalars, and it obeys the linearity and independence principles. However, a serious drawback of the IEM model is its inability to describe the evolution of the scalar PDF correctly, i.e., the initial PDF shape is preserved and does not relax to a Gaussian distribution, which violates criterion 5.

2. **Parameterized Scalar Profile (PSP) model** Meyer and Jenny[50,51] developed a model for molecular diffusion in PDF methods by constructing statistical distribu-

tions of one-dimensional scalar profiles at the diffusive scales. These profiles are assumed to be self-similar and are characterized by a number of parameters. The resulting model equations are simple, similar to the IEM model, however PSP models are able to predict the evolution of joint PDF of inert scalars to a joint Gaussian. It is able to produce accurate results at a relatively low computational cost. It can be extended to multiple scalars. However, PSP models only fulfill the weak localness requirement. By "localness" it means mixing is restricted only to nearest neighbors in composition space. The PSP models also violate the linearity and independence criterion. The effect of reaction on PSP models has yet to be studied.

3. **Particle interaction models** Frost[21], Pope[62] and Janicka et al.[28] proposed non-linear integral representations of the PDF molecular transport in terms of products of probabilities at two different states. These models can also be interpreted in terms of interactions of particles in composition space. Curl's model[11] can be recovered as a special case of this model. A difficulty these models have in common is that higher moments diverge in time, causing the PDF to not to relax to a Gaussian at long times. Pope[63] developed an improved version of Curl's model by introducing the age distribution to the particle population so that the resulting higher-order cumulants approach zero. Kosály[36] showed the short-time limit of the non-linear integral model reduces to IEM. Particle interaction models are also readily extended to multiple scalars.

4. **Langevin Model** Pope[64] proposed to use a diffusion process (Wiener process) to simulate stochastically the incremental changes of the composition field. Model parameters were obtained by matching decay rate of scalar variance to experiment measurements. An advantage of this model is the capability of relaxing an arbitrary shaped initial PDF to Gaussian. However, the unbounded nature of Wiener process leads to violation of the bounds of scalars.

5. **Binomial model** Binomial models[81] are a combination of IEM and a random contribution that preserves the bounds of a single scalar. Although at long times they lead to a Gaussian PDF, the evolution is not continuous in time, and the extension of the model to multiple scalars is difficult because one scalar's bound depends on the others'.

6. **Mapping closure** The mapping closure method[8,65] makes predictions in better agreement with DNS than earlier models due to its sound theoretical foundations. This is the first model to satisfy localness. This property is very important to a mixing model when applied to a diffusion flame test problem by Norris and Pope.[55] However, there are difficulties in extending mapping closure to multiple reactive scalars since the mappings are not unique and expensive to compute.[65] Subramaniam and Pope[73] developed a new mixing model to deal with mixing and reaction simultaneously, in which the change in particle composition is determined by particle interaction along the edges of a Euclidean minimum spanning tree(EMST) constructed in composition space. It succeeded as an extension of the mapping closure particle model to multiple scalars. An essential feature of the EMST model is the "localness". A superior performance over existing models was found when EMST model was applied to the diffusion flame test problem. However, EMST model again violates the linearity and independence principle. Later, the "multiple mapping condition" method was developed by Klimenko and Pope[35] to address this shortcoming. This model, which combines the principles of the mapping closure and the conditional moment closure, has been applied to non-premixed flames in combination with large eddy simulation (LES) by Klimenko.[34] This model is local, bounded, satisfies the linear and independent principle, and it is able to evolve the PDF to a Gaussian in appropriate limits, however, it cannot capture differential diffusion.

In general the inherent assumption shared by all single-point mixing models is that the mechanical-to-scalar time scale ratio is constant. This is known to be violated when the integral length scale of the scalar is different from that of the velocity.[14,29,80,85] To address this shortcoming, multi-point, multi-time information must be introduced. An effort made to fix this issue has led to a class of two-point mixing models, briefly reviewed below.

1.2 Two-point Mixing Models

1. **Joint scalar/scalar-gradient PDF** The joint PDF of scalar and the scalar gradient, $P(\phi, \nabla\phi)$, provides a partial remedy to some limitations of the single-point mixing models, although it still requires statistics for higher-order derivative that must be modeled. Meyers and O'Brien[52] modeled the unclosed term with one that relaxes the scalar to its mean. However it didn't correctly represent the evolution of scalar PDF from a non-Gaussian initial condition. Gao and O'Brien[22] showed that the PDF of the scalar gradient conditioned on the scalar is nearly Gaussian. This motivated them to use a Gram-Charlier expansion for $P(\nabla\phi \mid \phi)$ with coefficients found from DNS. Alternatively the conditional dissipation rate $\chi(\phi, t)$ can be expressed in terms of a two-point PDF, $P(\phi(\mathbf{x}_1), \phi(\mathbf{x}_2))$. Kuo and O'Brien[39] investigated the closure of this equation for a stochastically distributed reactant undergoing self-diffusion and a non-linear reaction using Ievlev's closure.[27] It yielded the correct initial evolution of the single-point PDF, among other desirable properties. However, it remains unclear how Ievlev's closure is affected by reactions, which modifies the scalar gradients.

2. **Mapping closure** Pope[65] tried to extend the mapping closure principles to close the joint PDF of ϕ and $\nabla\phi$. However certain encumbrances exist at this level. For example, the closure implies that for a scalar field with Gaussian PDF, the PDF of the derivative $\partial\phi/\partial x_1$ is also Gaussian, whereas it is known that $|\nabla\phi|$ is log-normal

through DNS.[14] The fact that mapping closure is hard to extend to multiple scalars is another hindrance.

3. **Lagrangian Spectral Relaxation (LSR) model** LSR model is used to account for the effect of the change in the spectral distribution of the scalar on the scalar dissipation rate. Fox and Yeung[20] developed a hybrid strategy which combines the LSR model for the mean scalar spectrum[17–19] with a Fokker Planck equation for the PDF.[15,16] The prediction of several Eulerian and Lagrangian statistics are in good agreement with DNS for both decaying and stationary Gaussian scalar. However, further closure assumptions for conditional scalar dissipation rate are required when extended to non-Gaussian fields. And since LSR is strictly a local closure to the spectral evolution equation, it does not inherently capture differential diffusion.[72] These effects were incorporated empirically by introducing model coefficients which are explicit functions of Reynolds number and all the Schmidt numbers.[19] This overcomes the shortcoming with differential diffusion of LSR model. However, to bring that capability into the PDF model, the stochastic differential equations governing the evolution of the PDF have to be multi-scale.

Besides these two-point models, there is a linear eddy model (LEM)[31,69] which provides a full range of lengthscales representation of mixing by reducing the description of the scalar field to one spatial dimension. A key feature of LEM is that convection is modeled as random rearrangement events of the scalar field along a line, while the molecular diffusion is accounted for explicitly. The LEM model has received a wide range of applications and overall accurate representations of turbulent mixing have been obtained.[32,33,49,70] However, an unavoidable consequence of the reduced one-dimensional formulation is the introduction of discontinuous derivatives, which will slow falloff of the scalar fluctuation intensity in the dissipation range. The fact that LEM was based on scalings applicable to high-Reynolds number turbulent flow also compromises its performance

at low-to-moderate Reynolds numbers.

As noted above, our goal is to incorporate a spectral representation into the PDF mixing model. There are a number of spectral models that describe scalar mixing adequately; however, this work has focused on the EDQNM closure. Below we review the relevant EDQNM literature.

1.3 EDQNM Model

Spectral models consider the evolution of second-order moments of the Fourier transform of the velocity and scalar fields. The nonlinear convection terms lead to higher-order moments that must be closed. It is the closure of these terms that define each of the spectral models. Whereas molecular mixing must be modeled within the PDF framework, these linear terms are closed within a spectral model. As spectral models naturally introduce the broad range of length and time scales found in turbulent flows, and they can treat molecular diffusion exactly, they provide a natural framework to address criteria $6-8$ of Subramaniam and Pope. The predictions of spectral models are remarkably insensitive to the modeling of the higher-order terms that are responsible for scalar transfer from low to high wavenumbers, leading to many successful spectral models in the literature.[26] However, only a few of them can be regarded as true spectral theories, defined here as formalisms that can be generalized to circumstances beyond those originally considered in their development. Rigorous spectral theories such as Lagrangian history direct interaction approximation (LHDIA)[37] and test field model (TFM)[38] are extremely computationally intensive (rivaling, and even exceeding the computational expense of DNS), and hence are not appropriate for a practical mixing model. On the other end, shell models[1] are simpler in mathematical form, but with a focus mainly on small scale phenomena such as

intermittency instead of global statistics. The EDQNM theory strikes a favorable balance between rigor and relative ease of computation. It pocesses all of the requisite properties such as spectral positivity, Kolmogorov inertial ranges and energy equipartition for inviscid flows. Therefore we choose EDQNM theory as the backbone for the stochastic mixing model that will be developed in this study. The name of the theory reveals the three major assumptions that were made in its derivation, namely quasi-normality, eddy-damping, and the Markovian approximation.

The quasi-normal assumption was first proposed to model turbulent velocity field independently by Chou[9] and Millionshtchikov.[53] It is essentially a moment closure to approximate the $4th$-order moments in the governing equations of $3rd$-order moments. By assuming the fluctuations have a joint-normal distribution, the $4th$-order moments can be approximated by

$$\langle abcd\rangle \approx \langle ab\rangle\langle cd\rangle + \langle ac\rangle\langle bd\rangle + \langle ad\rangle\langle bc\rangle \,, \tag{1.3}$$

where a, b, c and d are assumed to be joint-normal random variables with zero mean. These variables stand for any combination of velocity or scalar fluctuations in the EDQNM theory. However early attempts of applying the quasi-normal assumption yielded negative energy spectra over a range of wavenumbers, which is not physical.[56,58] To overcome this flaw and compensate for the cumulants that are inherently neglected by Eq. 1.3, Orszag[61] introduced eddy-damping to reduce the unphysical growth of the $3rd$-order moments. With this correction, the EDQNM model is able to predict an energy spectrum with the classical Kolmogorov scaling in the inertial range in the limit of infinitely large Reynolds number. However, this eddy-damping hypothesis alone cannot eliminate the "negative energy spectrum" problem completely. Orszag proposed a second correction in the same work commonly referred as Markovianization which eliminates the unrealizability problem. A Markov process is a stochastic process whose future evolution depends only on the current state of the system and not on the history of that system.[23,68,71] This

assumption together with the other two enables an analytical integration of the evolution equation for the 3*rd*-order moment and yields an explicit expression for the 3*rd*-order moment of interest. While it is certainly not necessary to make this Markovian approximation from a closure point of view, Orszag[60] showed that it is precisely this approximation that guarantees the positive definiteness of the energy spectrum throughout its temporal evolution.

EDQNM has been found to be able to predict turbulent energy spectra in fair agreement with experiment[82] and DNS.[44] It has been widely accepted and used to study different aspects of turbulent flows. Turner and Pratt[76] derived an EDQNM closure for magnetic-hydrodynamic turbulence and achieved a realizable model for this kind of flow. Lesieur and Ossia[54] used EDQNM theory to study the asymptotic behavior of the energy spectrum and backscatter at various wavenumbers in a three-dimensional isotropic turbulent flow with very high Reynolds number. And due to its capability of properly predicting the cascading of turbulent energy, EDQNM has been used to provide or validate subgrid scale models in large eddy simulations (LES).[7,30,41]

In addition, EDQNM theory has been extended to study turbulent mixing problems. Mixing of isotropic scalars with and without forcing was reviewed with this theory by Lesieur.[42] Later, Herr and Collins[25] extended the EDQNM framework to study the mixing of a scalar under the presence of mean gradient and obtained excellent agreement with DNS. Ulitsky and coworkers also extended EDQNM theory to multiple scalars with and without mean gradients.[78,79] Some corrections were made to ensure the model's realizability, and the resulting model is able to capture differential diffusion as expected. Orlandi and Antonia[59] studied the dependence of a passive scalar on the Reynolds and Schmidt numbers in decaying isotropic turbulence using the EDQNM model. It also has been recently used to provide subgrid scale models for passive scalars in LES.[3]

The application of EDQNM model to turbulent reacting flows has also been well documented. Tsai and O'Brien[75] used a physical space EDQNM model to study an isothermal homogeneous turbulent reacting flow and obtained good agreement with DNS data with respect to the governing parameters as Reynolds number, Schmidt number and Damköhler number. Ulitsky and Collins[77] studied the propagation of a premixed turbulent flame with EDQNM and found that the length scales where wrinkling of the flame interface occurred decrease as the size of inertial subrange increases, which is difficult to capture by single-point models. EDQNM has also been applied to study unpremixed bimolecular chemical reaction by Vaithianathan et al.[80] The model is able to capture the correlations between reactants and product quantitatively well when compared with DNS.

To sum up, EDQNM has many important extensions and applications since its birth, and we believe it can be used in more practical situations to describe and predict mixing of inert and reacting scalars in turbulent flows.

1.4 Objective and Outline

The PDF method provides an elegant and effective solution to the closure problems that arise from averaging or filtering the highly nonlinear chemical source terms and the terms that correspond to other one-point physical processes;[24] however, it requires a closure assumption for the mixing term. An ideal mixing model should be able to represent the information of the wide range of length and time scales embedded in turbulent flows. In this sense a spectral mixing model is most desirable because it inherently introduces all the scales, while it has difficulties with the highly nonlinear chemical source terms. This then motivates the idea to derive a hybrid model that exploits the advantages of each modeling framework in a complementary way. The EDQNM model has been chosen to provide the

spectral component of the hybrid model.

The main structure of this thesis consists of three papers, two of which have been published and the third will be submitted shortly.

Chapter 2 is the published paper entitled "Eddy damped quasi-normal Markovian theory for chemically reactive scalars in isotropic turbulence"[86] which presents a new EDQNM model for an isothermal bimolecular reaction in an isotropic homogeneous system. The derived model is first validated with DNS, then a parametric study is performed to investigate the dependence of the scalar fields on three important dimensionless parameters: Reynolds number, Schmidt number and Damköhler number. It also demonstrates that this model is able to capture the phenomenon of differential diffusion well. This paper proves that EDQNM can be applied to study turbulent reacting flows and establishes a base on which we can further develop the stochastic version of the model.

A second paper entitled, "Stochastic shell model for turbulent mixing of multiple scalars with mean gradients and differential diffusion",[87] is presented in Chapter 3. It shows the development of a stochastic shell mixing model (SSMM) based on EDQNM theory for multiple non-reacting scalars with the presence of uniform mean scalar gradients. The Langevin equations derived in this paper are proven to be statistically consistent with the EDQNM model. The model is implemented as an ensemble of notional "particles", each carrying velocity and scalar concentration distributed across the "spectral shells" that are evolved according to the independent Langevin equations. The model predicts Lagrangian characteristics for the velocity and scalar fields in good qualitative agreement with DNS by Yeung.[90] This paper mainly builds a bridge between the EDQNM model and the PDF method.

The third paper entitled, "Bounded stochastic shell model for turbulent mixing of mul-

tiple scalars with distinct diffusivities", corrects the model so that the scalar bounds are preserved. The paper begins with a DNS study of the influence of the initial PDF and spectral distribution of scalar fields. It demonstrates the importance of the spectral distribution on the mixing rate, as suggested by Viswanathan et al.[84] that "the passive scalar variance decay rate is uniquely determined by the wavenumber of the initial scalar fluctuations relative to the turbulence integral length scale", which supports the inherent assumption made in EDQNM theory. The problem with the bounds originates from the random terms. The problem is corrected by introducing a new so-called "zeroth" mode. The zeroth mode is used to cancel the residual advection resulting from the random terms, such that advection within each particle is precisely conservative. This eliminates the problem with the bounds. The paper then shows extensive comparisons of model predictions with DNS.

REFERENCES

[1] L. Biferale. Shell models of energy cascade in turbulence. *Annual Review of Fluid Mechanics*, 35:441 –468, 2003.

[2] R. W. Bilger and R. W. Dibble. Differential molecular diffusion effects in turbulent mixing. *Combust. Sci. Tech.*, 28:161 – 172, 1982.

[3] C. Brun, G. Balarac, C. B. da Silva, and O.Métais. Effects of molecular diffusion on the subgrid-scale modeling of passive scalars. *Phys. Fluids*, 20:025102, 2008.

[4] R. Cao and S.B. Pope. The influence of chemical mechanisms on PDF calculations of nonpremixed piloted jet flames. *Combust. Flame*, 143:450–470, 2005.

[5] R. Cao, S.B. Pope, and A.R. Masri. Turbulent lifted flames in a vitiated coflow investigated using joint PDF calculations. *Combust. Flame*, 142:438–453, 2005.

[6] Renfeng Richard Cao, Haifeng Wang, and S. B. Pope. The influence of chemical mechanisms on PDF calculations of nonpremixed piloted jet flames. *Combust. Flame*, 143:450–470, 2007.

[7] J. R. Chasnov. Simulation of the kolmogorov inertial subrange using an improved subgrid model. *Phys. Fluids A*, 3:188–200, 1991.

[8] H. Chen, S. Chen, and R. H. Kraichnan. Probability distribution of a stochastically advected scalar field. *Phys. Rev. Lett.*, 63:2657, 1989.

[9] P. Y. Chou. On an extension of Reynolds' method of finding apparent stress and the nature of turbulence. *Chinese Journal of Physics*, 4:1–33, 1940.

[10] S. Corrsin. On the spectrum of isotropic temperature fluctuations in isotropic turbulence. *J. Appl. Phys.*, 22:469 – 473, 1951.

[11] R. L. Curl. Dispersed phase mixing: I. Theory and effects of simple reactors. *AIChE J.*, 9:175–181, 1963.

[12] Robert W. Dibble and Marshall B. Long. Investigation of differential diffusion in turbulent jet flows using planar laser rayleigh scattering. *Combust. Flame*, 143:644–649, 2005.

[13] C. Dopazo and E. E. O'Brien. An approach to the autoignition of a turbulent mixture. *Acta Astronautica*, 1, 1974.

[14] V. Eswaran and S. B. Pope. Direct numerical simulation of the turbulent mixing of a passive scalar. *Phys. Fluids*, 31:506–520, 1988.

[15] R. O. Fox. The Fokker-Planck closure of turbulent molecular mixing: passive scalars. *Phys. Fluids A*, 4:1230–1244, 1992.

[16] R. O. Fox. Improve Fokker-Planck model for the joint scalar, scalar gradient pdf. *Phys. Fluids A*, 6:334–348, 1994.

[17] R. O. Fox. The spectral relaxation model of the scalar dissipation rate in homogeneous turbulence. *Phys. Fluids*, 7:1082, 1995.

[18] R. O. Fox. The Langrangian spectral relaxation model of the scalar dissipation in homogeneous turbulence. *Phys. Fluids*, 9:2364–2386, 1997.

[19] R. O. Fox. The Langrangian spectral relaxation model for differential diffusion in homogeneous turbulence. *Phys. Fluids*, 11:1550–1571, 1999.

[20] R. O. Fox and P. K. Yeung. Improved Lagrangian mixing models for passive scalars in isotropic turbulence. *Phys. Fluids*, 15:961–985, 2003.

[21] V. A. Frost. Model of a turbulent diffusion-controlled flame-jet. *Fluid Mech. Sov. Res*, 4:124–133, 1975.

[22] F. Gao and E. E. O'Brien. Joint probability density function of a scalar and its gradient in isotropic turbulence. *Phys. Fluids A*, 3:1625–1632, 1991.

[23] C. W. Gardiner. *Handbook of Stochastic Methods for Physics, Chemistry and the Natural Sciences*. Springer, 1985.

[24] D. C. Haworth. Progress in probability density function methods for turbulent reacting flows. *Progress in Energy and Combust. Sci.*, 36:168C259, 2010.

[25] S. Herr, L.-P. Wang, and L. R. Collins. EDQNM model of a passive scalar with a uniform mean gradient. *Phys. Fluids*, 8:1588–1608, 1996.

[26] J. R. Herring, D. Schertzer, D. Lesieur, G. R. Newman, J. R. Chollet, and M. Larcheveque. A comparative assessment of spectral closures as applied to passive scalar diffusion. *J. Fluid Mech.*, 124:411 – 437, 1982.

[27] V. M. Ievlev. Equations for the finite dimensional probability distributions of pulsating variables in a turbulent flow. *Dokl. Akad. S.S.S.R.*, 208:1044, 1973.

[28] J. Janicka, W. Kolbe, and W. Kollmann. Closure of the transport equation for the probability density function of turbulent scalar fields. *Journal of Non-Equilibrium Thermodynamics*, 4:47–66, 1979.

[29] A. Juneja and S. B. Pope. A dns study of turbulent mixing of two passive scalars. *Phys. Fluids*, 8:2161–2184, 1996.

[30] H. S. Kang and C. Meneveau. Experimental measurements of spectral subgridscale prandtl number in a heated turbulent wake flow, edqnm predictions and 4/3-law. *J. Turbulence*, 7:1–28, 2006.

[31] A. R. Kerstein. A linear- eddy model of turbulent scalar transport and mixing. *Combust. Sci. Tech.*, 60, 1988.

[32] A. R. Kerstein. Linear eddy modeling of turbulent transport ii: Application to shear layer mixing. *Combust. Flame,* 75:397, 1989.

[33] A. R. Kerstein. Linear eddy modeling of turbulent transport. part 3. mixing and differential molecular diffusion in jets. *J. Fluid Mech.,* 216:411, 1990.

[34] A. Y. Klimenko. Matching conditional moments in pdf modeling of nonpremixed combustion. *Combust. Flame,* 143:369–385, 2005.

[35] A. Y. Klimenko and S. B. Pope. The modeling of turbulent reactive flows based on multiple mapping conditioning. *Phys. Fluids,* 15:1907–1925, 2003.

[36] G. Kosaly. Theoretical remarks on a phenomenological model of turbulent mixing. *Combust. Sci. Tech.,* 49:227, 1986.

[37] R. H. Kraichnan. Lagrangian-history closure approximation for turbulence. *Phys. Fluids,* 8:575 –589, 1965.

[38] R. H. Kraichnan. An almost-markovian galilean-invariant turbulence model. *J. Fluid Mech.,* 47:523–524, 1971.

[39] Y-Y. Kuo and E. E. O'Brien. Two-point probability density function closure applied to a diffusive-reactive system. *Phys. Fluids,* 24:194–201, 1981.

[40] T. M. Lavertu, L. Mydlarski, and S. J. Gaskin. Differential diffusion of high-Schmidt-number passive scalars in a turbulent jet. *J. Fluid Mech.,* 612:439–475, 2008.

[41] M. Lesieur and S. Ossia. Energy backscatter in large-eddy simulations of threedimensional incompressible isotropic turbulence. *J. Turbulence,* 1:1 – 11, 2000.

[42] Marcell Lesieur. *Turbulence in fluids, stochastic and numerical modeling*. Martinus Nijhoff, Boston, 1987.

[43] D. O. Lignell, J. H. Chen, and P. J. Smith. Three-dimensional direct numerical simulation of soot formation and transport in a temporally-evolving, nonpremixed ethylene jet flame. *Combust. Flame*, 155:316–333, 2008.

[44] E. Lindborg, M. Hallback, and A. D. Burden. Edqnm and dns - comparative calculations. *Applied Scientific Research*, 51:353–358, 1993.

[45] R. P. Lindstedt and S. A. Louloudi. Joint scalar transported probability density function modeling of trubulent methanol jet diffusion flames. *Proc. Comb. Inst.*, 29: 2147–2154, 2002.

[46] R. P. Lindstedt, S. A. Louloudi, and E. M. Vaos. Joint scalar probability density function modeling of pollutant formation in piloted turbulent jet diffusion flames with comprehensive chemistry. *Proc. Comb. Inst.*, 28:149–156, 2000.

[47] R. P. Lindstedt, S. A. Louloudi, J. J. Driscoll, and V. Sick. Finite rate chemistry effects in turbulent reacting flows. *Flow, Turb. Combust.*, 72:407–426, 2004.

[48] K. Liu, S. B. Pope, and D. A. Caughey. Calculations of bluff-body stabilized flames using a joint PDF model with detailed chemistry. *Combust. Flame*, 141:89–117, 2005.

[49] P. A. McMurtry, T. C. Gansauge, A. R. Kerstein, and S. K. Krueger. Linear eddy simulations of mixing in a homogeneous turbulent flow. *Phys. Fluids A*, 5:1023, 1993.

[50] D. W. Meyer and P. Jenny. A mixing model for turbulent flows based on parameterized scalar profiles. *Phys. Fluids*, 18:035105, 2006.

[51] Daniel W. Meyer and Patrick Jenny. Micromixing models for turbulent flows. *J. Comput. Phys.*, 288, 2009.

[52] R. E. Meyers and E. E. O'Brien. The joint pdf of a scalar and its gradient at a point in a turbulent flow. *Combust. Sci. Tech.*, 26:123, 1981.

[53] M. Millionshtchikov. On the theory of homogeneous isotropic turbulence. *Dokl. Akad. Nauk. SSSR*, 32:615–618, 1941.

[54] M.Lesieur and S. Ossia. 3d isotropic turbulence at very high Reynolds numbers:edqnm study. *J. Turbulence*, 1:1–25, 2000.

[55] A. T. Norris and S. B. Pope. Turbulent mixing model based on order pairing. *Combust. Flame*, 83:27–42, 1991.

[56] E. E. O'Brien and G. C. Francis. A consequence of the zero fourth cumulant approximation. *J. Fluid Mech.*, 13:369–382, 1962.

[57] A. M. Obukhov. Structure of temperature field in turbulent flows. *Izv. Akad. Nauk SSSR, Geogmagn and Geophys. Ser.*, 13:58, 1949.

[58] Y. Ogura. A consequence of the zero-fourth-cumulant approximation in the decay of isotropic turbulence. *J. Fluid Mech.*, 16:33–40, 1963.

[59] P. Orlandi and R. A. Antonia. Dependence of a passive scalar in decaying isotropic turbulence on the Reynolds and Schmidt numbers using the edqnm model. *J. Turbulence*, 5(9), 2004.

[60] S. A. Orszag. *Les Houches Summer School of Theoretical Physics*. Gordon and Breach, London, 1973.

[61] Steven. A. Orszag. Analytical theories of turbulence. *J. Fluid Mech.*, 41:363–386, 1970.

[62] S. B. Pope. The probability approach to the modeling of turbulent reactive flows. *Combust. Flame*, 27:299–312, 1976.

[63] S. B. Pope. An improved turbulent mixing model. *Combust. Sci. Tech.*, 28:131–145, 1982.

[64] S. B. Pope. PDF methods for turbulent reactive flows. *Prog. Energy Combust. Sci.*, 11:119–192, 1985.

[65] S. B. Pope. Mapping closures for turbulent mixing and reaction. *Theor. Comput. Fluid Dyn.*, 2:255–270, 1991.

[66] S. B. Pope. Lagrangian pdf methods for turbulent flows. *Annual Review of Fluid Mechanics*, 26:23–63, 1994.

[67] V. Raman, R. O. Fox, and A. D. Harvey. Hybrid FV/PDF simulation of piloted methane/air flame analysis of the turbulence-chemistry interactions. *Combust. Flame*, 136:327–350, 2004.

[68] S. I. Resnick. *Adventures in Stochastic Processes*. Birkhauser, Boston, 1992.

[69] A. R.Kerstein. Linear eddy modeling of turbulent transport. part 6: Microstructure of diffusive scalar mixing fields. *J. Fluid Mech.*, 231:361, 1991.

[70] A. R.Kerstein. Linear eddy modeling of turbulent transport. part 7. finite-rate chemistry and multi-stream mixing. *J. Fluid Mech.*, 240:289, 1992.

[71] S. M. Ross. *Stochastic Processes*. Wiley, New York, 1983.

[72] J. R. Saylor and K. R. Sreenivasan. Differential diffusion in low Reynolds number water jets. *Phys. Fluids*, 10:1125–1146, 1998.

[73] S. Subramaniam and S. B. Pope. A mixing model for turbulent reactive flows based on Euclidean minimum spanning trees. *Combust. Flame*, 115:487–514, 1998.

[74] H. Tennekes and J. L. Lumley. *A First Course in Turbulence*. MIT Press, Cambridge, 1972.

[75] K. Tsai and E. E. O'Brien. A hybrid one-point and 2-point approach for isothermal reacting flows in homogeneous turbulence. *Phys. Fluids A*, 5:2901–2919, 1993.

[76] L. Turner and J. Pratt. Eddy-damped quasinormal markovian closure: a closure for magnetohydrodynamic turbulence? *Journal of Physics A - Mathematical and General*, 35:781–793, 2002.

[77] M. Ulitsky and L. R. Collins. Application of the eddy damped quasi-normal markovian spectral transport theory to premixed turbulent flame propagation. *Phys. Fluids*, 11:3410–3430, 1997.

[78] M. Ulitsky and L. R. Collins. On constructing realizable,conservative mixed scalar equations using the eddy-damped quasi-normal markovian theory. *J. Fluid Mech.*, 412:303–329, 2000.

[79] M. Ulitsky, T. Vaithianathan, and L. R. Collins. A spectral study of differential diffusion of passive scalars in isotropic turbulence. *J. Fluid Mech.*, 460:1–38, 2002.

[80] T. Vaithianathan, M. Ulitsky, and L. R. Collins. Comparison between a spectral and probability density function model for turbulent reacting flows. *Proc. Comb. Inst.*, 29:2139–2146, 2002.

[81] L. Valino and C. Dopazo. A binomial Langevin model for turbulent mixing. *Phys. Fluids A*, 3:3034–3037, 1991.

[82] J. Vignon, C. Cambon, and M. Lesieur. Comparison of spectral calculations using the edqnm theory with experiments of homogeneous thermal turbulence. *Comptes Rendus Hebdomadaires des Seances de L'Academie des Sciences, Series B*, 288: 335–338, 1979.

[83] J. Villermaux and J. C. Devillon. *In Proc. Second Int. Symp. On Chemical Reaction Engineering*, pages 1–13, 1972.

[84] Sharadha Viswanathan and S. B. Pope. Turbulent dispersion from line sources in grid turbulence. *Phys. Fluids*, 20:101514, 2008.

[85] Z. Warharft and J. L. Lumley. An experimental study of the decay of temperature fluctuations in grid generated turbulence. *J. Fluid Mech.*, 88:659 –684, 1978.

[86] Yanjun Xia, Yang Liu, T. Vaithianathan, and Lance R. Collins. Eddy damped quasi-normal markovian theory for chemically reactive scalars in isotropic turbulence. *Phys. Fluids*, 22:045103, 2010.

[87] Yanjun Xia, T. Vaithianathan, and Lance R. Collins. Stochastic shell model for turbulent mixing of multiple scalars with mean gradients and differential diffusion. *Flow, Turb. Combust.*, 2010.

[88] J. Xu and S. B. Pope. PDF calculations of turbulent nonpremixed flames with local extinction. *Combust. Flame*, 123:281–307, 2000.

[89] P. K. Yeung. Direct numerical simulation of two-particle relative diffusion in isotropic turbulence. *Phys. Fluids A*, 6:3416 – 3428, 1994.

[90] P. K. Yeung. Lagrangian characteristics of turbulence and scalar transport in direct numerical simulations. *J. Fluid Mech.*, 427:241–274, 2001.

CHAPTER 2

EDDY DAMPED QUASI-NORMAL MARKOVIAN THEORY FOR CHEMICALLY REACTIVE SCALARS IN ISOTROPIC TURBULENCE *

Abstract The eddy damped quasi-normal Markovian (EDQNM) theory has been applied to the mixing of three scalars undergoing an isothermal, bimolecular chemical reaction of the form: $A + B \rightarrow C$, with a reaction rate constant that is independent of the scalar concentrations. The model is an extension of the work by Vaithianathan, Ulitsky and Collins (*Proc. Combust. Inst.* **29**:2139–2146, 2002) to allow for unequal initial molar concentrations of the reactant species and differences in the molecular diffusivities of the three scalars, thereby enabling the effect of differential diffusion to be studied. Comparisons of the model with results from direct numerical simulations are in good agreement for the low-order statistics considered here. The model also was used to explore the effect of the parameters (Reynolds number, Schmidt number and Damköhler number) on the scalar statistics. The results show that differential diffusion effects decrease with increasing Reynolds number, as has been observed for non-reacting scalars. However, statistics involving the product species (e.g., cross correlation coefficients ρ_{AC} and ρ_{BC}) have the opposite trend with Damköhler number, which raises the question of the role of differential diffusion for the intermediate species in a turbulent flame, where the unity Lewis number assumption is often invoked on the basis of the high Reynolds number even though the Damköhler number too is quite large.

*Originally published as: Y. Xia, Y. Liu, T. Vaithianathan and L. Collins, *Physics of Fluids*, 22, 045103, (2010). The format is adapted to meet the requirement of this thesis.

2.1 Introduction

Chemically reactive scalars must be brought into molecular contact before the chemical reaction can proceed. As a result, the overall rate of reaction for an initially unmixed system will be controlled by the mixing rate and the intrinsic chemical reaction rate. In the limit of an infinitely fast or infinitely slow reaction, the mixing or the chemistry will be the controlling (rate limiting) rate for the system, respectively. However, in many practical circumstances, including most turbulent combustion processes, the two rates are nearly in balance leading to an overall rate that is determined by their complicated and coupled interaction. One successful framework for modeling the fully coupled process is the probability density function (PDF) approach, which replaces the instantaneous scalar fields with a high-dimensional joint probability that describes the distribution of states that occur at each point in the fluid. The PDF method has the great advantage of rendering the chemical source terms in the scalar equation closed, independent of their complexity.[28] Furthermore, other nonlinear couplings, such as those associated with radiative thermal emission for example, are also closed within this framework.[18,19] However, while these source terms are formally closed, molecular mixing, which involves two-point (i.e., higher order) statistics, must be modeled. Moreover, the qualitative behavior of the PDF is controlled by the mixing model; thus, the major strength of the PDF, that is the closed source terms, is lost if the mixing model is not effective.

Mixing results from the stretching and folding of scalar blobs by turbulent eddies of different scale, causing the breakup of the blobs until ultimately molecular mixing dissipates the scalar fluctuations. This conceptual picture of mixing can be well represented by a spectral model, which decomposes the scalar fluctuations into amplitudes associated with different wavenumbers. Classical scaling arguments set forth by Kolmogorov[13], Obukhov[26] and Corrsin[5] established that the scalar spectrum should have the following

form in the so-called inertial-convective subrange:[31]

$$E_B(k) = \beta\varepsilon^{-1/3}\chi k^{-5/3} \,, \tag{2.1}$$

where $E_B(k)$ is the three-dimensional scalar spectrum, ε is the energy dissipation rate, χ is the scalar dissipation rate and β is a universal constant (according to the theory). Equation (4.1) provides a good model for inertial range under equilibrium conditions; however, scalars undergoing a chemical reaction may not achieve an equilibrium, and even if they do it will not be the same as for the purely mixing case.

The eddy damped quasi-normal Markovian (EDQNM) theory[27] is a spectral closure procedure that has been used to model a range of turbulent flow spectra, including the isotropic energy spectrum[1,16], anisotropic turbulence[21,22], passive scalar mixing[9,10,17,23,24], and even premixed flame propagation.[32,34] In earlier work, we extended the model to multiple scalars; however, the formal EDQNM procedure led to a formulation that was not realizable without correcting the eddy damping terms.[33] The resulting model was found to be in good agreement with direct numerical simulations (DNS), including capturing the relative motion of the scalars and the associated reduction in their cross correlation due to differential diffusion.[35]

In this paper, we have extended the EDQNM closure to the case of two reactants undergoing an isothermal, bimolecular reaction in homogeneous, isotropic turbulence. This system (and the closely related series-parallel reactions) has been investigated using DNS by several investigators.[4,8,11,15,20,25] This paper presents a generalization of the model given in Ref.[37] in two ways: (i) the model can be applied to scalars with arbitrary mole fractions (the previous model was limited to equal mole fractions of the reactant species); and (ii) the molecular diffusivities of the reactant and product species can be arbitrarily set, thereby allowing the effects of differential diffusion to be investigated.

The paper is organized as follows. The EDQNM spectral equations are derived in

Section 2.2. Comparisons of the prediction of the EDQNM model with DNS are given in Section 2.3 followed by a full parameter study of the effect of differential diffusion in Section 2.4. Conclusions from the study are presented in Section 3.6.

2.2 Derivation of EDQNM Model

2.2.1 Governing Equations

We consider reactant species in solution at trace concentrations that undergo an isothermal, irreversible, bimolecular reaction: $A+B \rightarrow C$. Assuming constant molecular properties, the governing equation for each scalar is as follows[3]

$$\frac{\partial \phi_\alpha(\mathbf{x},t)}{\partial t} + \frac{\partial}{\partial x_j}\left[u_j(\mathbf{x},t)\phi_\alpha(\mathbf{x},t)\right] = \mathcal{D}_\alpha \frac{\partial^2 \phi_\alpha(\mathbf{x},t)}{\partial x_j \partial x_j} + z\tilde{k}\phi_A(\mathbf{x},t)\phi_B(\mathbf{x},t)\ , \tag{2.2}$$

where $\phi_\alpha(\mathbf{x},t)$ is the concentration of one of the three reacting species: A, B or C, $u_j(\mathbf{x},t)$ is the local fluid velocity obtained from the Navier-Stokes equation, $\mathcal{D}_\alpha$ is the molecular diffusivity of species α relative to the solvent species, $\tilde{k}$ is the reaction rate constant, and $z=-1$ for reactants (α is A or B), $z=1$ for the product (α is C). Note that we use Greek letters to signify arbitrary species, and hence the summation convention does not apply.

We introduce the Reynolds decomposition, $\phi_\alpha = \langle\phi_\alpha\rangle + \phi'_\alpha$, where $\langle\phi_\alpha\rangle$ is the ensemble average and ϕ'_α is the fluctuating component. For an isotropic turbulence, the mean velocity field $\langle\mathbf{u}\rangle$ always can be set to 0 according to Galilean invariance.[29] Then taking the ensemble average of Eq. (2.2) yields the mean scalar equation

$$\begin{aligned}\frac{\partial \langle\phi_\alpha(\mathbf{x},t)\rangle}{\partial t} + \frac{\partial}{\partial x_j}\langle u'_j(\mathbf{x},t)\phi'_\alpha(\mathbf{x},t)\rangle &= \mathcal{D}_\alpha \frac{\partial^2 \langle\phi_\alpha(\mathbf{x},t)\rangle}{\partial x_j \partial x_j} + z\tilde{k}\left[\ \langle\phi'_A(\mathbf{x},t)\phi'_B(\mathbf{x},t)\rangle\right. \\ &\quad \left. + \langle\phi_A(\mathbf{x},t)\rangle\langle\phi_B(\mathbf{x},t)\rangle\ \right]\ .\end{aligned} \tag{2.3}$$

Due to the assumption of homogeneity, all of the spatial derivatives of the mean quantities vanish, simplifying Eq. (3.5) to

$$\frac{d\langle\phi_\alpha\rangle}{dt} = z\tilde{k}\left[\ \langle\phi_A\rangle\langle\phi_B\rangle + \langle\phi'_A\phi'_B\rangle\ \right]\ . \tag{2.4}$$

Subtracting Eq. (3.5) from Eq. (2.2) yields the governing equation for the scalar fluctuation

$$\frac{\partial\phi'_\alpha(\mathbf{x},t)}{\partial t} + \frac{\partial}{\partial x_j}\left[u'_j(\mathbf{x},t)\phi'_\alpha(\mathbf{x},t)\right] = \mathcal{D}_\alpha\frac{\partial^2\phi'_\alpha(\mathbf{x},t)}{\partial x_j\partial x_j} + z\tilde{k}\left[\ \phi'_A(\mathbf{x},t)\phi'_B(\mathbf{x},t) + \phi'_A(\mathbf{x},t)\langle\phi_B\rangle + \phi'_B(\mathbf{x},t)\langle\phi_A\rangle - \langle\phi'_A\phi'_B\rangle\ \right]\ , \tag{2.5}$$

which is the starting equation for the EDQNM model. To simplify the nomenclature, hereafter we suppress t in the arguments for the variables, although it remains implied.

The only term in Eq. (2.4) that requires modeling is the second-order moment $\langle\phi'_A\phi'_B\rangle$. Rather than modeling this term directly, we introduce the spectral correlation function $\mathbf{B}(\mathbf{k})$

$$\mathbf{B}(\mathbf{k}) \equiv \begin{pmatrix} B^{AA}(\mathbf{k}) & B^{AB}(\mathbf{k}) & B^{AC}(\mathbf{k}) \\ B^{AB}(\mathbf{k}) & B^{BB}(\mathbf{k}) & B^{BC}(\mathbf{k}) \\ B^{AC}(\mathbf{k}) & B^{BC}(\mathbf{k}) & B^{CC}(\mathbf{k}) \end{pmatrix}, \tag{2.6}$$

where $B^{\alpha\beta}(\mathbf{k})\hat{\delta}(\mathbf{k}+\mathbf{p}) = \frac{1}{2}[\ \langle\phi'_\alpha(\mathbf{k})\phi'^*_\beta(\mathbf{p})\rangle + \langle\phi'^*_\alpha(\mathbf{k})\phi'_\beta(\mathbf{p})\rangle\ ]$, $\hat{\delta}(\mathbf{k}) = (2\pi)^3\delta(\mathbf{k})$, $\delta(\mathbf{k})$ is the three-dimensional Dirac delta function, $\phi'_\alpha(\mathbf{k})$ is the Fourier coefficient of $\phi'_\alpha(\mathbf{x})$, and $\phi'^*_\alpha(\mathbf{k})$ is the complex conjugate of $\phi'_\alpha(\mathbf{k})$. Tensor invariance theory applied to a homogeneous isotropic system yields that $\mathbf{B}(\mathbf{k}) = 2\,\mathbf{B}(k)$, where k is the magnitude of vector $\mathbf{k}$. It is common to define the scalar spectrum as

$$\mathbf{E}(k) = \frac{k^2\mathbf{B}(k)}{\pi^2}\ , \tag{2.7}$$

such that correlations such as $\langle\phi'_A\phi'_B\rangle$ and the dissipation rate χ_α can be obtained from integrals of the spectrum

$$\langle\phi'_\alpha\phi'_\beta\rangle = \int_0^\infty E^{\alpha\beta}(k)\,dk\,, \tag{2.8}$$

$$\chi_\alpha = \mathcal{D}_\alpha \langle \nabla\phi'_\alpha \cdot \nabla\phi'_\alpha \rangle = 2\mathcal{D}_\alpha \int_0^\infty k^2 E^{\alpha\alpha}(k)\, dk\,. \tag{2.9}$$

Closing Eq. (2.4) requires a transport equation for the spectral correlation function $\mathbf{B}(k)$.

2.2.2 Exact Spectral Equations

Applying the Fourier transform to Eq. (2.5) yields

$$\begin{aligned}\left[\frac{\partial}{\partial t} + \mathcal{D}_\alpha k^2\right]\phi'_\alpha(\mathbf{k}) &= -ik_j \iint \phi'_\alpha(\mathbf{q}')u'_j(\mathbf{p}')\,\hat{\delta}(\mathbf{p}'+\mathbf{q}'-\mathbf{k})\,d\hat{\mathbf{p}}'d\hat{\mathbf{q}}' \\ &\quad + z\tilde{k}\iint \phi'_A(\mathbf{q}')\phi'_B(\mathbf{p}')\hat{\delta}(\mathbf{p}'+\mathbf{q}'-\mathbf{k})\,d\hat{\mathbf{p}}'d\hat{\mathbf{q}}' \\ &\quad + z\tilde{k}[\,\phi'_A(\mathbf{k})\langle\phi_B\rangle + \phi'_B(\mathbf{k})\langle\phi_A\rangle - \langle\phi'_A\phi'_B\rangle\hat{\delta}(\mathbf{k})\,]\,, \end{aligned}\tag{2.10}$$

where $i \equiv \sqrt{-1}$ is the imaginary number, $d\hat{\mathbf{p}} = d\mathbf{p}/(2\pi)^3$ and $d\hat{\mathbf{q}}$ is analogously defined. We can construct the equation for $B^{\alpha\beta}(\mathbf{k})$ by multiplying the equation for $\phi'_\alpha(\mathbf{k})$ by $\phi'^*_\beta(\mathbf{p})$, summing the result with the equation for $\phi'_\beta(\mathbf{p})$ multiplied by $\phi'^*_\alpha(\mathbf{k})$ and averaging. It leads to the following exact equation for the correlation matrix $\mathbf{B}(\mathbf{k})$

$$\begin{aligned}\frac{d\mathbf{B}}{dt} + (k^2\boldsymbol{\mathcal{D}} + \boldsymbol{\Psi})\cdot\mathbf{B} + \mathbf{B}\cdot(k^2\boldsymbol{\mathcal{D}} + \boldsymbol{\Psi}^T) &= \underbrace{2\iint \hat{\delta}(\mathbf{p}+\mathbf{q}-\mathbf{k})\mathbf{M}(\mathbf{k},\mathbf{p},\mathbf{q})d\hat{\mathbf{p}}d\hat{\mathbf{q}}}_{\text{advection}} \\ &\quad - \underbrace{2\tilde{k}\iint \hat{\delta}(\mathbf{p}+\mathbf{q}-\mathbf{k})\mathbf{C}(\mathbf{k},\mathbf{p},\mathbf{q})d\hat{\mathbf{p}}d\hat{\mathbf{q}}}_{\text{reaction}}\end{aligned}\tag{2.11}$$

where

$$\mathcal{D} \equiv \begin{pmatrix} \mathcal{D}_A & 0 & 0 \\ 0 & \mathcal{D}_B & 0 \\ 0 & 0 & \mathcal{D}_C \end{pmatrix}, \quad \boldsymbol{\Psi} \equiv \begin{pmatrix} \tilde{k}\langle\phi_B\rangle & \tilde{k}\langle\phi_A\rangle & 0 \\ \tilde{k}\langle\phi_B\rangle & \tilde{k}\langle\phi_A\rangle & 0 \\ -\tilde{k}\langle\phi_B\rangle & -\tilde{k}\langle\phi_A\rangle & 0 \end{pmatrix}. \tag{2.12}$$

The terms on the right hand side of Eq. (2.11) are higher-order moments that must be

modeled. The advection term takes the form

$$\mathbf{M}(\mathbf{k},\mathbf{p},\mathbf{q}) \equiv -k_j \begin{pmatrix} M_j^{AA}(\mathbf{p},\mathbf{k},\mathbf{q}) & \frac{M_j^{AB}(\mathbf{p},\mathbf{k},\mathbf{q})+M_j^{AB}(\mathbf{p},\mathbf{q},\mathbf{k})}{2} & \frac{M_j^{AC}(\mathbf{p},\mathbf{k},\mathbf{q})+M_j^{AC}(\mathbf{p},\mathbf{q},\mathbf{k})}{2} \\ Sym & M_j^{BB}(\mathbf{p},\mathbf{k},\mathbf{q}) & \frac{M_j^{BC}(\mathbf{p},\mathbf{k},\mathbf{q})+M_j^{BC}(\mathbf{p},\mathbf{q},\mathbf{k})}{2} \\ Sym & Sym & M_j^{CC}(\mathbf{p},\mathbf{k},\mathbf{q}) \end{pmatrix}, \tag{2.13}$$

where '*Sym*' implies elements required to construct a symmetric matrix,

$$M_j^{\alpha\beta}(\mathbf{k},\mathbf{p},\mathbf{q}) \equiv \{ \langle u_j'(\mathbf{k})\phi_\alpha'(\mathbf{p})\phi_\beta'(\mathbf{q})\rangle \}^{\mathrm{Im}}, \tag{2.14}$$

and 'Im' implies the imaginary part of a complex variable. The reaction term in Eq. (2.11) is defined as

$$\mathbf{C}(\mathbf{k},\mathbf{p},\mathbf{q}) \equiv \begin{pmatrix} d_1 & (d_1+d_2)/2 & -(d_1+d_3)/2 \\ sym & d_2 & -(d_2+d_3)/2 \\ sym & sym & d_3 \end{pmatrix}, \tag{2.15}$$

where

$$d_1 \equiv \frac{C_{\mathbf{kpq}}^{AAB}+C_{\mathbf{kqp}}^{AAB}}{2}, d_2 \equiv \frac{C_{\mathbf{pkq}}^{ABB}+C_{\mathbf{qkp}}^{ABB}}{2}, d_3 \equiv -\frac{C_{\mathbf{pqk}}^{ABC}+C_{\mathbf{qpk}}^{ABC}}{2}, \tag{2.16}$$

$$C_{\mathbf{kpq}}^{\alpha\beta\gamma} \equiv \{ \langle \phi_\alpha'(\mathbf{k})\phi_\beta'(\mathbf{p})\phi_\gamma'(\mathbf{q})\rangle \}^{Re}, \tag{2.17}$$

and 'Re' means the real part of a complex variable. Closure approximations for $\mathbf{M}(\mathbf{k},\mathbf{p},\mathbf{q})$ and $\mathbf{C}(\mathbf{k},\mathbf{p},\mathbf{q})$ will be discussed in the next two sections.

2.2.3 EDQNM Closure for $\mathbf{M}(\mathbf{k},\mathbf{p},\mathbf{q})$

In this section, we apply the EDQNM formalism[27] to model the higher-order correlations in the advection term. In contrast to the case of a single scalar field,[10] this procedure here leads to a *coupled* system of ordinary differential equations for the triple correlations. The quasi-normal approximation for the velocity-scalar correlation $\mathbf{M}(\mathbf{k},\mathbf{p},\mathbf{q})$ is

$$\frac{d\mathbf{M}(\mathbf{k},\mathbf{p},\mathbf{q})}{dt} = \mathbf{A}\cdot\mathbf{M}(\mathbf{k},\mathbf{p},\mathbf{q}) + \mathbf{M}(\mathbf{k},\mathbf{p},\mathbf{q})\cdot\mathbf{A}^{\mathrm{T}} + \mathcal{M}(\mathbf{k},\mathbf{p},\mathbf{q}), \tag{2.18}$$

where

$$\mathbf{A} \equiv \begin{pmatrix} -\frac{\lambda+2\tilde{k}\langle\phi_B\rangle}{2} & -\tilde{k}\langle\phi_A\rangle & 0 \\ -\tilde{k}\langle\phi_B\rangle & -\frac{\lambda+2\tilde{k}\langle\phi_A\rangle}{2} & 0 \\ \tilde{k}\langle\phi_B\rangle & \tilde{k}\langle\phi_A\rangle & -\frac{\lambda}{2} \end{pmatrix}, \tag{2.19}$$

$$\mathcal{M}(\mathbf{k},\mathbf{p},\mathbf{q}) \equiv -k_j \begin{pmatrix} \mathcal{M}_j^{AA}(\mathbf{p},\mathbf{k},\mathbf{q}) & \frac{\mathcal{M}_j^{AB}(\mathbf{p},\mathbf{k},\mathbf{q})+\mathcal{M}_j^{AB}(\mathbf{p},\mathbf{q},\mathbf{k})}{2} & \frac{\mathcal{M}_j^{AC}(\mathbf{p},\mathbf{k},\mathbf{q})+\mathcal{M}_j^{AC}(\mathbf{p},\mathbf{q},\mathbf{k})}{2} \\ Sym & \mathcal{M}_j^{BB}(\mathbf{p},\mathbf{k},\mathbf{q}) & \frac{\mathcal{M}_j^{BC}(\mathbf{p},\mathbf{k},\mathbf{q})+\mathcal{M}_j^{BC}(\mathbf{p},\mathbf{q},\mathbf{k})}{2} \\ Sym & Sym & \mathcal{M}_j^{CC}(\mathbf{p},\mathbf{k},\mathbf{q}) \end{pmatrix}, \tag{2.20}$$

$$k_j \mathcal{M}_j^{\alpha\beta}(\mathbf{p},\mathbf{k},\mathbf{q}) = -2k_j \left[k_m P_{jm}(\mathbf{p}) R(p) B^{\alpha\beta}(q) + q_m P_{jm}(\mathbf{p}) R(p) B^{\alpha\beta}(k) \right] \hat{\delta}(\mathbf{k}+\mathbf{p}+\mathbf{q}), \tag{2.21}$$

$R(p)$ is the energy spectrum defined by $R(p)P_{jm}(\mathbf{p})\hat{\delta}(\mathbf{k}+\mathbf{p}) = \langle u_j'(\mathbf{k}) u_m'(\mathbf{p})\rangle$, $P_{jm}(\mathbf{p}) \equiv \delta_{jm} - p_j p_m / p^2$ is the projection operator, δ_{jm} is the Kronecker delta function and λ is an inverse timescale that has been determined to satisfy the realizability condition[33]

$$\lambda \equiv c_{M1}\mu^p + c_{M2}(\mu^k + \mu^q) + \nu \left(k^2 + p^2 + q^2\right) . \tag{2.22}$$

The eddy damping coefficients are $c_{M1} = c_{M2} = 0.36$, and μ^k (similarly for μ^p and μ^q) is obtained in the way suggested by Pouquet et al.[30]

$$\mu^k \equiv \frac{1}{\sqrt{2}\pi} \sqrt{\int_0^k k'^4 R(k') dk'} . \tag{2.23}$$

Note that μ^k has units of inverse time, it increases monotonically with k and asymptotically approaches the inverse Kolmogorov time scale, $(\varepsilon/\nu)^{1/2}$, at large k.

The Markovian approximation neglects the effects of the time dependence of the spectra (on the right hand side of Eq. (2.18)) on the evolution of the triple correlations. Under this assumption, the linearity of the equation allows an analytical solution for $\mathbf{M}(\mathbf{k},\mathbf{p},\mathbf{q})$

$$\mathbf{M}(\mathbf{k},\mathbf{p},\mathbf{q}) = \int_0^t ds \exp[(t-s)\mathbf{A}] \mathcal{M}(\mathbf{k},\mathbf{p},\mathbf{q}) \exp[(t-s)\mathbf{A}^{\mathrm{T}}], \tag{2.24}$$

where 'exp' denotes the matrix exponential,[2] and we have assumed that initially all triple correlations are zero (i.e., $\mathbf{M}(\mathbf{k},\mathbf{p},\mathbf{q})|_{t=0} = 0$) . Substituting $\mathcal{M}$ from Eq. (2.21) into Eq. (2.24), we obtain

$$\begin{aligned}\mathbf{M}(\mathbf{k},\mathbf{p},\mathbf{q}) &= \frac{2N^2}{p^2}\int_0^t ds\{-\exp[(t-s)\mathbf{A}]\mathbf{B}(\mathbf{k})\exp[(t-s)\mathbf{A}^{\mathrm{T}}] \\ &+ \exp[(t-s)\mathbf{A}]\mathbf{B}(\mathbf{q})\exp[(t-s)\mathbf{A}^{\mathrm{T}}]\}R(p)\hat{\delta}(\mathbf{k}+\mathbf{p}+\mathbf{q}). \qquad (2.25)\end{aligned}$$

Here N is twice the area of the triad formed by the $\mathbf{k},\mathbf{p},\mathbf{q}$ vectors. Note that when evaluating the time integral in Eq. (2.25), matrices $\mathbf{A}$ and $\mathbf{B}(\mathbf{k})$ are treated as independent of time due to Markovian approximation. Consequently the matrix exponentials can be evaluated analytically. The above form of the EDQNM closure explicitly guarantees $\mathbf{B}(\mathbf{k})$ will be a positive semi-definite matrix (i.e., is realizable).[33]

2.2.4 EDQNM Closure for $\mathbf{C}(\mathbf{k},\mathbf{p},\mathbf{q})$

Based on the definition given in Eq. (2.17), the governing equation for $C^{\alpha\beta\gamma}_{\mathbf{kpq}}$ can be derived from the transport equation for $\phi'_\alpha(\mathbf{k})$. However, the coupling is not as straightforward as for $\mathbf{M}(\mathbf{k},\mathbf{p},\mathbf{q})$. For example, the equation for $C^{AAB}_{\mathbf{kpq}}$ involves $C^{AAA}_{\mathbf{kpq}}$, $C^{ABB}_{\mathbf{kpq}}$ and $C^{ABB}_{\mathbf{pkq}}$. Although $C^{ABB}_{\mathbf{pkq}}$ is one of the terms that appears in the $\mathbf{C}$ matrix, the other term, $C^{ABB}_{\mathbf{kpq}}$ does not. Ultimately, this makes it necessary to generate simultaneous equations for the following 8 correlations: $C^{AAB}_{\mathbf{kpq}}$, $C^{AAB}_{\mathbf{kqp}}$, $C^{AAB}_{\mathbf{pqk}}$, $C^{ABB}_{\mathbf{kpq}}$, $C^{ABB}_{\mathbf{pkq}}$, $C^{ABB}_{\mathbf{qkp}}$, $C^{AAA}_{\mathbf{kpq}}$ and $C^{BBB}_{\mathbf{kpq}}$ for the reactants alone, and more equations when we consider the product species. The complete set of equations is summarized in the appendix for completeness.

To reduce the computational effort, we take a different approach. First, we define two new matrices: $\mathbf{P}(\mathbf{k},\mathbf{p},\mathbf{q})$ and $\mathbf{N}(\mathbf{k},\mathbf{p},\mathbf{q})$ (the mathematical definitions are given in Tables

2.1 and 2.2) and derive their evolution equations

$$\frac{d\mathbf{P}(\mathbf{k},\mathbf{p},\mathbf{q})}{dt} = \mathbf{U}_+ \cdot \mathbf{P}(\mathbf{k},\mathbf{p},\mathbf{q}) + \mathbf{P}(\mathbf{k},\mathbf{p},\mathbf{q}) \cdot \mathbf{U}_+^{\mathrm{T}} + \mathcal{P}(\mathbf{k},\mathbf{p},\mathbf{q}) \,, \tag{2.26}$$

$$\frac{d\mathbf{N}(\mathbf{k},\mathbf{p},\mathbf{q})}{dt} = \mathbf{X} \cdot \mathbf{N}(\mathbf{k},\mathbf{p},\mathbf{q}) + \mathbf{N}(\mathbf{k},\mathbf{p},\mathbf{q}) \cdot \mathbf{X}^{\mathrm{T}} + \mathcal{N}(\mathbf{k},\mathbf{p},\mathbf{q}) \,, \tag{2.27}$$

where the definitions for all of the tensors in this section are tabulated in Tables 2.1 and 2.2. The analytical solutions of the equations are then

$$\mathbf{P}(\mathbf{k},\mathbf{p},\mathbf{q}) = \int_0^t ds \, \exp\left[(t-s)\mathbf{U}_+\right] \mathcal{P}(\mathbf{k},\mathbf{p},\mathbf{q}) \, \exp\left[(t-s)\mathbf{U}_+^{\mathrm{T}}\right] \,, \tag{2.28}$$

$$\mathbf{N}(\mathbf{k},\mathbf{p},\mathbf{q}) = \int_0^t ds \, \exp\left[(t-s)\mathbf{X}\right] \mathcal{N}(\mathbf{k},\mathbf{p},\mathbf{q}) \, \exp\left[(t-s)\mathbf{X}^{\mathrm{T}}\right] \,. \tag{2.29}$$

The equation for $\mathbf{C}(\mathbf{k},\mathbf{p},\mathbf{q})$ is then

$$\frac{d\mathbf{C}(\mathbf{k},\mathbf{p},\mathbf{q})}{dt} = \mathbf{U}_- \cdot \mathbf{C}(\mathbf{k},\mathbf{p},\mathbf{q}) + \mathbf{C}(\mathbf{k},\mathbf{p},\mathbf{q}) \cdot \mathbf{U}_-^{\mathrm{T}} + \mathcal{C}(\mathbf{k},\mathbf{p},\mathbf{q}) \,, \tag{2.30}$$

with the analytical solution

$$\mathbf{C}(\mathbf{k},\mathbf{p},\mathbf{q}) = \int_0^t ds \, \exp\left[(t-s)\mathbf{U}_-\right] \mathcal{C}(\mathbf{k},\mathbf{p},\mathbf{q}) \, \exp\left[(t-s)\mathbf{U}_-^{\mathrm{T}}\right] \,. \tag{2.31}$$

Table 2.1: This table lists the definitions of all the matrices shown in the process of the closure of **C**. Here Matrix **I** is a 3×3 identity matrix, coefficients λ_C, f_1, f_2 and f_3 are defined in Table 2.2.

Matrix	Definition
E	$\begin{pmatrix} 1 & 1 & -1 \\ 1 & 1 & -1 \\ -1 & -1 & 1 \end{pmatrix}$
X	$\begin{pmatrix} -\frac{1}{2}(\lambda_C + 2\tilde{k}\langle\phi_B\rangle) & -\tilde{k}\langle\phi_A\rangle & 0 \\ -\tilde{k}\langle\phi_B\rangle & -\frac{1}{2}(\lambda_C + 2\tilde{k}\langle\phi_A\rangle) & 0 \\ \tilde{k}\langle\phi_B\rangle & \tilde{k}\langle\phi_A\rangle & -\frac{1}{2}\lambda_C \end{pmatrix}$
$\mathbf{U}_-$	$\mathbf{X} - \frac{1}{2}[\langle\phi_A\rangle + \langle\phi_B\rangle]\,\mathbf{I}$
$\mathbf{U}_+$	$\mathbf{X} + \frac{1}{2}[\langle\phi_A\rangle + \langle\phi_B\rangle]\,\mathbf{I}$
$\mathbf{\Phi}_1$	$\begin{pmatrix} \frac{B^{BB}(p)+B^{BB}(q)+B^{AB}(p)+B^{AB}(q)}{2} & \frac{B^{AA}(p)+B^{AA}(q)+B^{AB}(p)+B^{AB}(q)}{2} & 0 \\ \frac{B^{BB}(p)+B^{BB}(q)+B^{AB}(p)+B^{AB}(q)}{2} & \frac{B^{AA}(p)+B^{AA}(q)+B^{AB}(p)+B^{AB}(q)}{2} & 0 \\ -\left[\frac{B^{BB}(p)+B^{BB}(q)+B^{AB}(p)+B^{AB}(q)}{2}\right] & -\left[\frac{B^{AA}(p)+B^{AA}(q)+B^{AB}(p)+B^{AB}(q)}{2}\right] & 0 \end{pmatrix}$
$\mathbf{\Phi}_2$	$\begin{pmatrix} \frac{B^{BB}(p)+B^{BB}(q)-B^{AB}(p)-B^{AB}(q)}{2} & \frac{B^{AB}(p)+B^{AB}(q)-B^{AA}(p)-B^{AA}(q)}{2} & 0 \\ \frac{B^{BB}(p)+B^{BB}(q)-B^{AB}(p)-B^{AB}(q)}{2} & \frac{B^{AB}(p)+B^{AB}(q)-B^{AA}(p)-B^{AA}(q)}{2} & 0 \\ -\left[\frac{B^{BB}(p)+B^{BB}(q)-B^{AB}(p)-B^{AB}(q)}{2}\right] & -\left[\frac{B^{AB}(p)+B^{AB}(q)-B^{AA}(p)-B^{AA}(q)}{2}\right] & 0 \end{pmatrix}$
$\mathbf{P}(\mathbf{k},\mathbf{p},\mathbf{q})$	$\begin{pmatrix} \frac{C^{AAA}_{\mathbf{kpq}}+C^{ABB}_{\mathbf{kpq}}}{2} & \frac{C^{AAA}_{\mathbf{kpq}}+C^{AAB}_{\mathbf{pqk}}+C^{ABB}_{\mathbf{kpq}}+C^{BBB}_{\mathbf{kpq}}}{4} & \frac{C^{AAC}_{\mathbf{pqk}}-C^{AAA}_{\mathbf{kpq}}+C^{CBB}_{\mathbf{kpq}}-C^{ABB}_{\mathbf{kpq}}}{4} \\ sym & \frac{C^{AAB}_{\mathbf{pqk}}+C^{BBB}_{\mathbf{kpq}}}{2} & \frac{C^{AAC}_{\mathbf{pqk}}-C^{AAB}_{\mathbf{pqk}}+C^{CBB}_{\mathbf{kpq}}-C^{BBB}_{\mathbf{kpq}}}{4} \\ sym & sym & \frac{-C^{AAC}_{\mathbf{pqk}}-C^{CBB}_{\mathbf{kpq}}}{2} \end{pmatrix} - \mathbf{C}(\mathbf{k},\mathbf{p},\mathbf{q})$
$\mathcal{P}(\mathbf{k},\mathbf{p},\mathbf{q})$	$-2\tilde{k}\,f_2\mathbf{E}$
$\mathbf{N}(\mathbf{k},\mathbf{p},\mathbf{q})$	$\mathbf{C}(\mathbf{k},\mathbf{p},\mathbf{q}) - \begin{pmatrix} C^{AAA}_{\mathbf{kpq}} & \frac{C^{AAA}_{\mathbf{kpq}}+C^{AAB}_{\mathbf{pqk}}}{2} & \frac{C^{AAC}_{\mathbf{pqk}}-C^{AAA}_{\mathbf{kpq}}}{2} \\ Sym & C^{AAB}_{\mathbf{pqk}} & \frac{C^{AAC}_{\mathbf{pqk}}-C^{AAB}_{\mathbf{pqk}}}{2} \\ Sym & Sym & -C^{AAC}_{\mathbf{pqk}} \end{pmatrix}$
$\mathcal{N}(\mathbf{k},\mathbf{p},\mathbf{q})$	$-2\tilde{k}[\Phi_2\mathbf{B}(\mathbf{k}) + \mathbf{B}(\mathbf{k})\Phi_2^T] - 2\tilde{k}\,f_3\mathbf{E} - 2\tilde{k}\langle\Phi_A\rangle\mathbf{P}(\mathbf{k},\mathbf{p},\mathbf{q})$
$\mathcal{C}(\mathbf{k},\mathbf{p},\mathbf{q})$	$-2\tilde{k}[\Phi_1\mathbf{B}(\mathbf{k}) + \mathbf{B}(\mathbf{k})\Phi_1^T]$ $-2\tilde{k}\,f_1\mathbf{E} - 2\tilde{k}\langle\Phi_A\rangle\mathbf{P}(\mathbf{k},\mathbf{p},\mathbf{q}) + \tilde{k}\,[\langle\Phi_B\rangle - \langle\Phi_A\rangle]\mathbf{N}(\mathbf{k},\mathbf{p},\mathbf{q})$

Table 2.2: This table lists the definitions of the coefficients λ_C, f_1, f_2 and f_3, the arbitrary coefficient c_C is set to 0.36 to agree with the coefficient used in the expression for $\mathbf{M}(\mathbf{k},\mathbf{p},\mathbf{q})$.

Coefficient	Definition
λ_C	$c_C(\mu^p+\mu^k+\mu^q)+\nu\,(k^2+p^2+q^2)$
f_1	$B^{AA}(p)B^{BB}(q)+B^{AA}(q)B^{BB}(p)+2B^{AB}(p)B^{AB}(q)$
f_2	$B^{AA}(p)B^{AB}(q)+B^{AA}(q)B^{AB}(p)+B^{AB}(p)B^{BB}(q)+B^{AB}(q)B^{BB}(p)$ $-B^{AA}(p)B^{BB}(q)-B^{AA}(q)B^{BB}(p)-2B^{AB}(p)B^{AB}(q)$
f_3	$B^{AA}(p)B^{BB}(q)+B^{AA}(q)B^{BB}(p)+2B^{AB}(p)B^{AB}(q)$ $-2[B^{AA}(p)B^{AB}(q)+B^{AA}(q)B^{AB}(p)]$

2.2.5 Numerical Update of the EDQNM equations

Equation (2.11) can be rewritten in the following form

$$\frac{d\mathbf{B}}{dt}=\mathbf{\Pi}\cdot\mathbf{B}+\mathbf{B}\cdot\mathbf{\Pi}^{\mathrm{T}}+\mathbf{\Gamma}\,, \tag{2.32}$$

where $\mathbf{\Gamma}$ is a positive semi-definite matrix comprising the right hand side of Eq. (2.11) and $\mathbf{\Pi}$ is defined as

$$\mathbf{\Pi}\equiv-(k^2\mathcal{D}+\mathbf{\Psi})\,. \tag{2.33}$$

The mathematical form of Eq. (2.32) guarantees $\mathbf{B}$ remains positive semi-definite; however, time stepping errors can lead to a loss of that property, implying the scalar statistics may not satisfy the Cauchy-Schwartz realizability constraints. Hence the time update of the EDQNM equation must be carefully devised.

A numerical scheme developed by Vaithianathan and Collins[36] could be used to preserve the positive definiteness of $\mathbf{B}(k)$. However, due to the smooth behavior of the matrices, a much simpler first order scheme can be designed based on a backward Euler update.

Discretizing Eq. (2.32), we obtain

$$\frac{\mathbf{B}_{n+1}-\mathbf{B}_n}{\Delta t} = \mathbf{\Pi}_n \cdot \mathbf{B}_{n+1} + \mathbf{B}_{n+1} \cdot \mathbf{\Pi}_n^{\mathrm{T}} + \mathbf{\Gamma}_n. \tag{2.34}$$

Here, subscripts n and $n+1$ denote the quantities are evaluated at times t_{n+1} and t_n respectively. Rearranging Eq. (2.34) we get an algebraic Lyapunov equation[2]

$$\left[\Delta t\mathbf{\Pi}_n - \tfrac{1}{2}\mathbf{I}\right] \cdot \mathbf{B}_{n+1} + \mathbf{B}_{n+1} \cdot \left[\Delta t\mathbf{\Pi}_n - \tfrac{1}{2}\mathbf{I}\right]^{\mathrm{T}} = -\mathbf{B}_n - \Delta t\mathbf{\Gamma}_n, \tag{2.35}$$

where $\mathbf{I}$ is the 3×3 identity matrix. Since $\mathbf{B}_n \to \mathbf{O}$ (zero matrix) as $n \to \infty$, the analytical solution to the above equation can be written as[2]

$$\mathbf{B}_{n+1} = \int_0^\infty ds\ \exp[s(\Delta t\mathbf{\Pi}_n - \tfrac{1}{2}\mathbf{I})]\{\mathbf{B}_n + \Delta t\mathbf{\Gamma}_n\}\exp[s(\Delta t\mathbf{\Pi}_n - \tfrac{1}{2}\mathbf{I})^{\mathrm{T}}]. \tag{2.36}$$

The exponentials can be evaluated analytically if the eigenvalues of $\left(\Delta t\mathbf{\Pi}_n - \frac{1}{2}\mathbf{I}\right)$ are known. Since this is only a 3×3 matrix, the eigenvalues are calculated at each time step. By this updating scheme, the positive semi-definiteness of matrix $\mathbf{B}(\mathbf{k})$ is preserved.

2.3 Comparison with Direct Numerical Simulations

In this section, we compare the predictions of the EDQNM model with direct numerical simulations (DNS) performed in a cube of length 2π with 128^3 grid points. The DNS is similar to previous studies performed in our group (e.g., Herr et al.[9] or Vaithianathan et al.[37]). The turbulent kinetic energy was made stationary by forcing the first two wavenumbers in a manner similar to Eswaran and Pope[7]. The initial velocity field and forcing were fixed for all of the simulations. The energy spectrum was obtained by averaging the instantaneous spectrum over 40 large eddy turnover times. Scalar fields were not introduced until the velocity fields reached a statistically stationary state after about 20 eddy turnover times. The reactant fields were initialized with a pre-specified spectrum, but

following the method of Eswaran and Pope[6] so that they were nearly unmixed initially. The scalar fields were updated using the second-order, bound-preserving finite volume scheme developed by Kurgonov and Tadmor[14]. The parameters used in the comparison are summarized in Table 2.3.

Table 2.3: Parameters used in DNS and EDQNM calculations. Dimensional parameters are based on arbitrary units. Here ν is fluid viscosity, ε is dissipation rate, $u_{\rm rms}$ is turbulence intensity, $L \equiv \frac{\pi}{2u_{\rm rms}^2}\int_0^\infty \frac{E(k)}{k}dk$ is the integral length scale, $T \equiv L/u_{\rm rms}$ is the large eddy turn-over time, $Re_L \equiv u_{\rm rms}L/\nu$ is Reynolds number based on integral scales. $\langle\phi\rangle$ is the initial scalar mean concentration, ϕ' is the initial root mean square of the scalar fluctuation, ρ_{AB} is the initial cross correlation coefficient and L_ϕ/L is the initial ratio of the integral length scale of the scalar to that of the turbulent kinetic energy.

Simulation	ν	ε	$u_{\rm rms}$	L	T	Re_L	$\langle\phi\rangle$	ϕ'_A	ϕ'_B	ρ_{AB}	L_ϕ/L
DNS	0.015	0.21	0.87	1.03	1.18	60	2.66	0.91	0.91	-0.99	0.25
EDQNM	0.015	0.22	0.87	0.88	1.01	51	2.66	0.91	0.91	-0.99	0.28

In the EDQNM calculations, we did not solve for the energy spectrum, but substituted the stationary energy spectrum from the DNS, thus eliminating any error associated with the EDQNM prediction of the energy spectrum, particularly over the forced wavenumbers. This allows us to focus on the performance of the scalar equations. We matched the initial scalar spectra and updated them using the EDQNM model presented in Section 2.2. We ran six different combinations of Schmidt numbers ($Sc_\alpha \equiv \nu/\mathcal{D}_\alpha$) to analyze the effect of differential diffusion. They will be referred to as Cases 1–6 (see Table 2.4). However, comparisons with DNS will be done for Cases 1 and 2 only. We define the Damköhler number as the ratio of the turbulence time scale to the initial time scale of the chemical source term, the latter being defined as $1/(\tilde{k}\langle\phi_A\rangle|_{t=0})$. For the fluid time scale we have the option of using the large eddy turnover time, T or the Kolmogorov time $\tau_\eta \equiv \sqrt{\nu/\varepsilon}$, hence we define two Damköhler numbers as: $Da \equiv \tilde{k}\langle\phi_A\rangle|_{t=0}T$ and $Da_\eta \equiv \tilde{k}\langle\phi_A\rangle|_{t=0}\sqrt{\nu/\varepsilon}$. The

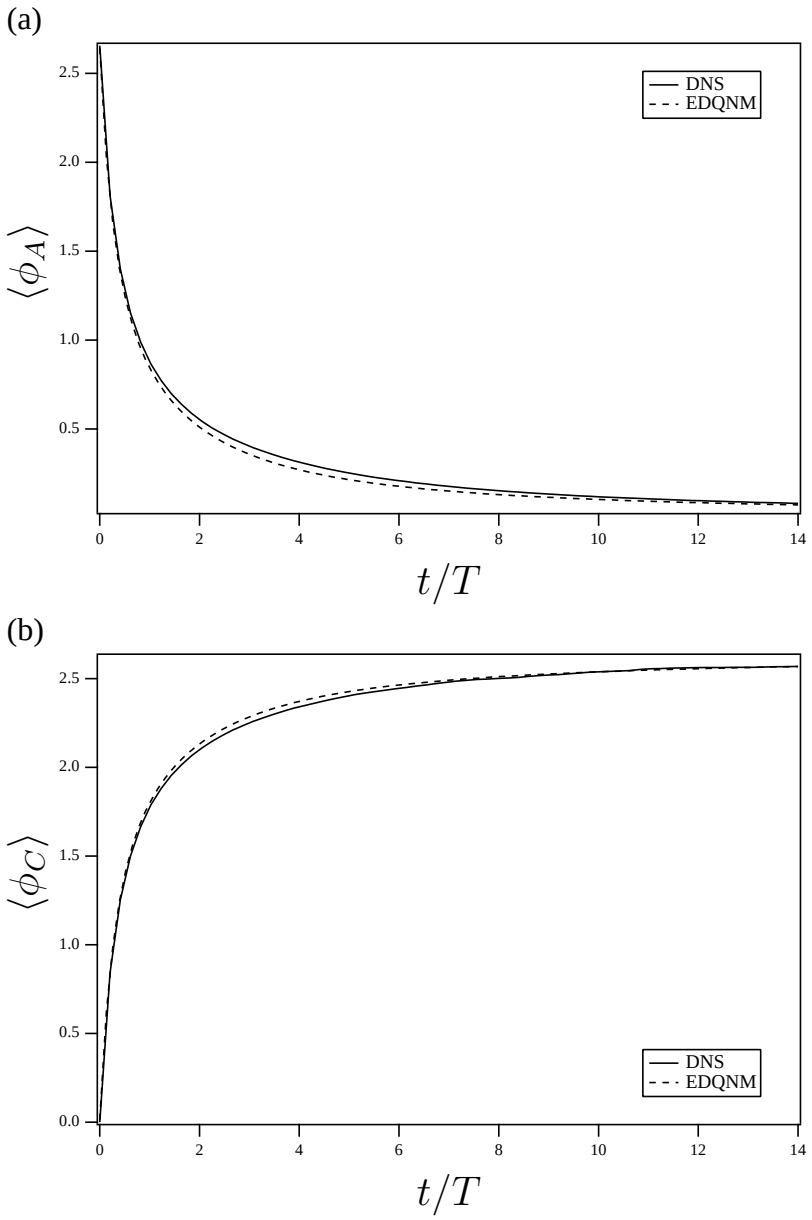

Figure 2.1: Comparison of the mean concentration of (a) reactant *A* and (c) product *C* between DNS and the EDQNM model for Case 1 with $Da = 3.1$.

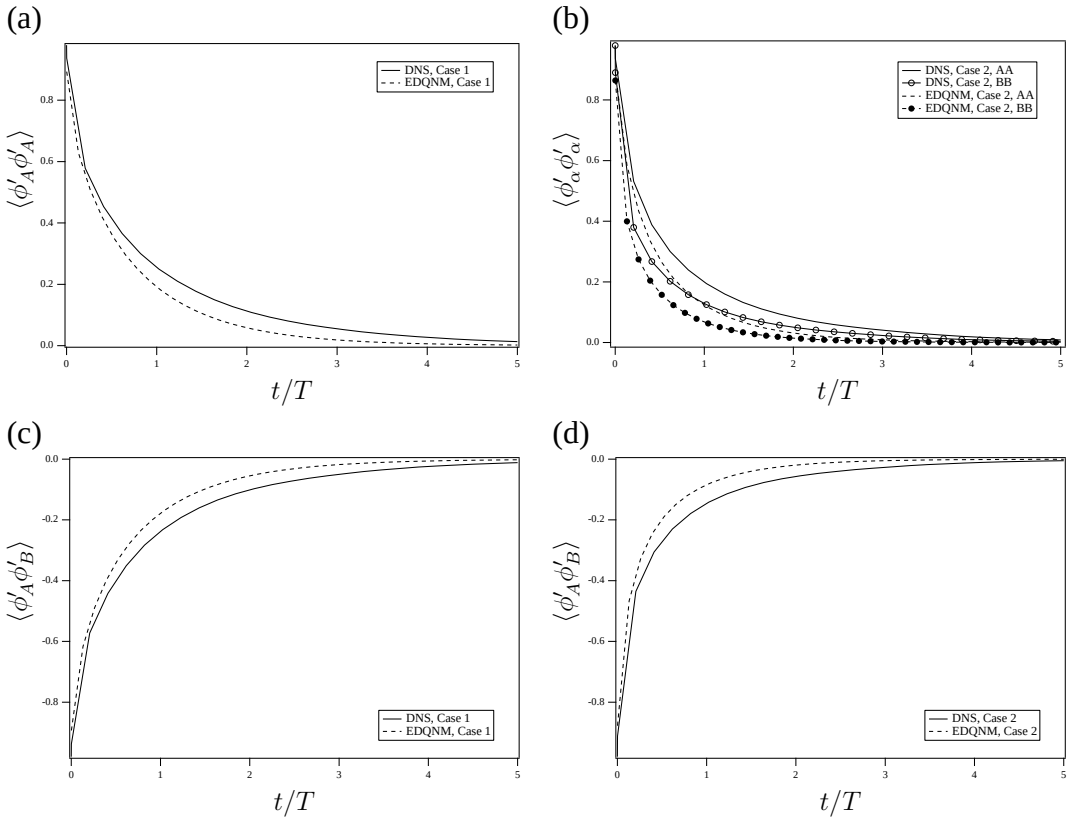

Figure 2.2: Reactant autocorrelations (a and b) and cross correlations (c and d) for Cases 1 (a and c) and 2 (b and d) at $Da = 3.1$. Solid lines are DNS and dashed lines are the EDQNM model.

comparisons are made at $Da = 3.1$, which corresponds to $Da_\eta = 0.7$. Figure 2.1 shows a comparison of the mean concentrations $\langle \phi_A \rangle$ and $\langle \phi_C \rangle$ for Case 1 (note $\langle \phi_B \rangle = \langle \phi_A \rangle$ for this case). The agreement is excellent; note that similar agreement was achieved for the other comparisons (not shown).

Table 2.4: Combinations of Schmidt numbers for the 6 cases we ran.

Case$\rightarrow$	1	2	3	4	5	6
Sc_A	1	$\frac{1}{4}$	$\frac{1}{4}$	$\frac{1}{4}$	1	$\frac{1}{16}$
Sc_B	1	1	$\frac{1}{4}$	1	1	$\frac{1}{4}$
Sc_C	1	1	1	$\frac{1}{4}$	$\frac{1}{4}$	1

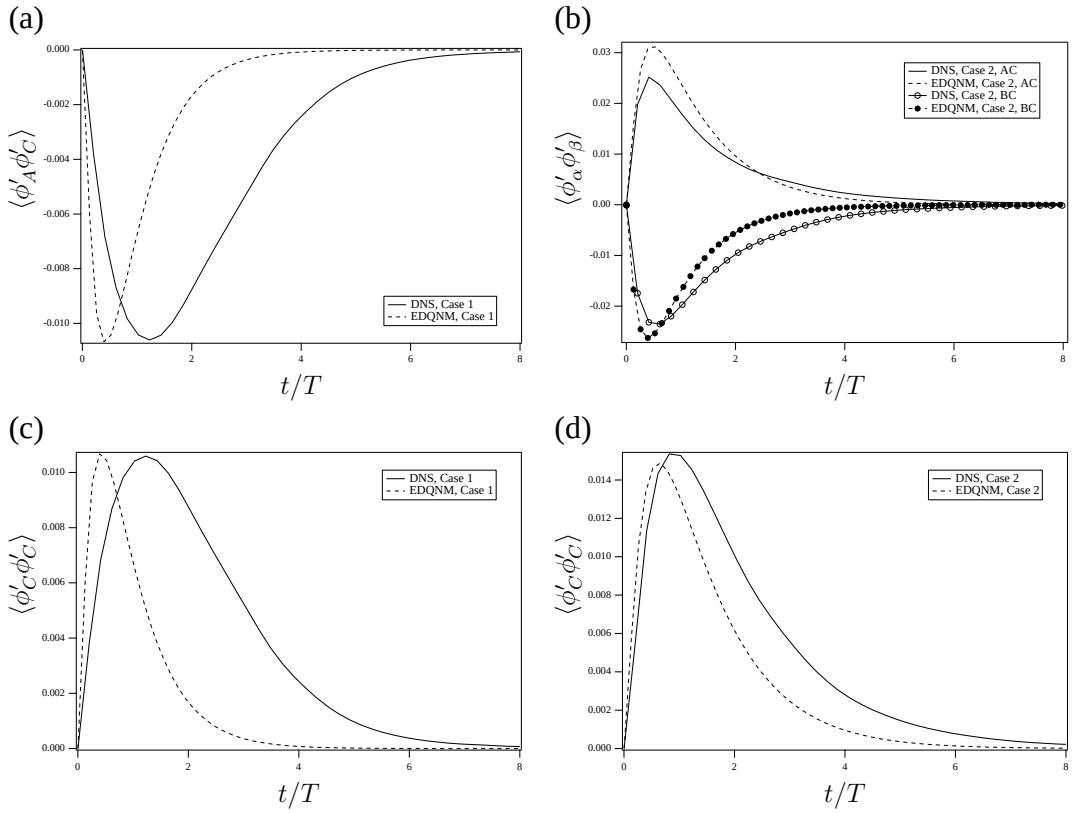

Figure 2.3: Product/reactant cross correlations (a and b) and product autocorrelations (c and d) for Cases 1 (a and c) and 2 (b and d) at $Da = 3.1$. Note that for Case 1 $\langle \phi'_A \phi'_C \rangle = \langle \phi'_B \phi'_C \rangle$ thus only the former is shown.

Figure 2.2 shows the autocorrelations and cross correlations of the reactant species for Cases 1 and 2. The EDQNM model again gives very good predictions for Case 1 without differential diffusion. The error is slightly larger for Case 2, but the predictions are still reasonably good.

A more stringent test of the model is shown in Fig. 2.3, which has comparisons of the product–reactant cross correlations and product-product autocorrelations. This is the first prediction of its kind for a spectral-based model. We note that the magnitude of the peak of the cross correlation for Case 1 (Fig. 2.3a) is well predicted, but the timing of the peak is not well captured, with the EDQNM model predicting a time scale roughly half that of the DNS. Interestingly, the agreement for the case with differential diffusion (Case 2) is much

better. The EDQNM model is able to capture the difference in the sign of $\langle \phi'_A \phi'_C \rangle$ versus $\langle \phi'_B \phi'_C \rangle$, which arises solely due to differential diffusion. That is, the fact that species A diffuses at four times the rate of species B and C causes a break in the symmetry of the cross correlations, as shown in Fig. 2.3b. The fact that EDQNM is able to correctly capture that break in symmetry is encouraging that the modified closure procedure developed by Ulitsky and Collins[33] is robust. The autocorrelations shown in Figs. 2.3c and 2.3d have similar trends as those of the cross correlations. Once again, EDQNM captures the peak in the autocorrelation for Case 1, but the timing is less accurate than was found for Case 2.

Note that no attempt was made to adjust any of the EDQNM parameters to improve the agreement with the DNS. In particular, we do not attempt to optimize the coefficients to improve the agreement for this chemically reacting system, as this might degrade the model's performance for the simpler case of pure mixing.The only new parameter that is not set by previous studies is the eddy damping coefficient for $\mathbf{C}(\mathbf{k},\mathbf{p},\mathbf{q})$, c_C, which we set to 0.36 to agree with the coefficient for $\mathbf{M}(\mathbf{k},\mathbf{p},\mathbf{q})$.

2.4 Parameter Study

Given the reasonably good comparisons with DNS shown in Section 2.3, it is now possible to use the model to investigate how differential diffusion affects the scalar statistics as a function of the parameters. For simplicity we employ a Pao spectrum,[29] with three different values of the Reynolds number. Table 2.5 gives a summary of the flow and scalar parameters. We simulated the combination of Schmidt numbers given in Table 2.4 at Damköhler numbers $Da = 0.01$, 0.1, 1 and 3, for a total of 72 different cases. (Note that the Kolmogorov scale Damköhler number $Da_\eta = Da/[T/\tau_\eta]$, where T/τ_η is given in Table 2.5.) For space reasons we cannot show all of the results, but we will show a

selection of results that highlight the important effects of differential diffusion. The scalar means for reactants A and B were initially $\langle\phi_A\rangle = \langle\phi_B\rangle = 2.5$, while the scalar fluctuations were precisely anti-correlated, i.e., $\phi'_B(\mathbf{x},t) = -\phi'_A(\mathbf{x},t)$, implying a correlation coefficient,

$$\rho_{AB} \equiv \frac{\langle\phi'_A\phi'_B\rangle}{\left(\langle\phi'^2_A\rangle\langle\phi'^2_B\rangle\right)^{1/2}} , \tag{2.37}$$

of $\rho_{AB} = -1$, corresponding to a perfectly unmixed condition. To assist us in quantifying the effect of differential diffusion, we define three parameters

$$\Lambda \equiv \langle\phi'_B\phi'_B\rangle / \langle\phi'_A\phi'_A\rangle , \qquad \text{(Case 2 only)} \tag{2.38}$$

$$\Gamma \equiv \langle\phi'_B\phi'_C\rangle - \langle\phi'_A\phi'_C\rangle , \qquad \text{(Case 2 only)} \tag{2.39}$$

$$\Psi \equiv \langle\phi'_A\phi'_C\rangle_{\text{Case 5}} - \langle\phi'_A\phi'_C\rangle_{\text{Case 1}} . \tag{2.40}$$

Note by definition, $\Lambda = 1$, $\Gamma = 0$ and $\Psi = 0$ in the absence of differential diffusion.

Table 2.5: Summary of velocity and initial scalar parameters in the parametric study. $R_\lambda \equiv u'^2_{\text{rms}}\sqrt{15/\nu\varepsilon}$ is the Reynolds number based on the Taylor microscale and $\eta \equiv \nu^{3/4}/\varepsilon^{1/4}$ is the Kolmogorov length scale. Note that the statistics for scalar B are not shown because they are identical to those of A (with B perfectly anti-correlated to A). See the caption for Table 2.3 for definitions of the other parameters.

Velocity	ν	ε	u_{rms}	L	T	R_λ	L/η	T/τ_η	$\langle\phi_A\rangle$	ϕ'_A	ρ_{AB}	L_ϕ/L
$R_{\lambda 1}$	1×10^{-3}	0.3	0.78	1.05	1.34	137	138	23	2.5	2.5	-1	0.62
$R_{\lambda 2}$	4×10^{-4}	0.3	0.80	1.01	1.27	225	265	35	2.5	2.5	-1	0.64
$R_{\lambda 3}$	2×10^{-4}	0.3	0.80	0.99	1.24	324	439	48	2.5	2.5	-1	0.66

2.4.1 Single-point Statistics

Figure 2.4 shows the time evolution for $\langle\phi_A\rangle$ and $\langle\phi_C\rangle$. According to Eq. (2.4), the mean concentration is determined by the correlation covariance $\langle\phi'_A\phi'_B\rangle$, which, as we will show,

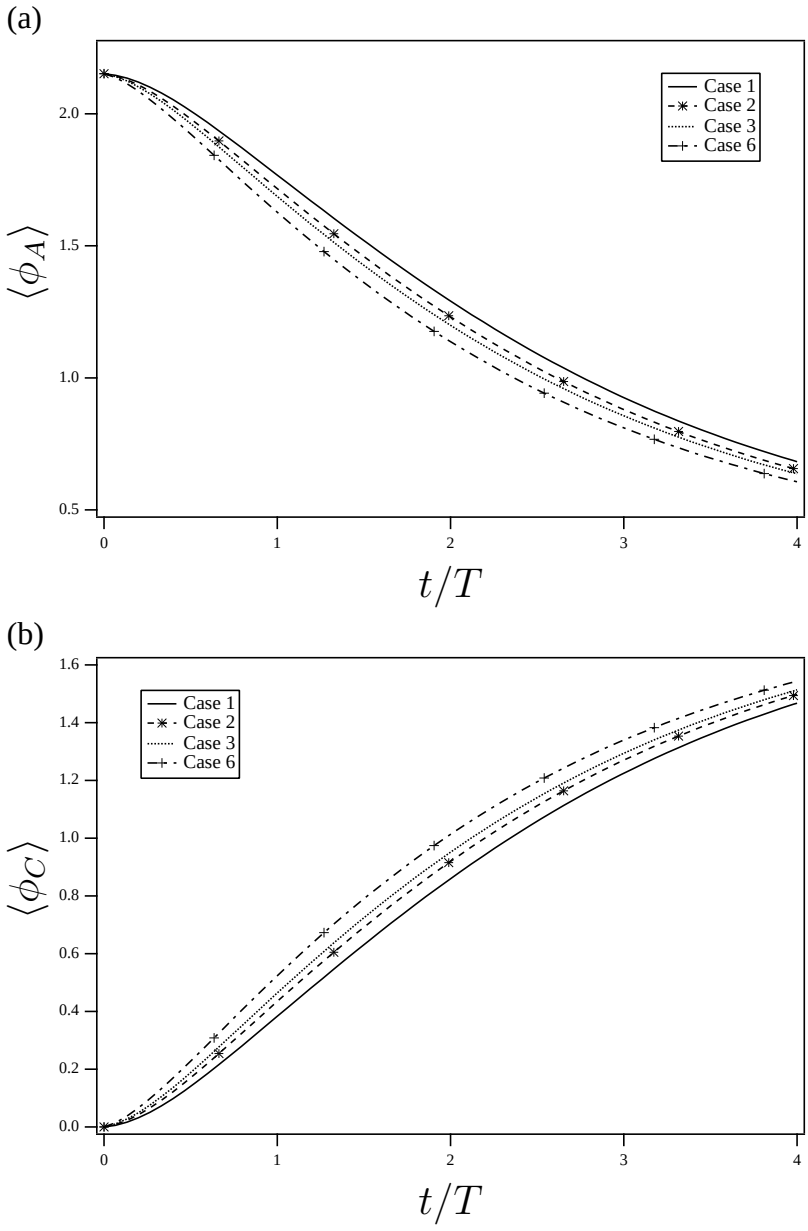

Figure 2.4: The mean concentration of species (a) A and (b) C for Cases 1, 2, 3 and 6 as indicated at $Da = 1$ ($Da_\eta = 1/23$) and $R_{\lambda 1}$.

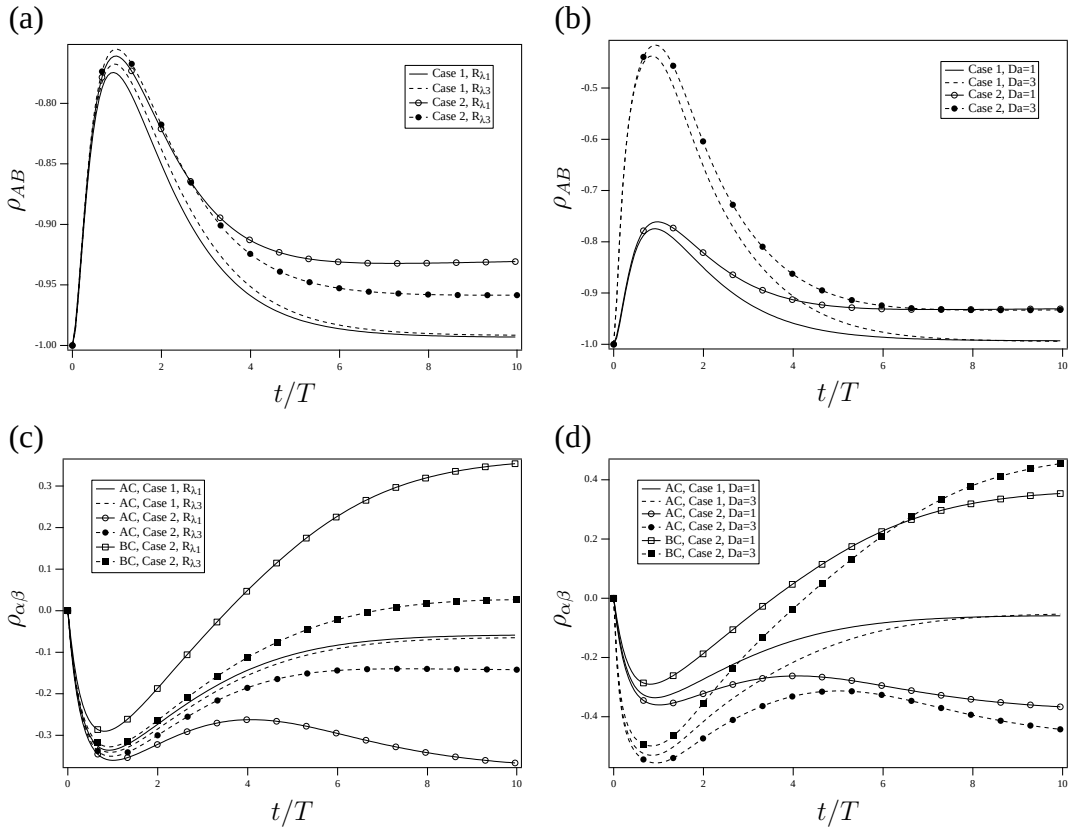

Figure 2.5: Cross correlation coefficients for Cases 1 and 2: (a) ρ_{AB} at $Da = 1$ and the indicated Reynolds number (note that $Da_\eta = 1/23$ and 1/48 for $R_{\lambda 1}$ and $R_{\lambda 3}$, respectively); (b) ρ_{AB} at $R_{\lambda 1}$ and the indicated Damköhler numbers ($Da_\eta = 1/23$ and $3/23$ for $Da = 1$ and 3, respectively); (c) ρ_{AC} and ρ_{BC} at $Da = 1$ and the indicated Reynolds number; and (d) ρ_{AC} and ρ_{BC} at $R_{\lambda 1}$ and the indicated Damköhler number.

is affected by differential diffusion. This explains the variations in $\langle \phi_A \rangle$ and $\langle \phi_C \rangle$ among the four cases shown in Fig. 2.4.

Ulitsky et al.[35] considered the effects of differential diffusion in the absence of chemical reaction. In their study, the scalars were initially perfectly correlated, and they calculated the change in correlation as the system mixed. For the case of equally diffusive scalars (equivalent to Case 1 in this study), the correlation coefficient will not change in time. The same would be true here for the initially anti-correlated scalars. Figure 2.5 shows the evolution of the cross correlation coefficients for Cases 1 and 2. If we consider

the evolution of ρ_{AB} for Case 1 in Fig. 2.5a (solid line), we can conclude immediately that the short-time behavior must be due to the chemical reaction. The cross correlation increases because locally species *A* and *B* are both consumed by the chemical reaction causing the local scalar fluctuation of the two species to be the same (negative) and hence better correlated. Eventually as the reactants are depleted and the chemical reaction rate approaches zero, the correlation coefficient returns to its initial value of -1. We also see the effect of Reynolds number on Case 1 is very weak. For Case 2, the diffusivity for species *A* is four times that for species *B*, introducing the effects of differential diffusion. The initial behavior of ρ_{AB} is only weakly affected by differential diffusion; however, beyond the peak at $t/T \approx 1$, there is a pronounced effect of differential diffusion. In particular, the asymptote approached at long times is apparently a function of the ratio of diffusivities. Furthermore, with increasing Reynolds number the asymptote approaches -1, indicating the effects of differential diffusion are diminished with increasing Reynolds number, which is consistent with our earlier findings[35] as well as those of others.[12] Figure 2.5b shows the effect of the Damköhler number on the correlation coefficient. With a change in *Da* from 1 to 3, we see the peak in the correlation coefficient also increases from -0.75 to nearly -0.4, indicating, not surprisingly, the effect of the chemical reaction is enhanced. At long times the curves approach an asymptote that is independent of the Damköhler number.

Figure 2.5c and d show the cross correlation coefficients between the reactants and product species, ρ_{AC} and ρ_{BC}. For Case 1, these curves are, by symmetry, equal and hence we do not show both curves. The curves start at zero and become negative as species *C* is produced. This can be explained by the fact that both species *A* and *B* are consumed to produce *C*, and hence they are anti-correlated. Once again, for Case 1 we see the dependence on the Reynolds number is relatively weak, whereas the minimum value decreases with increasing Damköhler number. The curves for Case 2 with differential

diffusion show rather complex behavior. In the early stages when chemical reaction is dominant, they are similar to Case 1; however, for mixing times beyond $t/T \approx 1$ we see ρ_{AC} and ρ_{BC} deviate strongly from each other, with neither curve looking at all like Case 1. Species *B* (the slower diffusiving species) has a much higher correlation with the product species at long times than species *A*. We attribute this to species *A* being able to diffuse from the pockets of high concentration deeper into the reaction zone than species *B*. As a consequence, a portion of the reaction zone will contain an excess of species *B* and hence the reaction in that region will be limited by species *A*. As species *A* is consumed and species *C* is produced, they will be anti-correlated, whereas the excess of species *B* will produce a positive correlation with species *C*. This effect of differential diffusion is diminished with increasing Reynolds number, while with increasing Damköhler number it is enhanced. Unlike ρ_{AB}, at long times the asymptotic behavior of ρ_{AC} and ρ_{BC} are both strong functions of the Reynolds *and* Damköhler numbers.

An alternative measure of the effect of differential diffusion on the reactant species is the variable Λ (see Eq. 2.38), which is shown in Fig. 2.6. Recall that $\Lambda = 1$ in the absence of differential diffusion, hence its value above unity is a measure of its effect. With increasing Reynolds number or Damköhler number we see Λ is diminished. The effect of Reynolds number is consistent with the results presented above; however, the trend with Damköhler number is contrary to the earlier trends. The rapid diffusion of species *A* into species *B* causes Λ to increase, but reaction consumes the limiting reagent, which in this case is species *A* since it has the higher diffusivity. Thus, increasing the reaction rate will diminish Λ.

Figure 2.7 shows the parameter Γ as a function of time (see Eq. 2.39). This function would be zero in the absence of differential diffusion (e.g., for Case 1). We see that its value decreases with increasing Reynolds number, but increases with increasing

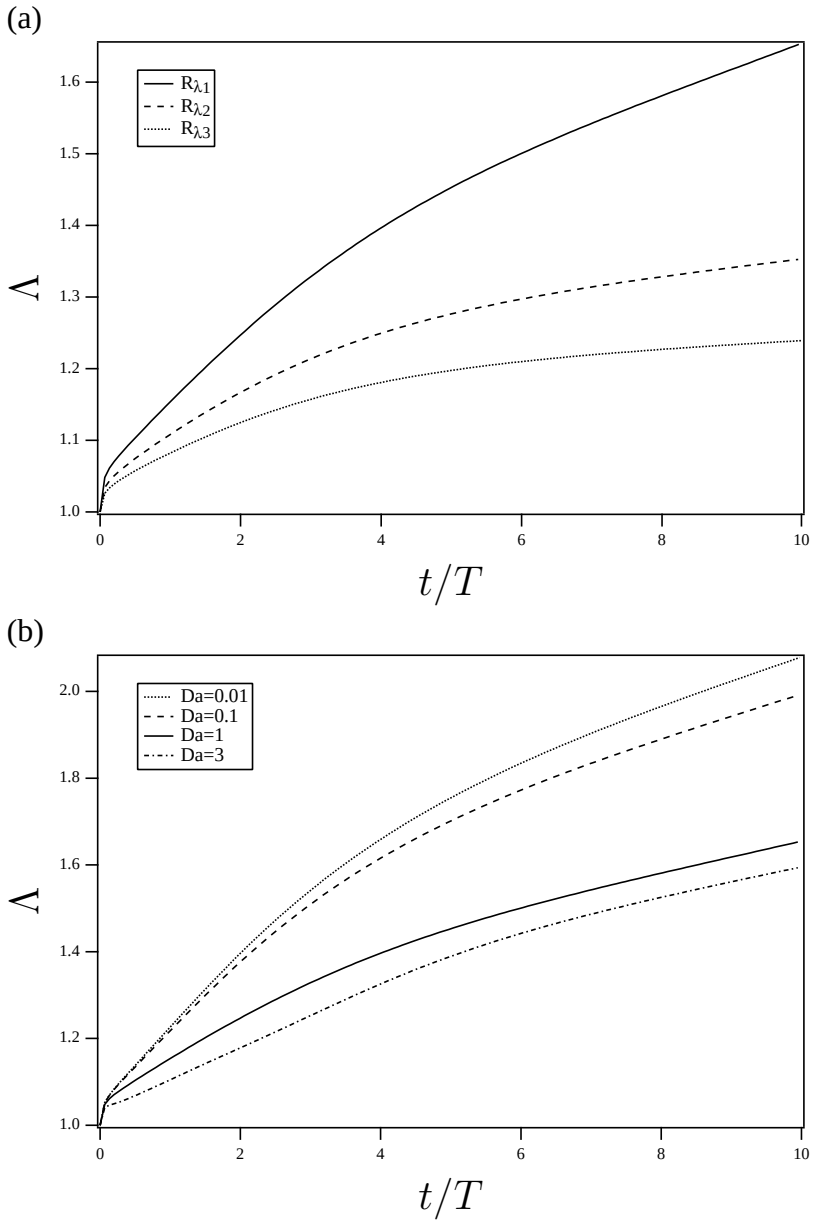

Figure 2.6: Evolution of $\Lambda \equiv \langle \phi'_B \phi'_B \rangle / \langle \phi'_A \phi'_A \rangle$ for Case 2 at: (a) $Da = 1$ and the indicated Reynolds number (note that $Da_\eta = 1/23$, $1/38$ and $1/45$ for $R_{\lambda 1}$, $R_{\lambda 2}$ and $R_{\lambda 3}$, respectively); and (b) $R_{\lambda 1}$ and the indicated Damköhler number (note that $Da_\eta = 0.01/23$, $0.1/23$, $1/23$ and $3/23$ for $Da = 0.01$, 0.1, 1 and 3, respectively).

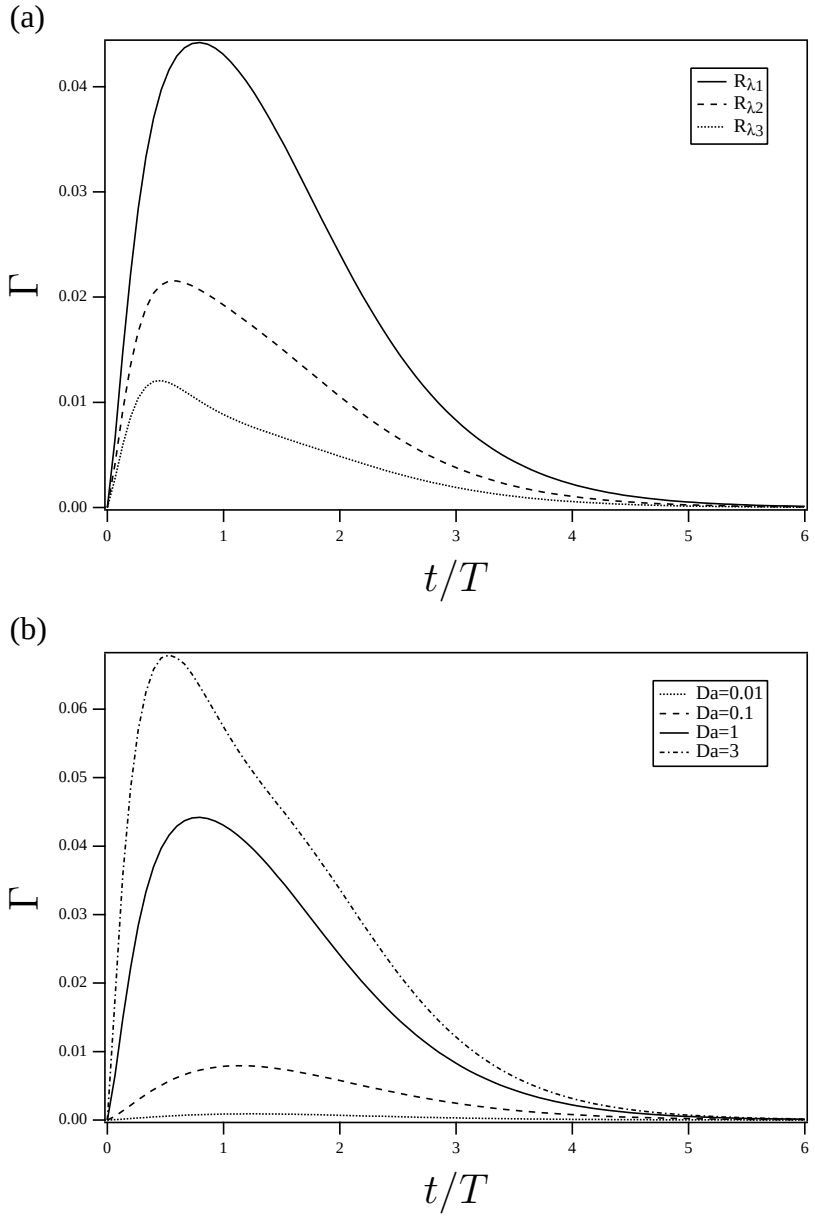

Figure 2.7: Evolution of $\Gamma \equiv \langle \phi'_B \phi'_C \rangle - \langle \phi'_A \phi'_C \rangle$ for Case 2 at: (a) $Da = 1$ and the indicated Reynolds number (note that $Da_\eta = 1/23$, $1/38$ and $1/45$ for $R_{\lambda 1}$, $R_{\lambda 2}$ and $R_{\lambda 3}$, respectively); and (b) $R_{\lambda 1}$ and the indicated Damköhler number (note that $Da_\eta = 0.01/23$, $0.1/23$, $1/23$ and $3/23$ for $Da = 0.01$, 0.1, 1 and 3, respectively).

Damköhler number. It is apparent that all of the differential diffusion statistics involving the product species are enhanced by increases in the chemical reaction rate. The effect of a higher diffusivity for the product species is shown in Fig. 2.8 for Case 5 (diffusivity of species C is four times that of species A and B). We see similar trends as were found for Γ in Fig. 2.7.

2.4.2 Scalar Spectra

Figure 2.9 shows the evolution of the three autocorrelation spectra under the influence of differential diffusion (Case 2). Two salient features can be observed. First, the autocorrelation spectra for the reactants A and B are nearly identical at low wavenumbers, but differ at high wavenumbers (small scales), which shows that differential diffusion originates from small scales. Second, the reactant spectra peak at wavenumber one, whereas the product spectrum is peaked at a higher wavenumber, which implies that the product is produced at smaller scales. In this non-premixed system, product C is predominantly produced in the thin reaction zone between the reactants, and then it diffuses towards the reactants, making the mixing of reactant and product species a small-scale phenomenon, which is captured well by the EDQNM model.

The cross-correlation spectra are given in Fig. 2.10 for Cases 1 and 2. We see that the cross correlation spectrum for the reactants is very different from the cross correlation spectra for each reactant with the product. The E^{AB} spectra, both for Cases 1 and 2, are peaked at small wavenumbers initially, while the E^{AC} spectra, are peaked at higher wavenumbers for the reasons discussed above. The differences between Cases 1 and 2 also occur at high wavenumbers, where molecular effects are most important.

The evolution of the E^{CC} in time is shown in Fig. 2.11; the inset shows the wavenumber

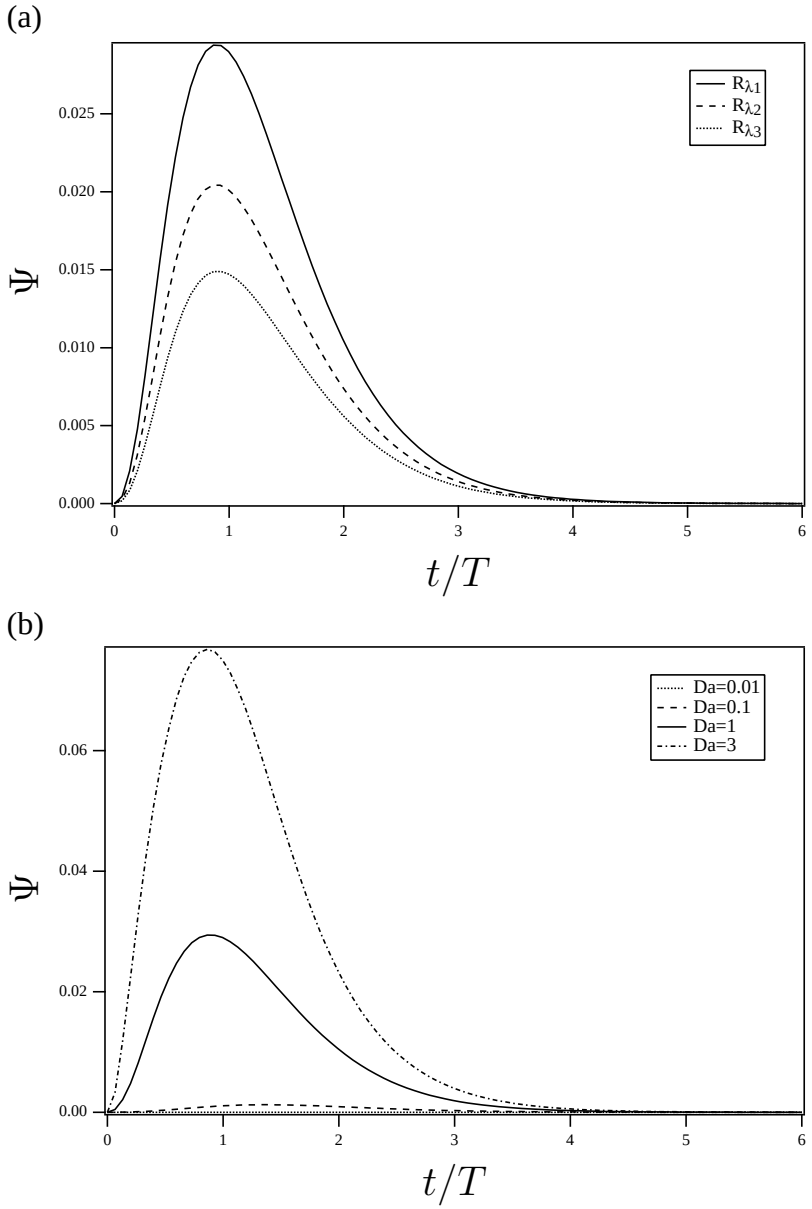

Figure 2.8: Evolution of $\Psi \equiv \langle \phi'_A \phi'_C \rangle_{\text{Case 5}} - \langle \phi'_A \phi'_C \rangle_{\text{Case 1}}$ at: (a) $Da = 1$ and the indicated Reynolds number (note that $Da_\eta = 1/23$, $1/38$ and $1/45$ for $R_{\lambda 1}$, $R_{\lambda 2}$ and $R_{\lambda 3}$, respectively); and (b) $R_{\lambda 1}$ and the indicated Damköhler number (note that $Da_\eta = 0.01/23$, $0.1/23$, $1/23$ and $3/23$ for $Da = 0.01$, 0.1, 1 and 3, respectively).

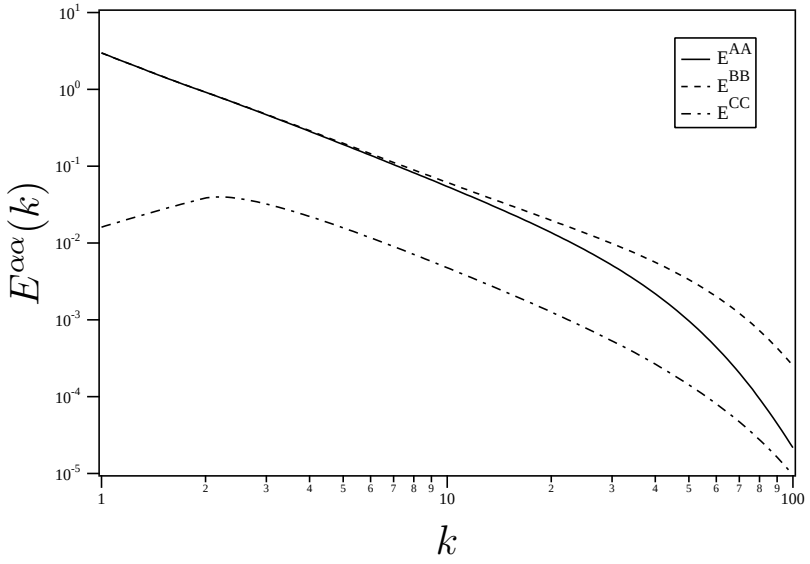

Figure 2.9: Autocorrelation spectra for Case 2 with $Da = 1$ ($Da_\eta = 1/23$) and $R_{\lambda 1}$ at time $t/T = 0.25$. The solid line is $E^{AA}(k)$, the dashed line is $E^{BB}(k)$, and the dash-dotted line is $E^{CC}(k)$.

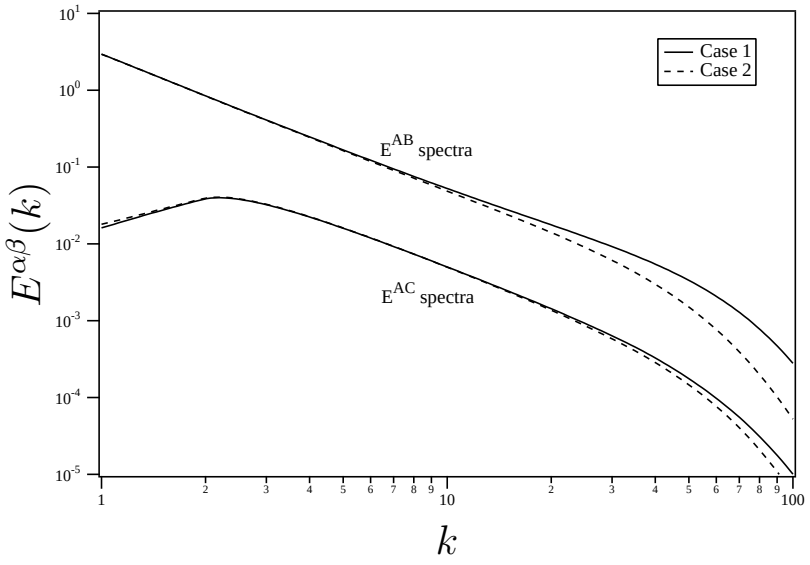

Figure 2.10: Cross correlation spectra for Cases 1 and 2 with $Da = 1$ ($Da_\eta = 1/23$) and $R_{\lambda 1}$ at time $t/T = 0.25$. The solid lines are for Case 1 and the dashed lines are for Case 2.

associated with the peak in the spectrum k_0. Notice that the peak in the spectrum moves to lower wavnumbers with time. This inverse cascade suggests the integral length scale of the autocorrelation of the product species is increasing with time due to the mixing by the turbulent eddies. As the EDQNM model is a non-local spectral model, it is able to capture all of these dynamics well.

2.5 Conclusions

In this paper, we have developed a spectral closure for scalars undergoing an isothermal bimolecular reaction in a homogeneous, isotropic turbulent flow. The model uses EDQNM theory to close the nonlinear turbulent transport terms and the reaction terms. Since EDQNM is a non-local model that inherently represents all of the scales present in a turbulent reacting system, it has the distinct advantage of describing the inter-scale dynamics of mixing, and is capable of capturing differential diffusion. The new model presented here also is able to capture the scales of the product species as they initially are formed in the gaps between the reactant species and as they mix outward. And since reaction is a complicated multi-scale phenomenon, the flexibility of the EDQNM model to represent all of the scales involved in the mixing and reaction process gives it certain advantages over single-point mixing models.

We made comparisons of the EDQNM model with DNS of two scalars that were initially nearly unmixed. The mean concentrations of both the reactant and product species were in excellent agreement with the DNS. Moreover, the EDQNM model was able to predict higher-order statistics such as the scalar cross correlations. Reactant–product cross correlations $\langle \phi'_A \phi'_C \rangle$ and $\langle \phi'_B \phi'_C \rangle$ were in agreement in terms of the magnitude, but the time scale for their variation was not that well predicted. However, the effects of differential

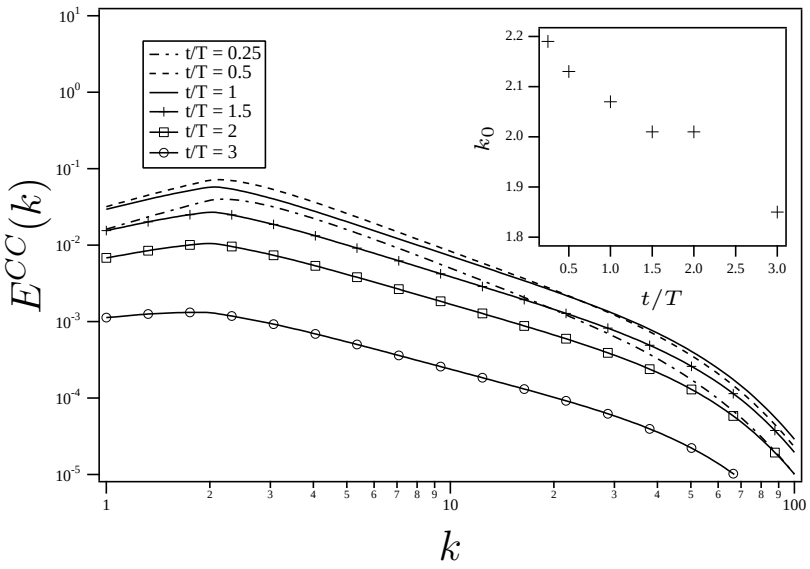

Figure 2.11: Evolution of the *C*–*C* autocorrelation spectrum for Case with $Da = 1$ and $R_{\lambda 1}$ and at the times indicated on the graph. Inset shows the location of the peak in the spectrum k_0 as a function of time. The integral length scale of the scalar is related to the inverse of this quantity.

diffusion, which led to $\langle \phi'_A \phi'_C \rangle > 0$ and $\langle \phi'_B \phi'_C \rangle < 0$, were well captured by the theory, even though we did not adjust any of the constants in the model.

We also did a parametric study of the dependence of differential diffusion on Reynolds number, Schmidt number and Damköhler number. From our calculations, we observed that differential diffusion decreases with increasing Reynolds number. The effect of differential diffusion on the reactant species also decreases with increasing Damköhler number; however, statistics involving the product species showed an increasing trend with increasing Damköhler number. These results are quite consistent with the previous studies. Moreover, they suggest that differential diffusion may be more important with intermediate species under fast chemistry conditions (i.e., high Damköhler number), as is often found in turbulent combustion under practical conditions.

We showed several auto- and cross-correlation spectra for Cases 1 and 2. We observe that differential diffusion, a molecular phenomenon, is initiated at high wavenumbers

and moves to lower wavenumbers through an inverse cascade. Additionally the EDQNM model predicts the product species are formed at a smaller scale than the reactant species. This manifests in the model as a peak in the spectra involving the product species at higher wavenumbers than the reactant-species spectra. Turbulence then causes the peak to move towards lower wavenumbers, as the action of the eddies progressively mixes the product species throughout the domain. The EDQNM spectral transport model is able to capture these complex dynamics without adjustment of any of the parameters.

This paper is a step towards a multi-scale mixing model we are developing. Here we have focused on a simple reaction (isothermal, bimolecular reaction) because it allowed us to implement the EDQNM model without introducing further approximations (since the nonlinearities are quadratic). Eventually we plan to relax this restriction, but our approach is systematic. We can use the present model to analyze the spectral distribution of the reaction term. This will prove invaluable in developing the closure for the more general source term.

Acknowledgments

This work was supported by the National Science Foundation under grant CTS-0121573.

APPENDIX

General Equations for $\mathbf{C}(\mathbf{k},\mathbf{p},\mathbf{q})$

The equations for the 3rd-order moments due to reaction are summarized as below:

$$\left[\frac{d}{dt}+\lambda_C+2\tilde{k}\langle\phi_B\rangle+\tilde{k}\langle\phi_A\rangle\right]C^{AAB}_{\mathbf{kpq}} = \mathcal{C}^{AAB}_{\mathbf{kpq}}-\tilde{k}\langle\phi_B\rangle C^{AAA}_{\mathbf{kpq}}-\tilde{k}\langle\phi_A\rangle(C^{ABB}_{\mathbf{kpq}}+C^{ABB}_{\mathbf{pkq}}) \quad (2.41)$$

$$\left[\frac{d}{dt}+\lambda_C+2\tilde{k}\langle\phi_A\rangle+\tilde{k}\langle\phi_B\rangle\right]C^{ABB}_{\mathbf{kpq}} = \mathcal{C}^{ABB}_{\mathbf{kpq}}-\tilde{k}\langle\phi_A\rangle C^{BBB}_{\mathbf{kpq}}-\tilde{k}\langle\phi_B\rangle(C^{AAB}_{\mathbf{kpq}}+C^{AAB}_{\mathbf{kqp}}) \quad (2.42)$$

$$\left[\frac{d}{dt}+\lambda_C+3\tilde{k}\langle\phi_B\rangle\right]C^{AAA}_{\mathbf{kpq}} = \mathcal{C}^{AAA}_{\mathbf{kpq}}-\tilde{k}\langle\phi_A\rangle C^{AAB}_{\mathbf{kpq}}-\tilde{k}\langle\phi_A\rangle(C^{AAB}_{\mathbf{pqk}}+C^{AAB}_{\mathbf{kqp}}), \quad (2.43)$$

$$\left[\frac{d}{dt}+\lambda_C+3\tilde{k}\langle\phi_A\rangle\right]C^{BBB}_{\mathbf{kpq}} = \mathcal{C}^{BBB}_{\mathbf{kpq}}-\tilde{k}\langle\phi_B\rangle C^{ABB}_{\mathbf{kpq}}-\tilde{k}\langle\phi_B\rangle(C^{ABB}_{\mathbf{pqk}}+C^{ABB}_{\mathbf{qkp}}), \quad (2.44)$$

$$\begin{aligned}\left[\frac{d}{dt}+\lambda_C+\tilde{k}\langle\phi_A\rangle+\tilde{k}\langle\phi_B\rangle\right](C^{ABC}_{\mathbf{pqk}}+C^{ABC}_{\mathbf{qpk}}) &= \mathcal{C}^{ABC}_{\mathbf{pqk}}+\mathcal{C}^{ABC}_{\mathbf{qpk}}-2\tilde{k}\langle\phi_B\rangle C^{AAC}_{\mathbf{pqk}}-2\tilde{k}\langle\phi_A\rangle C^{BBC}_{\mathbf{pqk}}\\ &+ \tilde{k}\langle\phi_B\rangle(C^{AAB}_{\mathbf{pkq}}+C^{AAB}_{\mathbf{qkp}})\\ &+ \tilde{k}\langle\phi_A\rangle(C^{ABB}_{\mathbf{pkq}}+C^{ABB}_{\mathbf{qkp}}), \quad (2.45)\end{aligned}$$

$$\begin{aligned}\left[\frac{d}{dt}+\lambda_C+2\tilde{k}\langle\phi_B\rangle\right]C^{AAC}_{\mathbf{pqk}} &= \mathcal{C}^{AAC}_{\mathbf{pqk}}-\tilde{k}\langle\phi_A\rangle(C^{ABC}_{\mathbf{pqk}}+C^{ABC}_{\mathbf{qpk}})\\ &+ \tilde{k}\langle\phi_A\rangle C^{AAB}_{\mathbf{pqk}}+\tilde{k}\langle\phi_B\rangle C^{AAA}_{\mathbf{kpq}}, \quad (2.46)\end{aligned}$$

$$\begin{aligned}\left[\frac{d}{dt}+\lambda_C+2\tilde{k}\langle\phi_A\rangle\right]C^{BBC}_{\mathbf{pqk}} &= \mathcal{C}^{BBC}_{\mathbf{pqk}}-\tilde{k}\langle\phi_B\rangle(C^{ABC}_{\mathbf{pqk}}+C^{ABC}_{\mathbf{qpk}})\\ &+ \tilde{k}\langle\phi_B\rangle C^{ABB}_{\mathbf{kpq}}+\tilde{k}\langle\phi_A\rangle C^{BBB}_{\mathbf{kpq}}. \quad (2.47)\end{aligned}$$

REFERENCES

[1] J. C. André and M. Lesieur. Influence of helicity on the evolution of isotropic turbulence at high reynolds number. *J. Fluid Mech.*, 81:187, 1977.

[2] R. Bellman. *Introduction to Matrix Analysis*. McGraw Hill, New York, 1960.

[3] R. B. Bird, W. E. Stewart, and E. N. Lightfoot. *Transport Phenomena*. John Wiley & Sons, Inc., New York, 1960.

[4] M. Chakrabarti, R. M. Kerr, and J. C. Hill. Direct numerical simulation of chemical selectivity in homogeneous turbulence. *AIChE J.*, 41:2356, 1995.

[5] S. Corrsin. On the spectrum of isotropic temperature fluctuations in isotropic turbulence. *J. Appl. Phys.*, 22:469, 1951.

[6] V. Eswaran and S. B. Pope. Direct numerical simulations of the turbulent mixing of a passive scalar. *Phys. Fluids*, 31:506, 1987.

[7] V. Eswaran and S. B. Pope. An examination of forcing in direct numerical simulations of turbulence. *Comput. Fluids*, 16:257, 1988.

[8] F. Gao. An analytical solution for the scalar probability density function in homogeneous turbulence. *Phys. Fluids A,* 3:511, 1991.

[9] S. Herr, L.-P. Wang, and L. R. Collins. Edqnm model of a passive scalar with a uniform mean gradient. *Phys. Fluids*, 8:1588, 1996.

[10] J. R. Herring, D. Schertzer, M. Lesieur, G. R. Newman, and J. P. Chollet. A comparitive assessment of spectral closures as applied to passive scalar diffusion. *J. Fluid Mech.*, 124:411, 1982.

[11] F. A. Jaberi, R. S. Miller, F. Mashayek, and P. Givi. Differential diffusion in binary scalar mixing and reaction. *Combust. Flame*, 109:561, 1997.

[12] A. R. Kerstein, M. A. Cremer, and P. A. McMurtry. Scaling properties of differential molecular effects in turbulence. *Phys. Fluids*, 7:1999, 1995.

[13] A. N. Kolmogorov. The local structure of turbulence in an incompressible viscous fluid for very large reynolds numbers. *Dokl. Akad. Nauk. SSSR*, 30:299, 1941.

[14] A. Kurgonov and E. Tadmor. New high-resolution central schemes for nonlinear conservation laws and convection-diffusion equations. *J. Comput. Phys.*, 160:241, 2000.

[15] A. D. Leonard and J. C. Hill. Scalar dissipation and mixing in turbulent reacting flows. *Phys. Fluids A*, 3:1286, 1991.

[16] M. Lesieur. *Turbulence in Fluids, Stochastic and Numerical Modeling*. M. Nijhoff, Boston, 1987.

[17] M. Lesieur and J. Herring. Diffusion of a passive scalar in two-dimensional turbulence. *J. Fluid Mech.*, 161:77, 1985.

[18] G. Li and M. F. Modest. Investigation of turbulence-radiation interactions in reacting flows using a hybrid fv/pdf monte carlo method. *J. Quantitative Spectroscopy and Radiative Transfer*, 73:461, 2002.

[19] S. Mazumder and M. F. Modest. A probability density function approach to modeling turbulence-radiation interactions in nonluminous flames. *Int. J. Heat and Mass Trans*, 42:971, 1998.

[20] P. A. McMurtry and P. Givi. Direct numerical simulations of mixing and reaction in a nonpremixed homogeneous turbulent flow. *Combust. Flame*, 77:171, 1989.

[21] N. Nakauchi. An application of the modified zero-fourth-cumulant approximation to homogeneous axisymmetric turbulance. *J. Phy. Soc. Japan*, 53:1682, 1984.

[22] N. Nakauchi. The return of strongly anisotropic turbulence to isotropy. *Phys. Fluids*, 30:3653, 1987.

[23] N. Nakauchi and S. Sega. The homogeneous axisymmetric passive scalar in isotropic turbulence. *Phys. Fluids*, 30:337, 1987.

[24] N. Nakauchi, H. Oshima, and Y. Saito. A passive scalar convected by homogeneous axisymmetric turbulence. *Phys. Fluids A*, 1:723, 1989.

[25] V. Nilsen and G. Kosály. Differential diffusion in turbulent reacting flows. *Combust. Flame*, 117:493, 1999.

[26] A. M. Obukhov. Structure of the temperature field in turbulent flows. *Izv. Akad. Nauk SSSR Geogmagn and Geophys. Ser.*, 13:58, 1949.

[27] S. A. Orszag. Analytical theories of turbulence. *J. Fluid Mech.*, 41:363, 1970.

[28] S. B. Pope. Pdf methods for turbulent reactive flows. *Prog. Energy Combust. Sci.*, 11:119, 1985.

[29] S. B. Pope. *Turbulent FLows*. Cambridge University Press, New York, 2000.

[30] A. Pouquet, M. Lesieur, J. C. Andre, and C. Basdevant. Evolution of high reynolds number two-dimensional turbulence. *J. Fluid Mech.*, 72:305, 1975.

[31] K. R. Sreenivasan. On local isotropy of passive scalar in turbulent shear flows. *Proc. R. Soc. London Ser. A*, 434:165, 1991.

[32] M. Ulitsky and L. R. Collins. Application of the eddy damped quasi-normal markovian spectral transport theory to premixed turbulent flame propagation. *Phys. Fluids*, 9:3410, 1997.

[33] M. Ulitsky and L. R. Collins. On constructing realizable, conservative mixed scalar equations using the eddy damped quasi-normal markovian theory. *J. Fluid Mech.*, 412:303, 2000.

[34] M. Ulitsky, C. Ghenaʹi, I. Gʹookalp, L.-P. Wang, and L. R. Collins. A comparison of a spectral edqnm model for premixed turbulent flame propagation to dns and experiments. *Combust. Theory and Modelling*, 4:241, 2000.

[35] M. Ulitsky, T. Vaithianathan, and L. R. Collins. A spectral study of differential diffusion of passive scalars in isotropic turbulence. *J. Fluid Mech.*, 460:1, 2002.

[36] T. Vaithianathan and L. R. Collins. Numerical approach to simulating turbulent flow of a viscoelastic polymer solution. *J. Comput. Phys.*, 187:1, 2003.

[37] T. Vaithianathan, M. Ulitsky, and L. R. Collins. Comparison between a spectral and pdf model for turbulent reacting flows. *Proc. Combust. Inst*, pages 2139–2146, 2002.

CHAPTER 3

STOCHASTIC SHELL MODEL FOR TURBULENT MIXING OF MULTIPLE SCALARS WITH MEAN GRADIENTS AND DIFFERENTIAL DIFFUSION*

Abstract In this paper, we develop a shell model for the velocity and scalar concentrations that, by design, is consistent with the eddy damped quasi-normal Markovian (EDQNM) model for multiple mixing scalars. We review the realizable form of the EDQNM model derived by Ulitsky & Collins (2000), which forms the basis for the shell model. The equations governing the velocity and scalar within each shell are stochastic ordinary differential equations with drift and diffusion terms chosen so that the velocity variance, velocity–scalar cross correlations, and scalar–scalar cross correlations within each shell precisely match the EDQNM model predictions. Consequently, shell averages can be thought of as a representation of the discrete three-dimensional spectrum. An advantage the shell model has over the original EDQNM equations is that the sum of each realization over the shells is a model for the fine-grained, joint velocity/scalar probability density function (PDF). Indeed, this provides some of the motivation for the development of the model. We cannot exploit this feature in the present study of the mixing of two scalars with uniform mean gradients, as the PDF is a joint Gaussian throughout (and hence the correlation matrix completely defines the distribution). The model is capable of predicting Lagrangian correlation functions for the scalar, scalar dissipation and velocity. We find the predictions of the model are in good qualitative agreement with direct numerical simulations by Yeung (2001). Eventually we will apply the shell model to scalars that are initially highly non-Gaussian (e.g., double delta function) and observe the relaxation towards a Gaussian. As the shell model contains information on the spectral distribution of the scalar field, the relaxation rate will depend upon the length and time scales of the tur-

*Originally published as: Y. Xia, T. Vaithianathan and L. Collins, *Flow, Turbulence and Combustion*, (2010). The format is adapted to meet the requirement of this thesis.

bulence and the scalar fields, as well as the molecular diffusivities of the species. The full capabilities of the PDF predictions of the model will be the subject of a future publication.

3.1 Introduction

Probability density function (PDF) methods are widely used for the computational modeling of turbulent flames[16,17,26,34,36] and other chemically reactive systems[11]. In the composition PDF method, the local temperature and species concentrations are replaced by a high-dimensional joint PDF that describes the local distribution of thermochemical states of the fluid. The PDF has the great advantage of rendering closed all single-point moments of the temperature and composition such as the chemical source terms and radiation emission[28,29], independent of their complexity. However, as the PDF contains only single-point information, the molecular mixing term, which involves two-point information, must be modeled. For example, the evolution of the scalar PDF, $P(c,t)$, in homogeneous turbulence is governed by

$$\frac{\partial P(c,t)}{\partial t} + \frac{1}{2}\frac{\partial^2}{\partial c^2}\left[\chi(c,t)P(c,t)\right] = 0 \ , \tag{3.1}$$

where $\chi(c,t) \equiv \langle 2\mathcal{D}\nabla\phi\cdot\nabla\phi|\phi = c\rangle$ is the average scalar dissipation rate conditioned on the scalar concentration, a quantity that cannot be computed from the scalar PDF and hence must be modeled.

Developing an accurate closure for the mixing term in the PDF equation is critical, as even the qualitative shape of the PDF is sensitive to this modeling. Hence, the reliability of the model to predict even the closed chemical source terms rests heavily on the quality of the mixing model. This is especially true when modeling flames near blow-out conditions (e.g., flames that are either chemically rich or lean, or stoichiometric flames at high gas velocities), where local fluctuations in the mixing can profoundly affect the reaction rate[39].

Subramaniam & Pope[43] (see also Pope[37]) identified eight features of an ideal mixing model: (i) mean scalar concentrations are not directly affected by mixing; (ii) mixing causes the monotonic decrease of the eigenvalues of the covariance matrix $\langle \phi_i' \phi_j' \rangle$, where ϕ_i' is the fluctuation in the concentration of the i^{th} species, and i and j run over all N species in the system; (iii) all scalars should satisfy bounds imposed by initial and boundary conditions; (iv) the model should satisfy the invariance properties of linearity and independence; (v) the joint composition PDF should relax towards a joint normal at long times; (vi) the model should account for differential diffusion resulting from differences in the scalar molecular diffusivities; (vii) the model should account for the influence of the length scales of the scalar fields; and (viii) the model should account for the influence of reaction on mixing. A mixing model that satisfies all eight criteria has yet to be developed, although several satisfy different subsets of these criteria. One important example is the interaction by exchange with the mean (IEM) model developed by Dopazo[5], which has been used widely in PDF calculations. IEM assumes that the rate of mixing is controlled by the integral time scale of the turbulence, which is usually represented by q^2/ε, where q^2 is the kinetic energy of the turbulence and ε is the turbulent kinetic energy dissipation rate. IEM satisfies criteria (i)–(iv); however, it cannot predict the changes in the shape of the PDF in homogeneous turbulence. Furthermore, the assumption that the mechanical-to-scalar time-scale ratio is constant is known to not be valid when the integral length scale of the scalar is different than that of the energy[6,22,49]. Indeed, our earlier study[47] showed that predictions for the rate of mixing of the product species based on this assumption can result in errors greater than an order of magnitude at high Damköhler numbers.

The problems with the IEM model can be traced to the lack of information about the spectrum of length and time scales of the turbulence and scalars. A partial remedy is found by considering the joint PDF for the scalar and scalar gradient, $P(c, \nabla c)$. The equation for this PDF requires statistics for higher-order derivatives that must be closed.

Meyers & O'Brien[30] closed this equation by replacing the unclosed term by one that relaxes the scalar to its mean. However, the solution to this equation did not correctly represent the evolution of the scalar PDF from a non-Gaussian initial condition. Gao & O'Brien[14] analyzed some of the properties of the joint PDF and showed that the PDF of scalar gradient conditioned on the scalar is nearly Gaussian, motivating them to use a Gram-Charlier expansion for $P(\nabla c|c)$ with coefficients found from DNS.

Alternatively, the conditional dissipation rate $\chi(c,t)$ can be expressed in terms of a two-point PDF, $P(c(\boldsymbol{x}_1),c(\boldsymbol{x}_2))$. Kuo & O'Brien[25] investigated the closure of this equation for a stochastically distributed reactant undergoing self-diffusion and a nonlinear reaction employing Ievlev's closure[21]. Apart from reproducing many desirable properties such as coincidence, separation and reduction of the two-point PDF into a single-point PDF, they showed that the equation for the two-point PDF yielded the correct initial evolution of the single-point PDF. However, there has been no investigation of how turbulence, which modifies the scalar gradients, affects the efficacy of Ievlev's closure.

Fox & Yeung[12] developed a hybrid strategy that combined the Lagrangian spectral relaxation (LSR) model for the mean scalar spectrum[9,10] with a Fokker–Planck equation for the PDF[7,8]. The LSR model was used to account for the effect of changes in the spectral distribution of scalar on the scalar dissipation rate. The model captured several Eulerian and Lagrangian statistics in good accord with DNS for a decaying, Gaussian scalar; however, the extension of the modeling to non-Gaussian fields requires further closure assumptions for the conditional scalar dissipation rate. Furthermore, as the LSR model is strictly a local closure to the spectral evolution equation, it does not inherently capture differential diffusion, which aries due to differences in the molecular diffusivities of the scalars[40,42,51]. The model brings in these effects empirically by introducing model coefficients that are explicit functions of the Reynolds number and of all the Schmidt numbers[10]. This enables

the spectral model to capture some of the effects of differential diffusion, but in order to bring that capability into the PDF model, the stochastic differential equations that govern the evolution of the PDF would have to be multi-scale, an extension they are planning for the future.

We adopt a "shell-model" approach, in which each realization of the velocity and scalar concentrations are decomposed into wavenumber bands or shells. The evolution of the velocity and scalar within each shell, for each realization, is governed by a stochastic differential equation. Averages within a particular shell then can be thought of as loosely defining a spectrum for the energy or scalar fluctuations. The approach has a long history dating back to the so-called GOY model developed by Gledzer[15] and Ohkitani & Yamada[32]. The reader is referred to the excellent review by Biferale[2] for more information on how shell models have been used to analyze the multifractal energy cascade and small scale intermittency. In our approach, the ODEs for the shell model are stochastic differential equations that are derived to satisfy the eddy damped quasi-normal Markovian (EDQNM) theory[27,33]. EDQNM is computationally the least expensive of the family of two-point statistical closures with nonlocal interactions (e.g., direct interaction approximation[24]). It has been shown to predict the energy spectrum[1] and scalar transport well[18,20,31,48], including small-scale phenomena such as differential diffusion[44,45] without introducing additional modeling assumptions. Hybrid approaches that couple EDQNM to the mapping closure[4,35] have yielded some success[13]. Here we formulate a Langevin equation for each shell that produces statistics consistent with the EDQNM equation. The approach is based on the one used by Ulitsky & Collins[44], but is extended to the case of scalars with mean gradients. It is somewhat reminiscent of the large-eddy-simulation closure developed by She & Jackson[41], in which they modeled the 'implicit' (missing) modes in spectral space as a linear damping of the 'explicit' (resolved) modes, such that the rate of removal of energy from a particular mode is proportional to the energy in that

mode. However, their model discretizes the three-dimensional wavevector space, whereas we are performing a much more severe truncation to wavenumber shells in order to gain the efficiency required for a general purpose mixing model.

The goal of this paper is to present the derivation of the stochastic shell model and verify its consistency with the EDQNM theory. Additionally, we show how the model will be used to determine the evolution of the joint scalar PDF, although we leave the full exploration of this aspect of the model to a future publication. The paper is organized as follows. The governing equations for the velocity and scalar, as well as the EDQNM closure for the relevant spectra are summarized in §3.2. The stochastic shell model is then developed in §3.3. Comparisons between the EDQNM and shell model predictions are given in §3.4 followed by a discussion of Lagrangian statistics predicted by the model in §3.5 and conclusions in §3.6.

3.2 Governing Equations and Summary of EDQNM Models

3.2.1 Governing Equations

Assuming constant molecular properties, the governing equations for each scalar and for velocity field are as follows

$$\frac{\partial u_i}{\partial x_i} = 0 \,, \tag{3.2}$$

$$\frac{\partial u_i}{\partial t} + u_j \frac{\partial u_i}{\partial x_j} + \frac{1}{\rho}\frac{\partial p}{\partial x_i} = \nu \frac{\partial^2 u_i}{\partial x_j^2} \,, \tag{3.3}$$

$$\frac{\partial \phi_\alpha}{\partial t} + u_i \frac{\partial \phi_\alpha}{\partial x_i} = \mathcal{D}_\alpha \frac{\partial^2 \phi_\alpha}{\partial x_i^2} \,, \tag{3.4}$$

where u_i is fluctuating velocity, p is pressure, ρ is fluid density, ν is kinematic viscosity, $\phi_\alpha(\mathbf{x},t)$ is concentration of scalar α, and $\mathcal{D}_\alpha$ is the molecular diffusivity of species α

relative to the solvent species. Note that Greek letters signify arbitrary species, and hence the summation convention does not apply to them. In this study, we will consider the mixing of two scalars, labeled A and B (corresponding to $\alpha = A$ and $\alpha = B$); however, the method can be generalized to an arbitrary number of scalars.

For the sake of simplicity, we align the scalar mean gradients with the x_3 direction. Although under this circumstance the correlations involving the scalar fields are no longer isotropic, they remain homogeneous. Introducing the Reynolds decomposition: $\phi'_\alpha = \phi_\alpha - \langle\phi_\alpha\rangle$ (we assume the mean velocity $\langle u_i\rangle = 0$ without loss of generality), we can derive the equations governing the mean and fluctuating scalar fields

$$\frac{\partial\langle\phi_\alpha\rangle}{\partial t} = 0\,, \tag{3.5}$$

$$\frac{\partial\phi'_\alpha}{\partial t} + \frac{\partial(u_i\phi'_\alpha)}{\partial x_i} = \mathcal{D}_\alpha\frac{\partial^2\phi'_\alpha}{\partial x_i^2} - u_3\Gamma_\alpha\,, \tag{3.6}$$

where $\Gamma_\alpha = d\langle\phi_\alpha\rangle/dx_3$ is the constant mean gradient of species α.

For completeness, we provide a summary of the EDQNM equations for the energy spectrum, velocity-scalar cross correlation spectrum, and the scalar-scalar spectrum.

3.2.2 EDQNM Model for Energy Spectrum

The energy spectrum is derived from the two-point Reynolds stress $R_{ij}(\boldsymbol{x}_1,\boldsymbol{x}_2) = \langle u_i(\boldsymbol{x}_1)u_j(\boldsymbol{x}_2)\rangle$. The reciprocal Fourier transform relations for the Reynolds stress are[27]

$$R_{ij}(\boldsymbol{k},\boldsymbol{p}) = \int\int R_{ij}(\boldsymbol{x}_1,\boldsymbol{x}_2)e^{-i(\boldsymbol{k}\cdot\boldsymbol{x}_1+\boldsymbol{p}\cdot\boldsymbol{x}_2)}d\boldsymbol{x}_1 d\boldsymbol{x}_2\,, \tag{3.7}$$

$$R_{ij}(\boldsymbol{x}_1,\boldsymbol{x}_2) = \int\int R_{ij}(\boldsymbol{k},\boldsymbol{p})e^{i(\boldsymbol{k}\cdot\boldsymbol{x}_1+\boldsymbol{p}\cdot\boldsymbol{x}_2)}d\hat{\boldsymbol{k}}d\hat{\boldsymbol{p}}\,, \tag{3.8}$$

where $d\hat{\boldsymbol{k}} = d\boldsymbol{k}/(2\pi)^3$, and $d\hat{\boldsymbol{p}}$ is defined by analogy. (Note that we have suppressed the explicit dependence of all correlations on time to simplify the nomenclature.) We assume

the velocity statistics are isotropic, and further neglect the effect of helicity, allowing us to reduce the two-point Reynolds stress to

$$R_{ij}(\boldsymbol{k},\boldsymbol{p}) = R(k)P_{ij}(\boldsymbol{k})\hat{\delta}(\boldsymbol{k}+\boldsymbol{p}) \,, \tag{3.9}$$

where the projection operator $P_{ij}(\boldsymbol{k}) = \delta_{ij} - k_i k_j/k^2$, $\hat{\delta}(\boldsymbol{k}+\boldsymbol{p}) = (2\pi)^3\delta(\boldsymbol{k}+\boldsymbol{p})$, $\delta(\boldsymbol{k}+\boldsymbol{p})$ is the three-dimensional Dirac delta function and δ_{ij} is the Kronecker delta function. The turbulence intensity, u', is related to $R(k)$ by

$$\frac{3}{2}u'^2 = \int_0^\infty \frac{k^2 R(k)}{2\pi^2}dk = \int_0^\infty E_u(k)dk \,, \tag{3.10}$$

where $E_u(k) = k^2R(k)/(2\pi^2)$ is the turbulent energy spectrum.

The EDQNM model transport equation for $E_u(k)$ can be written as follows[27]

$$\left[\frac{\partial}{\partial t} + 2\lambda_u(k)\right] E_u(k) = T_u(k) \,, \tag{3.11}$$

where

$$\begin{aligned}
T_u(k) &= \int\int_{\triangle} \Theta_R^{kpq} V_1 E_u(p) E_u(q) dpdq \,, && (3.12)\\
\lambda_u(k) &= \nu k^2 + \frac{1}{2}\int\int_{\triangle} \Theta_R^{kpq} V_2 \, E_u(q) dpdq \,, && (3.13)\\
V_1 &= \frac{3k^2}{2q}(xy - z^3) \,, && (3.14)\\
V_2 &= \frac{3p^2}{2q}(xy - z^3) \,, && (3.15)\\
\Theta_R^{kpq} &= \frac{1}{\mu_R^{kpq}} \,, && (3.16)\\
\mu_R^{kpq} &= c_1(\mu_k + \mu_p + \mu_q) + \nu(k^2 + p^2 + q^2) \,, && (3.17)
\end{aligned}$$

the constant $c_1 = 0.36$ to ensure that at infinite Reynolds number the energy spectrum obeys the Kolmogorov inertial range scaling[1], and the frequency μ_k is defined as[38]

$$\mu_k = \frac{1}{\sqrt{2}\pi}\sqrt{\int_0^k k'^4 R(k')dk'} \,. \tag{3.18}$$

The wave vectors $\boldsymbol{k}, \boldsymbol{p}$ and $\boldsymbol{q}$ compose a closed triad (i.e., $\boldsymbol{k}+\boldsymbol{p}+\boldsymbol{q}=\boldsymbol{0}$), and the coefficients x, y and z denote the cosines of its interior angles.

$$x = \frac{\boldsymbol{p}\cdot\boldsymbol{q}}{pq} = \frac{k^2-p^2-q^2}{2pq}\,, \tag{3.19}$$

$$y = \frac{\boldsymbol{k}\cdot\boldsymbol{q}}{kq} = \frac{p^2-k^2-q^2}{2kq}\,, \tag{3.20}$$

$$z = \frac{\boldsymbol{k}\cdot\boldsymbol{p}}{kp} = \frac{q^2-k^2-p^2}{2kp}\,. \tag{3.21}$$

The integrals in Eqs. 3.12 and 3.13 are over all possible closed triads that can be constructed for wave vector $\boldsymbol{k}$.

3.2.3 EDQNM Model for the Scalar-Velocity Cross-Correlation Spectrum

The two-point velocity-scalar cross correlation for species α is defined as $Q_i^\alpha(\boldsymbol{x}_1,\boldsymbol{x}_2) = \langle u_i(\boldsymbol{x}_1)\phi'_\alpha(\boldsymbol{x}_2)\rangle$. The reciprocal Fourier transforms are given by

$$Q_i^\alpha(\boldsymbol{k},\boldsymbol{p}) = \int\int Q_i^\alpha(\boldsymbol{x}_1,\boldsymbol{x}_2)e^{-i(\boldsymbol{k}\cdot\boldsymbol{x}_1+\boldsymbol{p}\cdot\boldsymbol{x}_2)}\,d\boldsymbol{x}_1 d\boldsymbol{x}_2\,, \tag{3.22}$$

$$Q_i^\alpha(\boldsymbol{x}_1,\boldsymbol{x}_2) = \int\int Q_i^\alpha(\boldsymbol{k},\boldsymbol{p})e^{i(\boldsymbol{k}\cdot\boldsymbol{x}_1+\boldsymbol{p}\cdot\boldsymbol{x}_2)}\,d\hat{\boldsymbol{k}}d\hat{\boldsymbol{p}}\,. \tag{3.23}$$

The presence of the mean scalar gradients reduces the symmetry of the scalar fluctuations from isotropic to axisymmetric about the x_3 axis. Thus, the only nonzero component of the cross correlation vector is $Q_3^\alpha(\boldsymbol{x}_1,\boldsymbol{x}_2)$ (and $Q_3^\alpha(\boldsymbol{k},\boldsymbol{p})$). Taking advantage of homogeneity, axisymmetry, and the continuity relationship yields[18]

$$Q_3^\alpha(\boldsymbol{k},\boldsymbol{p}) = Q^\alpha(k)(1-\mu^2)\hat{\delta}(\boldsymbol{k}+\boldsymbol{p})\,, \tag{3.24}$$

where μ is the cosine of the angle between the wave vector $\boldsymbol{k}$ and the direction of the mean gradient, i.e., $\mu = \boldsymbol{k}\cdot\mathbf{e}_3/k$, where $\mathbf{e}_3$ is the unit vector pointing in $\boldsymbol{x}_3$ direction. The single-point scalar flux, defined as $Q_3^\alpha \equiv \langle u_3\phi'_\alpha\rangle$, is related to an integral of the cross correlation

spectrum as follows

$$Q_3^\alpha = \int_0^\infty \frac{k^2}{3\pi^2} Q^\alpha(k)dk = \int_0^\infty E_Q^\alpha(k)dk \,, \tag{3.25}$$

where $E_Q^\alpha(k) \equiv k^2 Q^\alpha(k)/3\pi^2$.

Based on the standard EDQNM closure procedure, Herr et al.[18] derived the following integro-differential equation for $E_Q^\alpha(k)$

$$\left[\frac{\partial}{\partial t} + (\nu + \mathcal{D}_\alpha)k^2\right] E_Q^\alpha(k) = -\Gamma_\alpha E_u(k) + T_Q^\alpha(k) \tag{3.26}$$

where

$$\begin{aligned} T_Q^\alpha(k) = \int\int_\triangle dpdq \times \\ \Theta_T^{kpq}\Big\{ -\Theta_R^{kqp}\,\Gamma_\alpha\, [H_1 E_u(k)E_u(p) + H_2 E_u(k)E_u(q) + H_3 E_u(p)E_u(q)] \\ + H_4 E_u(p)E_Q^\alpha(k) + H_5 E_u(k)E_Q^\alpha(q) + H_6 E_u(p)E_Q^\alpha(q) + H_7 E_u(k)E_Q^\alpha(p)\Big\} \\ + \frac{1}{2}\Theta_T^{qpk}\Big\{ -\Theta_R^{qkp}\Gamma_\alpha\,[J_1 E_u(k)E_u(p) + J_2 E_u(k)E_u(q) + J_3 E_u(p)E_u(q)] \\ + J_4 E_u(q)E_Q^\alpha(k) + J_5 E_u(p)E_Q^\alpha(q) + J_6 E_u(q)E_Q^\alpha(p) + J_7 E_u(p)E_Q^\alpha(k)\Big\} \end{aligned} \tag{3.27}$$

$$\Theta_T^{kpq} = \frac{1 - e^{-\mu_T^{kpq} t}}{\mu_T^{kpq}} \,, \tag{3.28}$$

$$\mu_T^{kpq} = c_2(\mu_k + \mu_p) + c_3\mu_q + \nu(k^2 + p^2 + q^2) \,, \tag{3.29}$$

with the coefficients $c_2 = 0$ and $c_3 = 1.03$. The dependence on the angle μ cancels out of the equation. The definitions of the geometric factors H_1–H_7 and J_1–J_7 are summarized in Table 3.1[18].

Table 3.1: This table lists the definitions of the coefficients for the $Q^{\alpha}(k)$ equation. Here x, y and z are the cosines of angles between the wave vectors $\boldsymbol{k}$, $\boldsymbol{p}$ and $\boldsymbol{q}$, which forms a closed triad (see Eq. (3.21)), and N is twice the area of the triad, given by $N^2 = \frac{1}{4}(k+p+q)(k+p-q)(k+q-p)(p+q-k)$.

Name	Expression	Name	Expression
H_1	$\frac{3N^2}{8}\frac{q}{pk}\left(\frac{xy}{kp}-\frac{1+y^2}{p^2}\right)$	J_1	$\frac{3N^2}{8}\frac{1}{p^2}\left(-\frac{2q}{kp}-\frac{2yp}{k^2}\right)$
H_2	$\frac{3N^2}{8}\frac{p}{kq}\left(\frac{yz}{pq}-\frac{xy}{kp}\right)$	J_2	$\frac{3N^2}{8}\frac{1}{q^2}\left(-\frac{2p}{kq}-\frac{2zq}{k^2}\right)$
H_3	$\frac{3N^2}{8}\frac{k}{pq}\left(\frac{1+y^2}{p^2}-\frac{yz}{pq}\right)$	J_3	$\frac{3N^2}{8}\frac{k}{pq}\left(\frac{1+y^2}{p^2}+\frac{1+z^2}{q^2}-2\frac{yz}{pq}\right)$
H_4	$-\frac{3N^2q}{4p^3k}$	J_4	$\frac{3N^2}{8}\frac{1}{q^2}\left(-\frac{2p}{kq}-\frac{2zq}{k^2}\right)$
H_5	$\frac{3N^2}{8}\frac{p}{kq}\left(\frac{yz}{pq}-\frac{xy}{kp}\right)$	J_5	$\frac{3N^2}{8}\frac{k}{pq}\left(\frac{1+y^2}{p^2}-\frac{yz}{pq}\right)$
H_6	$\frac{3N^2}{8}\frac{k}{pq}\left(\frac{1+y^2}{p^2}-\frac{yz}{pq}\right)$	J_6	$\frac{3N^2}{8}\frac{k}{pq}\left(\frac{1+z^2}{q^2}-\frac{yz}{pq}\right)$
H_7	$\frac{3N^2}{8}\frac{qz}{p^2k}$	J_7	$\frac{3N^2}{8}\frac{1}{p^2}\left(-\frac{2q}{kp}-\frac{2yp}{k^2}\right)$

3.2.4 EDQNM Model for the Scalar-Scalar Correlation Spectrum

The scalar auto- and cross-correlation can be written generically as $B^{\alpha\beta}(\boldsymbol{x}_1,\boldsymbol{x}_2) = \langle\phi'_{\alpha}(\boldsymbol{x}_1)\phi'_{\beta}(\boldsymbol{x}_2)\rangle$, where α and β can represent species A or B, i.e., $B^{\alpha\beta}(\boldsymbol{x}_1,\boldsymbol{x}_2)$ is a representation of $B^{AA}(\boldsymbol{x}_1,\boldsymbol{x}_2)$, $B^{AB}(\boldsymbol{x}_1,\boldsymbol{x}_2) = B^{BA}(\boldsymbol{x}_2,\boldsymbol{x}_1)$ and $B^{BB}(\boldsymbol{x}_1,\boldsymbol{x}_2)$. The reciprocal Fourier transforms are then given by

$$B^{\alpha\beta}(\boldsymbol{k},\boldsymbol{p}) = \int\int B^{\alpha\beta}(\boldsymbol{x}_1,\boldsymbol{x}_2)e^{-i(\boldsymbol{k}\cdot\boldsymbol{x}_1+\boldsymbol{p}\cdot\boldsymbol{x}_2)}\,d\boldsymbol{x}_1 d\boldsymbol{x}_2\,, \tag{3.30}$$

$$B^{\alpha\beta}(\boldsymbol{x}_1,\boldsymbol{x}_2) = \int\int B^{\alpha\beta}(\boldsymbol{k},\boldsymbol{p})e^{i(\boldsymbol{k}\cdot\boldsymbol{x}_1+\boldsymbol{p}\cdot\boldsymbol{x}_2)}\,d\hat{\boldsymbol{k}}d\hat{\boldsymbol{p}}\,. \tag{3.31}$$

Again, homogeneity and axisymmetry leads to the following relation

$$B^{\alpha\beta}(\boldsymbol{k},\boldsymbol{p}) = 2B^{\alpha\beta}(k,\mu)\,\hat{\delta}(\boldsymbol{k}+\boldsymbol{p})\,. \tag{3.32}$$

The scalar correlation $\langle \phi'_\alpha \phi'_\beta \rangle$ is related to $B^{\alpha\beta}(k,\mu)$ by

$$\langle \phi'_\alpha \phi'_\beta \rangle = \frac{1}{2\pi^2} \int_0^\infty \int_{-1}^1 B^{\alpha\beta}(k,\mu) k^2 d\mu dk \,. \tag{3.33}$$

The dependence of $B^{\alpha\beta}(k,\mu)$ on the angle μ can be explicitly represented by a Legendre polynomial series in μ[19], and because $B^{\alpha\beta}(k,\mu)$ is an even function of μ, only the even-order powers of the series are non-zero, which yields

$$B^{\alpha\beta}(k,\mu) = \sum_{i=0}^{\infty} B_{2i}^{\alpha\beta}(k) P_{2i}(\mu) \,. \tag{3.34}$$

As the 4$^{\text{th}}$ and higher-order terms have no source, and are initialized to zero, the infinite series can be formally truncated after the second term

$$B^{\alpha\beta}(k,\mu) = B_0^{\alpha\beta}(k) + \frac{1}{2}(3\mu^2 - 1) B_2^{\alpha\beta}(k) \,. \tag{3.35}$$

The first term accounts for the isotropic spectrum and the second accounts for anisotropy introduced by the mean scalar gradient. Herr et al.[18] found that the anisotropy was driven primarily by the source term, and therefore $B_2^{\alpha\beta}(k) \approx -B_0^{\alpha\beta}(k)$, implying

$$B^{\alpha\beta}(k,\mu) = \frac{3}{2}(1-\mu^2) B_0^{\alpha\beta}(k) \,. \tag{3.36}$$

Thus Eq. (3.33) becomes

$$\langle \phi'_\alpha \phi'_\beta \rangle = \frac{1}{\pi^2} \int_0^\infty B_0^{\alpha\beta}(k) k^2 dk = \int_0^\infty E_B^{\alpha\beta}(k) dk \,, \tag{3.37}$$

where $E_B^{\alpha\beta}(k) \equiv k^2 B_0^{\alpha\beta}(k)/\pi^2$. The final EDQNM equation for $E_B^{\alpha\beta}(k)$ is (see Ref.[44] for details)

$$\left[\frac{\partial}{\partial t} + (\mathcal{D}_\alpha + \mathcal{D}_\beta) k^2 \right] E_B^{\alpha\beta}(k) = -\Gamma_\alpha E_Q^\beta(k) - \Gamma_\beta E_Q^\alpha(k) + T_B^{\alpha\beta}(k) \,, \tag{3.38}$$

where

$$
\begin{aligned}
T_B^{\alpha\beta}(k) = \int\int_{\triangle} dpdq \times \\
&\Theta_M^{pkq;pkq}\Big\{\Theta_R^{pqk}\Gamma_\alpha\Gamma_\beta\left[F_1E_u(k)E_u(p)+F_2E_u(k)E_u(q)+F_3E_u(p)E_u(q)\right] \\
&-\frac{1}{2}\Gamma_\alpha\left[F_4E_u(p)E_Q^\beta(k)+F_5E_u(k)E_Q^\beta(p)+F_6E_u(k)E_Q^\beta(q)+F_7E_u(p)E_Q^\beta(q)\right] \\
&-\frac{1}{2}\Gamma_\beta\left[F_4E_u(p)E_Q^\alpha(k)+F_5E_u(k)E_Q^\alpha(p)+F_6E_u(k)E_Q^\alpha(q)+F_7E_u(p)E_Q^\alpha(q)\right]\Big\} \\
&+\Theta_M^{pkq;pqk}\Big\{\Theta_R^{pkq}\Gamma_\alpha\Gamma_\beta\left[G_1E_u(k)E_u(p)+G_2E_u(k)E_u(q)+G_3E_u(p)E_u(q)\right] \\
&-\frac{1}{2}\Gamma_\beta\left[G_4E_u(p)E_Q^\alpha(k)+G_5E_u(k)E_Q^\alpha(p)+G_6E_u(k)E_Q^\alpha(q)+G_7E_u(p)E_Q^\alpha(q)\right] \\
&-\frac{1}{2}\Gamma_\alpha\left[G_4E_u(p)E_Q^\beta(k)+G_5E_u(k)E_Q^\beta(p)+G_6E_u(k)E_Q^\beta(q)+G_7E_u(p)E_Q^\beta(q)\right]\Big\} \\
&+\Theta_M^{pkq}\Big[M_1E_Q^\alpha(k)E_Q^\beta(p)+M_2E_Q^\alpha(k)E_Q^\beta(q)+M_3E_Q^\alpha(p)E_Q^\beta(q) \\
&+M_4E_u(p)E_B^{\alpha\beta}(k)+M_5E_u(p)E_B^{\alpha\beta}(q)\Big]\ , \qquad (3.39)
\end{aligned}
$$

$$
\Theta_M^{kpq} = \frac{1-e^{-\mu_M^{kpq}t}}{\mu_M^{kpq}}\ , \qquad (3.40)
$$

$$
\Theta_M^{kpq;k'p'q'} = \frac{1}{\mu_T^{k'p'q'}}\begin{cases}\left[\frac{1-e^{-\mu_M^{kpq}t}}{\mu_M^{kpq}}+\frac{e^{-\mu_M^{kpq}t}-e^{-\mu_T^{k'p'q'}t}}{\mu_M^{kpq}-\mu_T^{k'p'q'}}\right], & \mu_M^{kpq}\neq\mu_T^{k'p'q'} \\ \left[\frac{1-e^{-\mu_M^{kpq}t}}{\mu_M^{kpq}}-te^{-\mu_M^{kpq}t}\right], & \mu_M^{kpq}=\mu_T^{k'p'q'}\end{cases}\ , \qquad (3.41)
$$

$$
\mu_M^{kpq} = c_4\mu_k + c_5(\mu_p+\mu_q) + \nu(k^2+p^2+q^2)\ . \qquad (3.42)
$$

The coefficients c_4 and c_5 are set to 0.36, and the other coefficients F_1–F_7, G_1–G_7 and M_1–M_5 are given in Table 3.2.

Table 3.2: Definitions of the coefficients for the $B^{\alpha\beta}(k)$ equation. Here x, y, z and N are defined as in Table 3.1.

Name	Expression	Name	Expression	Name	Expression
F_1	$\frac{3N^2}{4}\frac{q}{kp}\left(\frac{xy}{kp}-\frac{1+y^2}{p^2}\right)$	G_1	$\frac{3N^2}{4}\frac{q}{kp}\left(\frac{xy}{kp}-\frac{1+y^2}{p^2}\right)$	M_1	$\frac{3N^2}{4}\frac{q}{kp}\left(\frac{z}{kp}-\frac{xy}{kp}\right)$
F_2	$\frac{3N^2}{4}\frac{p}{kq}\left(\frac{yz}{pq}-\frac{xy}{kp}\right)$	G_2	$\frac{3N^2}{4}\frac{p}{kq}\left(\frac{yz}{pq}-\frac{xy}{kp}\right)$	M_2	$\frac{3N^2}{4}\frac{p}{kq}\left(\frac{yz}{pq}-\frac{xy}{kp}\right)$
F_3	$\frac{3N^2}{4}\frac{k}{pq}\left(\frac{1+y^2}{p^2}-\frac{yz}{pq}\right)$	G_3	$\frac{3N^2}{4}\frac{k}{pq}\left(\frac{1+y^2}{p^2}-\frac{yz}{pq}\right)$	M_3	$-\frac{3N^2kx}{4p^2q^2}$
F_4	$-\frac{3N^2q}{2p^3k}$	G_4	$\frac{3N^2}{4}\frac{q}{pk}\left(\frac{xy}{kp}-\frac{1+y^2}{p^2}\right)$	M_4	$-\frac{3N^2q}{2p^3k}$
F_5	$\frac{3N^2}{4}\frac{q}{kp}\left(\frac{z}{kp}-\frac{xy}{kp}\right)$	G_5	$\frac{3N^2}{4}\frac{p}{kq}\left(\frac{yz}{pq}-\frac{xy}{kp}\right)$	M_5	$\frac{3N^2k}{2p^3q}$
F_6	$\frac{3N^2}{4}\frac{p}{kq}\left(\frac{yz}{pq}-\frac{xy}{kp}\right)$	G_6	$-\frac{3N^2kx}{4p^2q^2}$		
F_7	$\frac{3N^2}{4}\frac{k}{pq}\left(\frac{1+y^2}{p^2}-\frac{yz}{pq}\right)$	G_7	$\frac{3N^2k}{2p^3q}$		

3.3 'Shell' Model for the Velocity and Scalar Fields

'Shell' models are based on a discrete representation of the three-dimensional wave vector space in concentric spherical shells of radius $k_n = k_0\lambda^{n-1}$, where n is an integer, $n = 1,2,\cdots,N+1$ and λ is the intershell ratio. The wavenumber range of the model is $k_0 \leq k \leq k_0\lambda^N$ with a shell distribution that is logarithmic, which enables the model to span a broad range of scales with a moderate value of N. The discrete form of the EDQNM model can be solved on a logarithmic grid as well (see for example Lesieur[27] for details), providing the necessary inputs to the shell model. In this section, we derive stochastic differential equations (SDEs) for real variables $u_n(t)$ and $\phi_n^\alpha(t)$ ($\alpha = A$ or B), which are the fluctuations associated with shell n. The SDEs are defined such that an ensemble of

realizations of these variables satisfies the following relationships

$$\langle u_n(t)u_m(t)\rangle = \delta_{nm}E_u(k_n,t)\ , \tag{3.43}$$

$$\langle u_n(t)\phi_m^{\alpha}(t)\rangle = \delta_{nm}E_Q^{\alpha}(k_n,t)\ , \tag{3.44}$$

$$\langle \phi_n^{\alpha}(t)\phi_m^{\beta}(t)\rangle = \delta_{nm}E_B^{\alpha\beta}(k_n,t)\ . \tag{3.45}$$

3.3.1 Langevin Equation for the Velocity

The SDE for $u_n(t)$ takes the form of an Ornstein–Uhlenbeck process

$$du_n(t) + \lambda_u(k_n)u_n(t)dt = r_1(k_n)dW_n^{[1]}(t)\ , \tag{3.46}$$

where $dW_n^{[1]}(t)$ is a vector-valued Wiener process increment satisfying independence and the standard time correlation, i.e.,

$$\langle dW_n^{[1]}(t)dW_m^{[1]}(s)\rangle = \delta_{mn}\delta(t-s)dsdt\ .$$

If we multiply Eq. 3.46 by $u_m(t)$ and average based on Ito calculus[23], we can derive the following differential equation

$$\left[\frac{\partial}{\partial t} + 2\lambda_u(k_n)\right]E_u(k_n) = r_1^2(k_n) \tag{3.47}$$

Comparing this equation with the discrete form of Eq. (4.8), we find that for consistency

$$r_1^2(k_n) = T_u(k_n)\ . \tag{3.48}$$

However, Eq. (4.8) reflects a decaying energy spectrum without forcing, while in our study we will consider a statistically stationary turbulent flow. In the stationary case, the time derivative is zero, and hence we can redefine $r_1^2(k_n)$ as follows

$$r_1^2(k_n) = 2\lambda_u(k_n)E_u(k_n)\ , \tag{3.49}$$

with $E_u(k_n)$ being the desired stationary energy spectrum, and $\lambda_u(k_n)$ retains the definition given in Eq. (3.13).

3.3.2 Langevin Equations for the Scalar Fields

We introduce two stochastic equations for the scalar concentrations

$$\begin{aligned} d\phi_n^A(t) + \lambda_\phi^A(k_n)\phi_n^A(t)dt &= -\Gamma_A u_n(t)dt + r_2(k_n)dW_n^{[1]}(t) \\ &\quad + r_3(k_n)dW_n^{[2]}(t) \ , \end{aligned} \tag{3.50}$$

$$\begin{aligned} d\phi_n^B(t) + \lambda_\phi^B(k_n)\phi_n^B(t)dt &= -\Gamma_B u_n(t)dt + r_4(k_n)dW_n^{[1]}(t) \\ &\quad + r_5(k_n)dW_n^{[2]}(t) + r_6(k_n)dW_n^{[3]}(t) \ , \end{aligned} \tag{3.51}$$

where $dW_n^{[1]}(t)$, $dW_n^{[2]}(t)$ and $dW_n^{[3]}(t)$ are independent Wiener process increments (i.e., $\langle dW_n^{[i]}(t)dW_n^{[j]}(s)\rangle = 0$ for $i \neq j$). Relationships for the coefficients $\lambda_\phi^A(k_n)$, $\lambda_\phi^B(k_n)$, and $r_2(k_n)$–$r_6(k_n)$ are derived below.

Multiplying Eq. (3.50) by $u_n(t)$, summing the result with the product of Eq. (3.46) and $\phi_n^A(t)$, and averaging using Ito calculus yields

$$\left[\frac{\partial}{\partial t} + \lambda_u(k_n) + \lambda_\phi^A(k_n)\right] E_Q^A(k_n) = -\Gamma_A E_u(k_n) + r_1(k_n)r_2(k_n) \ . \tag{3.52}$$

Performing the analogous operations on Eqs. (3.46) and (3.51) yields

$$\left[\frac{\partial}{\partial t} + \lambda_u(k_n) + \lambda_\phi^B(k_n)\right] E_Q^B(k_n) = -\Gamma_B E_u(k_n) + r_1(k_n)r_4(k_n) \ . \tag{3.53}$$

Comparing Eqs. (3.52) and (3.53) with the discrete form of Eq. (3.26), we see that for consistency

$$\lambda_\phi^A(k_n) = (\nu + \mathcal{D}_A)k_n^2 - \lambda_u(k_n) \ , \tag{3.54}$$

$$\lambda_\phi^B(k_n) = (\nu + \mathcal{D}_B)k_n^2 - \lambda_u(k_n) \ , \tag{3.55}$$

$$r_1(k_n)r_2(k_n) = T_Q^A(k_n) \ , \tag{3.56}$$

$$r_1(k_n)r_4(k_n) = T_Q^B(k_n) \ . \tag{3.57}$$

Using the same procedure, we derive scalar auto- and cross-correlation equations

$$\left[\frac{\partial}{\partial t}+2\lambda_\phi^A(k_n)\right]E_B^{AA}(k_n) = -2\Gamma_A E_Q^A(k_n)+r_2^2(k_n)+r_3^2(k_n)\;, \tag{3.58}$$

$$\left[\frac{\partial}{\partial t}+2\lambda_\phi^B(k_n)\right]E_B^{BB}(k_n) = -2\Gamma_B E_Q^B(k_n)+r_4^2(k_n)+r_5^2(k_n)+r_6^2(k_n)\;, \tag{3.59}$$

$$\left[\frac{\partial}{\partial t}+\lambda_\phi^A(k_n)+\lambda_\phi^A(k_n)\right]E_B^{AB}(k_n) = -\Gamma_A E_Q^A(k_n)-\Gamma_B E_Q^B(k_n) + r_2(k_n)r_4(k_n)+r_3(k_n)r_5(k_n)\;. \tag{3.60}$$

Comparing these equations to the discrete version of Eq. (4.20) yields

$$r_2^2(k_n)+r_3^2(k_n) = 2\left[\lambda_\phi^A(k_n)-\mathcal{D}_A k_n^2\right]E_B^{AA}(k_n)+T_B^{AA}(k_n)\;, \tag{3.61}$$

$$r_4^2(k_n)+r_5^2(k_n)+r_6^2(k_n) = 2\left[\lambda_\phi^B(k_n)-\mathcal{D}_B k_n^2\right]E_B^{BB}(k_n)+T_B^{BB}(k_n)\;, \tag{3.62}$$

$$r_2(k_n)r_4(k_n)+r_3(k_n)r_5(k_n) = \left[\lambda_\phi^A(k_n)+\lambda_\phi^B(k_n)-(\mathcal{D}_A+\mathcal{D}_B)k_n^2\right]E_B^{AB}(k_n)+T_B^{AB}(k_n)\;. \tag{3.63}$$

3.3.3 Numerical Implementation

The 'shell' model consists of the SDEs for the velocity (see Eq. 3.46) and scalars (see Eqs. 3.50 and 3.51) that will be advanced for an ensemble of realizations. We refer to each realization as a 'particle' that is designated by an integer index $m = 1, 2, \cdots, M$, where M is the total number of realizations. We will augment the nomenclature given in the previous section to include the particle (or realization) number; for example, we define $u_{m,n}(t)$ to be the random velocity in the n^{th} shell of the m^{th} particle at time t. Each particle obeys the same equations, but is an independent realization of that equation. Spectral expectations

are then approximated by ensemble averages as follows

$$E_u(k_n) = \frac{1}{M}\sum_{m=1}^{M} u_{m,n}^2(t)\ , \tag{3.64}$$

$$E_Q^{\alpha}(k_n) = \frac{1}{M}\sum_{m=1}^{M} u_{m,n}(t)\phi_{m,n}^{\alpha}(t), \tag{3.65}$$

$$E_B^{\alpha\beta}(k_n) = \frac{1}{M}\sum_{m=1}^{M} \phi_{m,n}^{\alpha}(t)\phi_{m,n}^{\beta}(t), \tag{3.66}$$

which approach the expectation in the limit $M \to \infty$. The initial conditions for the scalars were set to zero, i.e., $\phi_{m,n}^{\alpha}(0) = \phi_{m,n}^{\beta}(0) = 0$, for all m and n. The turbulent velocities, being stationary, were initialized as follows

$$u_{m,n}(0) = E_u^{1/2}(k_n) N_{m,n}[0,1]\ , \tag{3.67}$$

where $N_{m,n}[0,1]$ is an independent Gaussian random number with zero mean and unit variance. The initial velocity is consistent with the spectral relationship given in Eq. (3.64).

In order to advance the shell model equations (Eqs. 3.46, 3.50 and 3.51), we must first evaluate the coefficients $\lambda_u(k_n)$, $\lambda_\phi^A(k_n)$ and $\lambda_\phi^B(k_n)$, as well as $r_1(k_n)$–$r_6(k_n)$. The first three are given as explicit functions of the spectra and known coefficients (see Eqs. 3.13, 3.54 and 3.55). At every instant in time, the spectra can be reconstructed from the ensemble of realizations of $u_{m,n}(t)$, $\phi_{m,n}^A(t)$ and $\phi_{m,n}^B(t)$, per Eqs. (3.64)–(3.66). The coefficients $r_1(k_n)$–$r_6(k_n)$ can be calculated by recognizing that for each shell the following relation holds

$$\begin{bmatrix} r_1(k_n) & 0 & 0 \\ r_2(k_n) & r_3(k_n) & 0 \\ r_4(k_n) & r_5(k_n) & r_6(k_n) \end{bmatrix} \cdot \begin{bmatrix} r_1(k_n) & r_2(k_n) & r_4(k_n) \\ 0 & r_3(k_n) & r_5(k_n) \\ 0 & 0 & r_6(k_n) \end{bmatrix} = \mathbf{\Lambda}\ ,$$

where $\mathbf{\Lambda}$ is the following *symmetric* matrix

$$\mathbf{\Lambda} \equiv \begin{bmatrix} 2\lambda_u(k_n)E_u(k_n) & T_Q^A(k_n) & T_Q^B(k_n) \\ \text{Sym} & \text{RHS Eq. (3.61)} & \text{RHS Eq. (3.63)} \\ \text{Sym} & \text{Sym} & \text{RHS Eq. (3.62)} \end{bmatrix}\ , \tag{3.68}$$

For space purposes, we use 'Sym' to refer to symmetric elements of the matrix, and 'RHS' refers to the 'right hand side' of the specified equation. As you can see, the coefficients $r_1(k_n)$–$r_6(k_n)$ form the lower triangular Cholesky decomposition of the symmetric matrix $\mathbf{\Lambda}$, which exists so long as this matrix remains positive definite (i.e., with positive real eigenvalues). This is a realizability constraint that is satisfied by the EDQNM model[44,46].

The stochastic differential equations that constitute the shell model were updated using a 3/2–order scheme[3]. To illustrate the approach, the numerical update for Eq. (3.46) can be written as follows

$$u_n(t+\Delta t) = u_n(t) - \lambda_u(k_n)\left[\frac{1}{3}u'_n(t) + \frac{2}{3}u''_n(t)\right]\Delta t + r_1(k_n)N_1[0,1]\,\sqrt{\Delta t}\;, \tag{3.69}$$

where

$$u'_n(t) = u_n(t) - \frac{1}{2}\lambda_u(k_n)u_n(t)\Delta t\;, \tag{3.70}$$

$$u''_n(t) = u'_n(t) + \frac{3}{2}r_1(k_n)\frac{1}{2}\left(N_1[0,1] + \frac{1}{\sqrt{3}}N_2[0,1]\right)\sqrt{\Delta t}\;, \tag{3.71}$$

and $N_1[0,1]$ and $N_2[0,1]$ are two independently chosen Gaussian random numbers (zero mean and unit variance). The same numerical update was used with Eqs. (3.50) and (3.51).

3.3.4 Probability Density Function

Although not the focus of the present study, we would like to point out that the stochastic shell model, in addition to modeling the energy, scalar and cross spectra through averages within each shell, also provides a model for the PDF of scalar and velocity fluctuations. We arrive at these relationships by first recalling that single-point second-order moments

can be determined from the spectra as shown below

$$\langle \phi_A'^2 \rangle = \sum_{n=1}^{N} E_B^{AA}(k_n) \,, \tag{3.72}$$

$$\langle \phi_B'^2 \rangle = \sum_{n=1}^{N} E_B^{BB}(k_n) \,, \tag{3.73}$$

$$\langle \phi_A' \phi_B' \rangle = \sum_{n=1}^{N} E_B^{AB}(k_n) \,, \tag{3.74}$$

$$\langle u \phi_A' \rangle = \sum_{n=1}^{N} E_Q^{A}(k_n) \,, \tag{3.75}$$

$$\langle u \phi_B' \rangle = \sum_{n=1}^{N} E_Q^{B}(k_n) \,. \tag{3.76}$$

Alternatively, we could arrive at a particle based velocity or scalar fluctuation by summing over the wavenumber shells as shown below for the m^{th} particle

$$u(t) = \sum_{n=1}^{N} u_{m,n}(t) \,, \tag{3.77}$$

$$\phi_A'(t) = \sum_{n=1}^{N} \phi_{m,n}^{A}(t) \,, \tag{3.78}$$

$$\phi_B'(t) = \sum_{n=1}^{N} \phi_{m,n}^{B}(t) \,, \tag{3.79}$$

which can be thought of as a single representation of the fine-grained PDF[34]. The correlations obtained from the PDF are consistent with those from the spectral shell representation. This can be easily demonstrated for the variance of the velocity by recognizing

$$\langle u^2 \rangle = \underbrace{\frac{1}{M} \sum_{m=1}^{M} \left[\sum_{n=1}^{N} u_{m,n}(t) \right]^2}_{\text{particle}} = \underbrace{\sum_{n=1}^{N} \left[\frac{1}{M} \sum_{m=1}^{M} u_{m,n}^2(t) \right]}_{\text{spectral}} \,.$$

The ‘particle’ and ‘spectral’ representations of the variance are the same because the velocity in each shell is independent, i.e., $\langle u_{m,n}(t) u_{m',n'}(t) \rangle = 0$ for $m \neq m'$ and/or $n \neq n'$. More generally, the single-point joint velocity–scalar PDF that is generated by binning the individual particle values for u, ϕ_A' and ϕ_B' has auto- and cross-correlation statistics that are consistent with the spectral representation. In light of the initial condition for the velocity

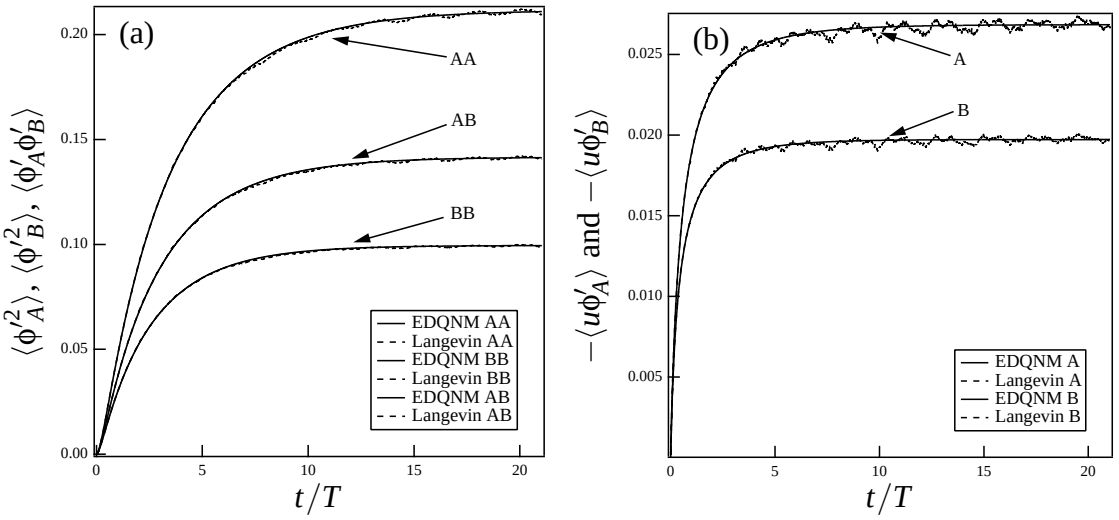

Figure 3.1: Evolution of (a) the scalar auto- and cross-correlations and (b) the velocity–scalar cross correlations (turbulent scalar flux), predicted by the EDQNM model (solid lines) and stochastic shell mixing model (dashed lines) as a function of time, normalized by the large eddy turnover time T. Aside from the statistical fluctuations in the latter due to the finite size of the ensemble, the agreement is excellent.

and scalars in the present study, the joint PDF for the velocity and scalars will remain a joint Gaussian for all times; hence for the example in this study, the PDF is completely determined by the correlation matrix. However, this need not be the case, and for circumstances in which the initial scalar PDF is non-Gaussian, the stochastic shell mixing model will provide a model for the evolution of the PDF.

3.4 Comparison of EDQNM and Shell Model

Numerical experiments of the stochastic shell mixing model were carried out using a Pao spectrum for the velocity defined as follows

$$E_u(k_n) = C\varepsilon^{2/3} k_n^{-5/3} \exp\left[-\frac{3}{2} C (k_n \eta)^{4/3}\right] , \tag{3.80}$$

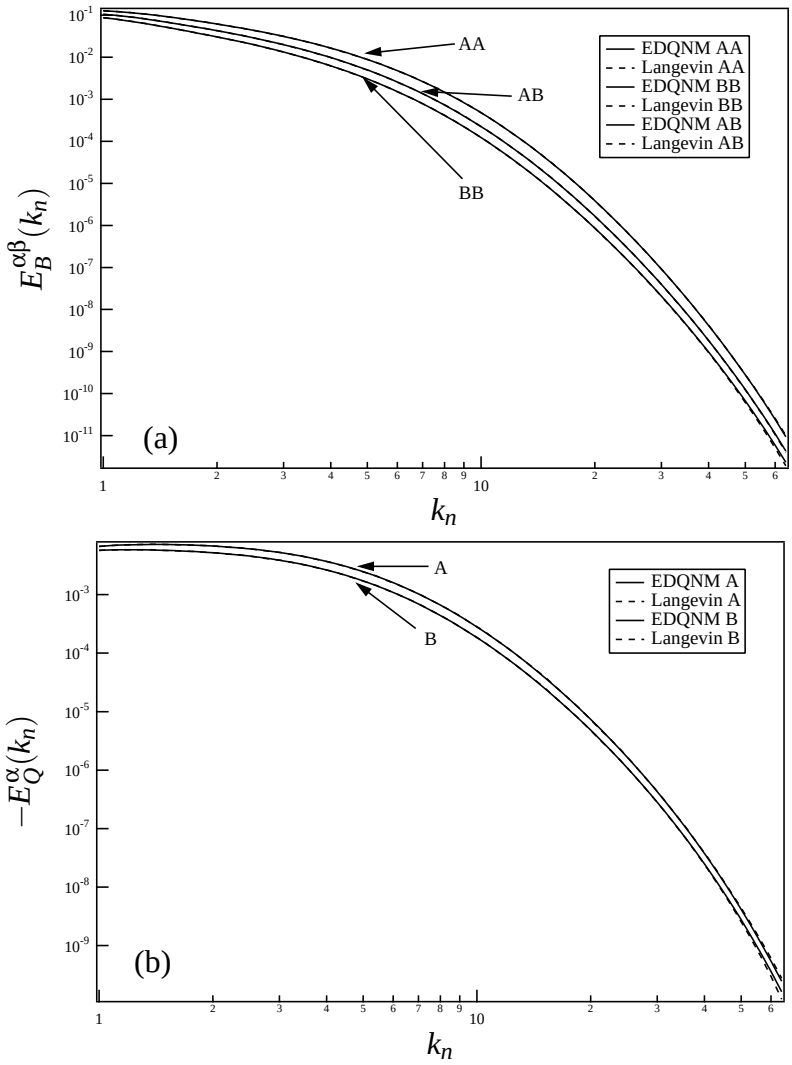

Figure 3.2: Plot of (a) scalar auto- and cross-correlation spectra and (b) velocity–scalar cross correlation spectra at time $t/T = 8$, predicted by the EDQNM model (solid lines) and stochastic shell mixing model (dashed lines). The specific spectra are indicated on the graph.

where the constant $C = 1.5$, the dissipation rate was set to $\varepsilon = 0.18$, the kinematic viscosity was $\nu = 0.015$, implying the Kolmogorov length scale was $\eta \equiv \nu^{3/4}/\varepsilon^{1/4} = 0.0658$. These parameters produced a turbulence with a root mean square fluctuating velocity of $\langle u^2 \rangle^{1/2} = 0.68$, integral length scale $L = 1.3$, large eddy turnover time $T = 1.92$ and Reynolds number (based on the integral length scale) $Re_L = 60$. The Schmidt numbers ($Sc_\alpha \equiv \nu/\mathcal{D}_\alpha$) for the two diffusing species were set to $Sc_A = 1.0$ and $Sc_B = 0.5$. The calculations were performed with $M = 10^5$, $N = 64$, $k_0 = 1$ and $k_{65} = 64$, implying a shell ratio $\lambda = 1.067$. The scalars were initially set to zero, i.e., $\phi^A_{m,n}(0) = \phi^B_{m,n}(0) = 0$.

Figure 3.1 shows the comparison between the EDQNM model and the ensemble averages of the stochastic shell model. The single-point quantities were obtained from Eqs. (3.72)–(3.76) using both the EDQNM prediction for the spectrum (solid lines) and the stochastic shell mixing model prediction for the spectrum (dashed lines). As you can see, aside from the statistical fluctuations in the stochastic shell model due to the finite size of the ensemble, the agreement is excellent. Comparisons of the spectra themselves are given in Fig. 3.2, and the agreement is once again excellent.

3.5 Lagrangian Statistics from Shell Model

We determined in §3.4 that the shell model reproduces the single-time statistics predicted by EDQNM. Because we are evolving primitive variables for each particle, it is possible to predict Lagrangian correlation functions in time. For arbitrary statistically stationary variables $X(t)$ and $Y(t)$ associated with each particle, we define the correlation function as

$$\rho(X,Y;t) \equiv \frac{\langle X(s)Y(s+t)\rangle}{\sqrt{\langle X^2\rangle\ \langle Y^2\rangle}}\ , \tag{3.81}$$

where X and Y stand for the species concentration ϕ'_α (Greek letters α and β signify species A or B), velocity u', concentration difference $z \equiv \phi'_B - \phi'_A$ or the local scalar dissipation rate

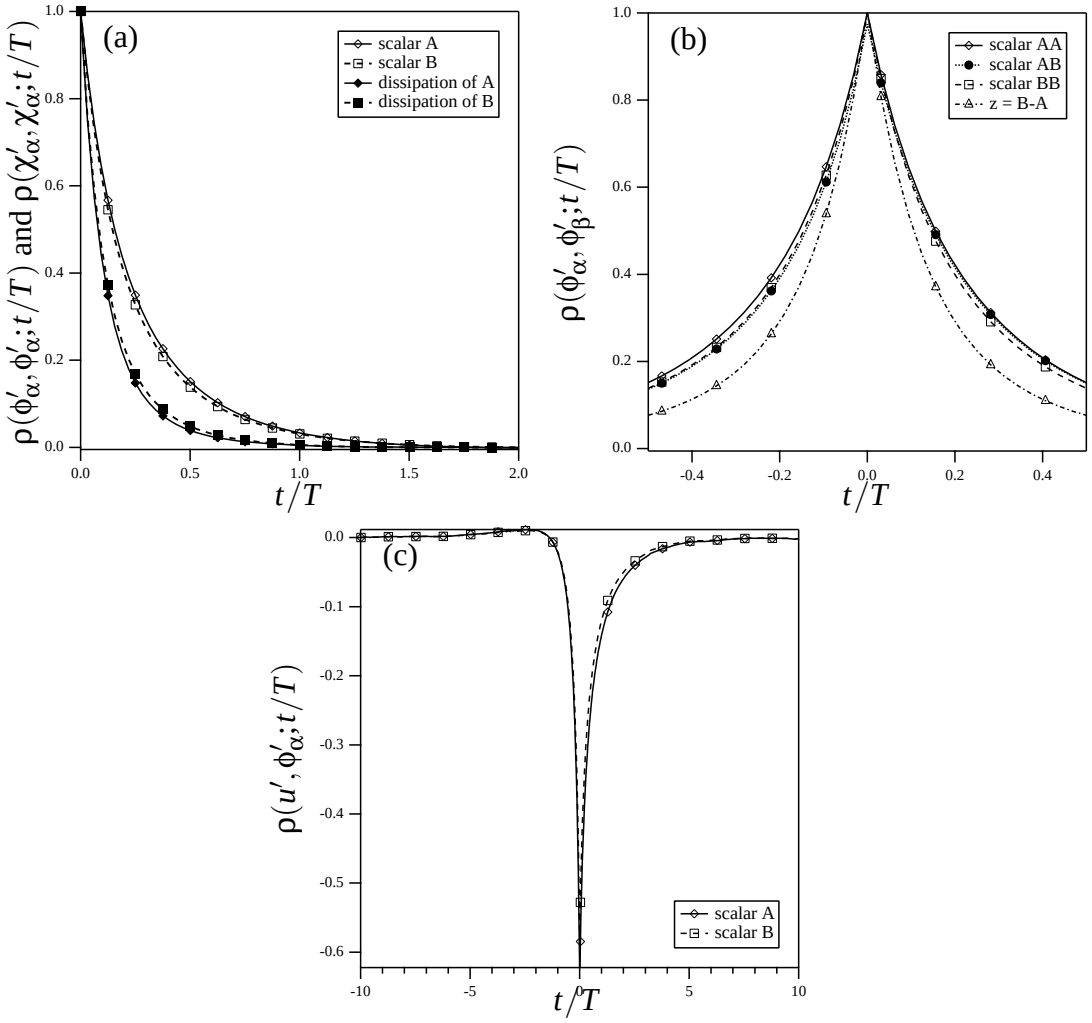

Figure 3.3: Evolution of Lagrangian temporal correlation functions: (a) autocorrelation of species concentrations and species dissipation rates; (b) auto- and cross-correlation of species A, B and $z \equiv \phi'_B - \phi'_A$; (c) velocity–scalar cross correlation function, for $Sc_A = 1.0$ and $Sc_B = 0.5$.

$\chi'_\alpha(t) \equiv -2\mathcal{D}_\alpha \sum_{n=1}^{N} k_n^2 \left[\phi_{m,n}^\alpha(t)\right]^2$. Note that we first ran the shell model until all the scalar statistics reached a statistically stationary state before constructing the various correlation functions defined by Eq. (3.81).

The shell model predictions for the Lagrangian statistics are summarized in Fig. 3.3. We can compare the qualitative trends with the direct numerical simulation (DNS) study by Yeung[52]. In particular, Fig. 3.3(a), (b) and (c) can be compared respectively with Figs. 10, 13 and 7 from Ref.[52]. The relative behavior between the autocorrelation function for the scalar and scalar dissipation are in good qualitative agreement with Yeung's DNS. Moreover, the trend with the Schmidt number, albeit weak, is also captured by the model; that is, the scalar with the higher diffusivity (scalar B) decays more quickly than the slower diffusiving scalar, whereas the opposite tend is observed for the scalar dissipation rate, all in accord with the DNS. The cross correlation curves shown in Fig. 3.3(b) look similar to Yeung's DNS. For example, they have a qualitatively similar asymmetry at the origin ($t/T = 0$). The major difference is with the sharpness of the curves near $t = 0$. The shell model generates a discontinuity in the slope of the correlation curves at $t = 0$ that arises from the Wiener process. The velocity-scalar correlations shown in Fig. 3.3(c) likewise are in qualitative agreement with the DNS, except near the origin. We consistently find the peak (largest negative value) in the correlation occurs at $t = 0$, whereas the peak in the DNS is shifted to $t/T > 0$. The model inherently cannot capture this feature. Nevertheless, the overall performance of the model is encouraging considering we are not tuning any adjustable parameters.

3.6 Conclusions

The main objective of this paper has been the development of a new 'shell' model for the velocity and multiple scalar species based on the EDQNM theory. The equations governing the velocity and scalar within a shell take on a particular form of the Ornstein–Uhlenbeck SDE, with drift and diffusion terms chosen so that ensemble averages of scalar–scalar auto- and covariances, and velocity–scalar covariances are precisely those predicted by the EDQNM theory. We use a generalized form of the EDQNM theory that has been shown to be realizable[44], enabling this advancement. The resulting equations are shown to reproduce the EDQNM predictions to within the statistical error resulting from the finite size of the ensemble. To further test the model, we compute Lagrangian correlation functions involving the scalar concentrations, scalar dissipation rate and velocity fluctuations along the particle paths and compare them to DNS by Yeung[52]. Overall the results are in good qualitative agreement, reproducing the correct trends with the scalar Schmidt number, for example. However, the stochastic nature of the model leads to a discontinuity in the slope of the correlation function at $t = 0$, a result of the Wiener process in the model equation. This discontinuity is not consistent with the DNS[52]. Fortunately the resulting errors are important only at small times $t/T \ll 1$.

The stochastic shell model has the advantage of predicting the probability density function (PDF) of the scalar fluctuations, when the velocity and/or scalar are summed over the shells. Indeed, this development is a step towards a new mixing model for the PDF that takes into account spectral information for the velocity and scalar fields. The spectral information is embedded in the distributions across the shells. For example, scalars with identical PDFs, but different length scales will mix at different rates because the spectral distributions will be different. Such a dependency is not easily reproduced by traditional single-point closures that contain no scale information. Furthermore, we have demon-

strated that the shell model takes into account differential diffusion at a level equivalent to the EDQNM theory, which previously has been shown to reproduce a number of key features in agreement with direct numerical simulations[45]. Finally, we note that the stochastic nature of the model ensures that the scalar fluctuations will relax towards a Gaussian at long times. Placing the stochastic shell model in the context of Subramaniam & Pope's eight requirements for a sound mixing model, the stochastic shell model automatically satisfies: (i), (ii), (iv), (v), (vi), and (vii). The issue of the bounds (iii) is a challenge for all stochastic mixing models, including this one, and we defer further discussion of this point until a future publication. The issue of the effect of chemical reaction (viii) has been realized; however, only for simple bimolecular reactions up to this point[50]. The generalization of the method for more complex chemistry remains an important open challenge.

ACKNOWLEDGEMENTS

We are grateful to Mr. Yang Liu for several theoretical contributions he made during the early stages of this work. LRC and YX acknowledge financial support from the National Science Foundation under grant 0121573.

REFERENCES

[1] J. C. Andre and M. Lesieur. Influence of helicity on the evolution of isotropic turbulence at high Reynolds number. *J. Fluid Mech.*, 81:187, 1977.

[2] L. Biferale. Shell models of energy cascade in turbulence. *Ann. Rev. Fluid Mech.*, 35:441–468, 2003.

[3] C.-C. Chang. Numerical solutions of stochastic differential equations with constant diffusion coefficients. *Math. Comput.*, 49:523–542, 1987.

[4] H. Chen, S. Chen, and R. H. Kraichnan. Probability distribution of a stochastically advected scalar field. *Phys. Rev. Letters*, 63:2657–2660, 1989.

[5] Cesar Dopazo. Probability density function approach for a turbulent axisymmetric heated jet. Centerline evolution. *Phys. Fluids*, 18:397–404, 1975.

[6] V. Eswaran and S. B. Pope. Direct numerical simulations of the turbulent mixing of a passive scalar. *Phys. Fluids*, 31:506–520, 1988.

[7] R. O. Fox. The Fokker-Planck closure for turbulent molecular mixing: Passive scalars. *Phys. Fluids A*, 4:1230–1244, 1992.

[8] R. O. Fox. Improved Fokker-Planck model for the joint scalar, scalar gradient PDF. *Phys. Fluids A*, 6:334–348, 1994.

[9] R. O. Fox. The Lagrangian spectral relaxation model of the scalar dissipation in homogeneous turbulence. *Phys. Fluids*, 9:2364–2386, 1997.

[10] R. O. Fox. The Lagrangian spectral relaxation model for differential diffusion in homogeneous turbulence. *Phys. Fluids*, 11:1550–1571, 1999.

[11] R. O. Fox. *Computational models for turbulent reacting flows*. Cambridge University Press, New York, 2003.

[12] R. O. Fox and P. K. Yeung. Improved Lagrangian mixing models for passive scalars in isotropic turbulence. *Phys. Fluids*, 15:961–985, 2003.

[13] S. Frankel, T.-L. Jiang, and P. Givi. Modeling of isotropic reacting turbulence by a hybrid mapping-EDQNM closure. *AIChE Journal*, 38:535–543, 1992.

[14] F. Gao. An analytical solution for the scalar probability density function in homogeneous turbulence. *Phys. Fluids A*, 3:511, 1991.

[15] E. B. Gledzer. System of hydrodynamic type admitting two quadratic integrals of motion. *Sov. Phys. Dokl.*, 18:216–217, 1973.

[16] D. C. Haworth. Progress in probability density function methods for turbulent reacting flows. *Prog. Energy Combust. Sci.*, pages 1–92, 2010. in press.

[17] S. Heinz. *Statistical Mechanics of Turbulent Flows*. Springer-Verlag, 2003.

[18] S. Herr, L.-P. Wang, and L. R. Collins. EDQNM model of a passive scalar with a uniform mean gradient. *Phys. Fluids*, 8:1588–1608, 1996.

[19] J. R. Herring. Approach of axisymmetric turbulence to isotropy. *Phys. Fluids*, 17: 859, 1974.

[20] J. R. Herring, D. Schertzer, M. Lesieur, G. R. Newman, J. P. Chollet, and M. Larcheveque. A comparitive assessment of spectral closures as applied to passive scalar diffusion. *J. Fluid Mech.*, 124:411–438, 1982.

[21] V. M. Ievlev. Equations for finite-dimensional distributions of pulsating value possibilities in a turbulent flow. *Dokl. Akad. Nauk SSSR*, 208:1044–1047, 1973.

[22] A. Juneja and S. B. Pope. A DNS study of turbulent mixing of two passive scalars. *Phys. Fluids*, 8:2161–2184, 1996.

[23] Fema C. Klebaner. *Introduction to stochastic calculus with applications*. Imperial College Press, 2005.

[24] Robert H. Kraichnan. The structure of isotropic turbulence at very high Reynolds numbers. *J. Fluid Mech.*, 5:497–543, 1959.

[25] Ying-Yan Kuo and E. E. O'Brien. Two-point probability density function closure applied to a diffusive-reactive system. *Phys. Fluids*, 24(2):194–201, 1981.

[26] V. R. Kuznetsov and V. A. Sabel'nikov. *Turbulence and Combustion*. Hemisphere, 1990.

[27] M. Lesieur. *Turbulence in fluids, stochastic and numerical modeling*. M. Nijhoff, Boston, 1987.

[28] G. Li and M. F. Modest. Investigation of turbulence-radiation interactions in reacting flows using a hybrid FV/PDF Monte Carlo method. In *Proceedings of the ICHMT 3rd Int. Sym. on Rad. Trans.*, 2001.

[29] S. Mazumder and M. F. Modest. A PDF approach to modeling turbulence-radiation interactions in nonluminous flames. *Int. J. Heat and Mass Trans.*, 42:971–991, 1998.

[30] R. E. Meyers and E. E. O'Brien. The joint PDF of a scalar and its gradient at a point in a turbulent flow. *Combust. Sci. Technol.*, 26:123, 1981.

[31] N. Nakauchi, H. Oshima, and Y. Saito. A passive scalar convected by homogeneous axisymmetric turbulence. *Phys. Fluids A*, 1:723, 1989.

[32] K. Ohkitani and M. Yamada. Temporal intermittency in the energy cascade process and local Lyapunov analysis in fully developed model of turbulence. *Prog. Theor. Phys.*, 89:329–341, 1989.

[33] S. A. Orszag. Analytical theories of turbulence. *J. Fluid Mech.*, 41:363–386, 1970.

[34] S. B. Pope. PDF methods for turbulent reactive flows. *Prog. Energy Combust. Sci.*, 11:119–192, 1985.

[35] S. B. Pope. Mapping closures for turbulent mixing and reaction. *Theor. Comput. Fluid Dyn.*, 2:255–270, 1991.

[36] S. B. Pope. Lagrangian PDF methods for turbulent flows. *Ann. Rev. Fluid Mech.*, 26: 23–63, 1994.

[37] Stephen B. Pope. *Turbulent Flows*. Cambridge University Press, New York, 2000.

[38] A. Pouquet, M. Lesieur, J. C. Andre, and C. Basdevant. Evolution of high Reynolds number two-dimensional turbulence. *J. Fluid Mech.*, 72:305–319, 1975.

[39] Z. Ren and S. B. Pope. Sensitivity calculations in PDF particle methods. *Combust. Flame*, 153:202–215, 2008.

[40] J. R. Saylor and K. R. Sreenivasan. Differential diffusion in low Reynolds number water jets. *Phys. Fluids*, 10:1135–1146, 1998.

[41] Z.-S. She and E. Jackson. Constrained Euler system for Navier-Stokes turbulence. *Phys. Rev. Lett.*, 70(9):1255–1258, 1993.

[42] L. L. Smith, R. W. Dibble, L. Talbot, R. S. Barlow, and C. D. Carter. Laser raman scattering measurements of differential molecular diffusion in nonreacting turbulent jets of H_2 / CO_2 mixing with air. *Phys. Fluids*, 7:1455–1466, 1995.

[43] S. Subramaniam and Stephen B. Pope. A mixing model for turbulent reactive flows based on Euclidean Minimum Spanning Trees. *Combust. Flame*, 115:487–514, 1998.

[44] M. Ulitsky and L. R. Collins. On constructing realizable, conservative mixed scalar equations using the eddy damped quasi-normal markovian theory. *J. Fluid Mech.*, 412:303–329, 2000.

[45] M. Ulitsky, T. Vaithianathan, and L. R. Collins. A spectral study of differential diffusion of passive scalars in isotropic turbulence. *J. Fluid Mech.*, 460:1–38, 2002.

[46] T. Vaithianathan. *A New Multi-Scale Mixing Model for Turbulent Reacting Flows*. PhD thesis, Penn State University, 2003.

[47] T. Vaithianathan, M. Ulitsky, and L. R. Collins. Comparison between a spectral and PDF model for turbulent reacting flows. *Proc. Comb. Inst.*, 29:2139–2146, 2002.

[48] Jean-Marc Vignon and Claude Cambon. Thermal spectral calculation using eddy-damped quasi-normal markovian theory. *Phys. Fluids*, 23:1935–1937, 1980.

[49] Z. Warhaft and J. L. Lumley. An experimental study of the decay of temperature fluctuations in grid generated turbulence. *J. Fluid Mech.*, 88:659–684, 1978.

[50] Yanjun Xia, Yang Liu, T. Vaithianathan, and Lance R. Collins. Eddy damped quasi normal Markovian theory for chemically reactive scalars in isotropic turbulence. *Phys. Fluids*, 22(4):045103, 2010.

[51] P. K. Yeung. Multi-scalar triadic interactions in differential diffusion with and without mean scalar gradients. *J. Fluid Mech.*, 321:235, 1996.

[52] P. K. Yeung. Lagrangian characteristics of turbulence and scalar transport in direct numerical simulations. *J. Fluid Mech.*, 427:241–274, 2001.

CHAPTER 4

BOUNDED STOCHASTIC SHELL MODEL FOR TURBULENT MIXING OF MULTIPLE SCALARS WITH DISTINCT DIFFUSIVITIES

Abstract In the paper by Xia et al. (2010), we derived a stochastic shell mixing model (SSMM) for turbulent mixing of multiple scalars with mixed diffusivities. The framework uses a Monte Carlo scheme to advance notional particles that move with the fluid, and have scalar concentrations that are subdivided into "shells" that loosely represent a spectral decomposition of the scalar fluctuations. The variance within each shell is equivalent to the scalar spectrum evaluated at the corresponding wavenumber. Small-scale phenomena such as differential diffusion and the dependence of mixing on the scalar length scale are captured by the inherently spectral nature of the model. Furthermore, the sum of the scalar over shells for each notional particle simultaneously provides a fine-grained representation of the joint scalar probability density function (PDF). This aspect of the model was introduced, but not fully explored in the earlier paper, which focused on scalar fluctuations arising from a uniform mean gradient. At the level of this model, the scalar PDF reduces to a joint Gaussian. In this study, we explore more complex mixing scenarios, including the initial double delta function, which arises when two streams are brought into sudden contact. This introduces two important complexities that are the focus of this paper. The first is the shape changes to the PDF that result as the scalar PDF relaxes into a Gaussian form. The second is due to the bounds the scalar must satisfy. Monte Carlo schemes inherently violate bounds; we modify the model so as to ensure the bounds are satisfied by nearly all of the particles. Extensive comparisons between the SSMM predictions and direct numerical simulations (DNS) are made for two decaying scalars (with different diffusivities) in forced, isotropic turbulence. Overall the agreement is very good. Additionally, we test a conjecture made in deriving the SSMM, namely that the rate of mixing of a scalar is a function of its spectrum, but not its PDF. Using DNS, we contrast

the mixing rate of two scalars with identical PDFs, but different spectra against two scalars with identical spectra, but different PDFs. We conclude from this comparison that the mixing rate is sensitive to the spectrum, but not the PDF, in support of the assumption used to derive the SSMM.

4.1 Introduction

There are a multitude of frameworks for studying the mixing of scalars by turbulence, each designed to address different aspects of the process. The two of greatest significances to this study are: (i) the spectral analysis of the auto- and cross correlations of the scalar fields; and (ii) the joint composition probability density function (PDF).

In the classical picture of mixing, turbulent eddies, through the actions of stretching and folding, break up large-scale inhomogeneities (blobs) of the scalar field into smaller and smaller scales until ultimately molecular mixing dissipates the remaining scalar fluctuations, homogenizing the system. The rates of stretching and folding depend upon the length and time scales of the eddies. While a formal analysis of this process is not feasible due to the closure problem, this conceptual picture of progressive granularity of the scalar by the action of the turbulence can be captured by a spectral model, which decomposes the scalar fluctuations into wavenumbers that loosely correspond to inverse length scales. Classical scaling arguments set forth by Kolmogorov[22], Obukhov[32] and Corrsin[5] established the scalar spectrum should have the following form in the so-called inertial-convective subrange:[38]

$$E_B(k) = \beta\varepsilon^{-1/3}\chi k^{-5/3} \,, \tag{4.1}$$

where $E_B(k)$ is the three-dimensional scalar spectrum, ε is the energy dissipation rate, χ is the scalar dissipation rate and β is a presumed universal constant. The argument assumes a constant flux of scalar fluctuations through the inertial-convective subrange equal to the

scalar dissipation rate, which effectively links small-scale dissipation to the larger-scale eddies that control the flux.

The PDF representation replaces the local concentration of scalars by the joint distribution of scalar fluctuations. PDF methods are particularly attractive for chemically reactive systems,[13,16,17,25,33,34] as the chemical source terms are closed in this representation, regardless of their complexity. However, the molecular mixing responsible for the evolution of the PDF is not closed and hence must be modeled. For example, the evolution of the scalar PDF, $P(c,t)$, in homogeneous turbulence is governed by

$$\frac{\partial P(c,t)}{\partial t} + \frac{1}{2}\frac{\partial^2}{\partial c^2}\left[\chi(c,t)P(c,t)\right] = 0 \ , \tag{4.2}$$

where $\chi(c,t) \equiv \langle 2\mathcal{D}\nabla\phi\cdot\nabla\phi|\phi = c\rangle$ is the average scalar dissipation rate conditioned on the scalar concentration, a quantity that cannot be computed from the scalar PDF and hence must be modeled. Recognizing the PDF is a single-point statistic, the modeled term can be thought of as providing two-point information.[23]

Both paradigms of mixing provide complementary information. The spectrum inherently provides two-point information about the scalar field and can represent derivatives of arbitrary (even) order as weighted integrals of the spectrum; however, it only contains information about second-order moments. The PDF framework, in contrast, can evaluate arbitrary-order moments through weighted integrals of the PDF, but only at a single point. It is natural to think of combining these two descriptions of the scalar field so as to exploit the strengths of each representation. Meyers and O'Brien[29] derived a two-point PDF equation with this in mind, and closed the equation by replacing the unclosed term by one that relaxes the scalar to its mean. However, the solution to this equation did not correctly represent the evolution of the scalar PDF from a non-Gaussian initial condition. Gao and O'Brien[15] analyzed some of the properties of the joint PDF and showed that the PDF of scalar gradient conditioned on the scalar is nearly Gaussian, motivating them to

use a Gram-Charlier expansion for $P(\nabla c|c)$ with coefficients found from DNS. Fox & Yeung[14] developed a hybrid strategy that combined the Lagrangian spectral relaxation (LSR) model for the mean scalar spectrum[11,12] with a Fokker–Planck equation for the PDF.[9,10] The LSR model was used to account for the effect of changes in the spectral distribution of scalar on the scalar dissipation rate. The model captured several Eulerian and Lagrangian statistics in good accord with DNS for a decaying, Gaussian scalar; however, the extension of the modeling to non-Gaussian fields requires further analysis.

In an earlier study, Xia et al.[45] developed a novel hybrid approach called the stochastic shell mixing model (SSMM) that uses a Monte Carlo scheme to advance the velocity and scalar concentrations on notional particles that have been subdivided into wavenumber bands or 'shells.' Averages across the particles of the scalar co-variance within each shell can be thought of as defining the scalar covariance spectrum; whereas the sum of concentrations over the shells of an individual particle provides a single realization of the fine-grained PDF.[33] Coefficients in the SSMM were chosen so that the spectra match the eddy damped quasi-normal Markovian (EDQNM) spectral model,[27] which in earlier work has been shown to predict single-point and spectral statistics in good agreement with DNS.[18,39,40,44] There are several inherent strengths of the model relative to single-point closures. First, as molecular mixing is explicitly accounted for, the model can describe molecular-driven processes such as differential diffusion. Second, the spectral decomposition provides length scale information that, for example, allows the mixing rate to depend upon the integral length scale of the scalar, a phenomenon known to be true.[43]

The model was first applied to the mixing of scalars with uniform mean gradients.[45] In this scenario, the model predicts a joint Gaussian PDF for all time, so the main feature of the model was that it captured the covariance matrix accurately. Additionally, we computed Lagrangian time correlations for the same flow and found them to be in qualitative

agreement with direct numerical simulations (DNS) in the literature.[48]

There are two aspects of the model that were not considered by Xia et al.[45]: (i) the ability of the model to describe the evolution of an initially non-Gaussian PDF (the double delta function being an important example[7]); and (ii) whether the model can be made to obey the scalar bounds, a challenge for any stochastic mixing model. We address both questions in this study. Additionally, we investigate an inherent assumption in the model, namely that the mixing rate depends upon the scalar spectrum, but not its PDF. To test this hypothesis, we investigate four mixing cases with DNS, two in which the PDFs are matched, but the spectra are different, and two in which the spectra are matched, but the PDFs are different. From this study we conclude that the assumption made in the model is valid. The remainder of the paper is devoted to comparisons between the model and DNS of isotropic mixing of scalars with initial PDFs that are nearly double delta functions. We use the algorithm by Eswaran and Pope[7] to create the initial condition, and study the evolution of the PDF towards a Gaussian, making detailed comparisons between the model predictions and the DNS.

The paper is organized as follows. The governing equations for the velocity and scalar are given in Sec. 4.2, along with a summary of the EDQNM model. The bounded SSMM is then presented in Sec. 4.3. Section 4.4 contains the DNS study comparing the significance of the scalar spectrum and its PDF on mixing. The result supports the assumption made in the SSMM. Comparisons of the predictions of the SSMM with DNS are given in Sec. 4.5, followed by the conclusions in Sec. 4.6.

4.2 Governing Equations and EDQNM Model Summary

4.2.1 Governing Equations

This paper focuses on the mixing of two passive scalars A and B in a homogeneous isotropic system, where the mean velocity and scalar concentrations are set to 0 without loss of generality. Under the assumption of constant molecular properties, the governing equations for fluctuating velocity u_i and scalar concentration ϕ_α for species α are as follows:*

$$\frac{\partial u_j(\boldsymbol{x})}{\partial x_j} = 0 \,, \tag{4.3}$$

$$\frac{\partial u_i(\boldsymbol{x})}{\partial t} + \frac{\partial [u_i(\boldsymbol{x}) u_j(\boldsymbol{x})]}{\partial x_j} + \frac{1}{\rho}\frac{\partial p(\boldsymbol{x})}{\partial x_i} = \nu \frac{\partial^2 u_i(\boldsymbol{x})}{\partial x_j^2} \,, \tag{4.4}$$

$$\frac{\partial \phi_\alpha(\boldsymbol{x})}{\partial t} + \frac{\partial [u_i(\boldsymbol{x}) \phi_\alpha(\boldsymbol{x})]}{\partial x_i} = \mathcal{D}_\alpha \frac{\partial^2 \phi_\alpha(\boldsymbol{x})}{\partial x_i^2} \,. \tag{4.5}$$

where p is pressure, ρ is fluid density, ν is kinematic viscosity, $\mathcal{D}_\alpha$ is the molecular diffusivity of species α relative to the solvent species. Note that we use Greek letters to signify arbitrary species, i.e., $\alpha = A$ or B, and that there is no summation over repeated Greek suffixes.

The next two sections provide concise summaries of the EDQNM equations for the turbulent energy and scalar spectra, respectively. Refer to Herr et al.[18] and Xia et al.[45] for the detailed derivations of the equations.

*To simplify the nomenclature we suppress the explicit dependence of all variables on time.

4.2.2 EDQNM Model for Energy Spectrum

For homogeneous isotropic turbulence, the energy spectrum $E_u(k)$ is all that is required to specify $R_{ij}(\boldsymbol{k},\boldsymbol{p})$, which is the Fourier transform of the two-point velocity correlation $R_{ij}(\boldsymbol{x}_1,\boldsymbol{x}_2) \equiv \langle u_i(\boldsymbol{x}_1)u_j(\boldsymbol{x}_2)\rangle$. The formal relationship is

$$R_{ij}(\boldsymbol{k},\boldsymbol{p}) = \frac{2\pi^2 E_u(k)}{k^2} P_{ij}(\boldsymbol{k})\hat{\delta}(\boldsymbol{k}+\boldsymbol{p}) \,, \tag{4.6}$$

where $P_{ij}(\boldsymbol{k})$ is the projection operator defined as $P_{ij}(\boldsymbol{k}) \equiv \delta_{ij} - k_i k_j/k^2$, $\hat{\delta}(\boldsymbol{k}+\boldsymbol{p}) \equiv (2\pi)^3\delta(\boldsymbol{k}+\boldsymbol{p})$, $\delta(\boldsymbol{k}+\boldsymbol{p})$ is the three-dimensional Dirac delta function and δ_{ij} is the Kronecker delta function. The energy spectrum $E_u(k)$ is related to the turbulence intensity as follows

$$\frac{3}{2}u'^2 = \int_0^\infty E_u(k)dk \,. \tag{4.7}$$

The transport equation for $E_u(k)$, closed by EDQNM theory, can be written as

$$\left[\frac{\partial}{\partial t} + 2\lambda_u(k)\right] E_u(k) = \int\int_\triangle \Theta_R^{kpq} V_1 \, E_u(p)E_u(q) \, dpdq \,, \tag{4.8}$$

where

$$\lambda_u(k) = \nu k^2 + \frac{1}{2}\int\int_\triangle \Theta_R^{kpq} V_2 \, E_u(q) \, dpdq \,, \tag{4.9}$$

$$V_1 = \frac{3k^2}{2q}(xy - z^3) \,, \tag{4.10}$$

$$V_2 = \frac{3p^2}{2q}(xy - z^3) \,, \tag{4.11}$$

$$\Theta_R^{kpq} = \frac{1}{\mu_R^{kpq}} \,, \tag{4.12}$$

$$\mu_R^{kpq} = c_1(\mu_k + \mu_p + \mu_q) + \nu(k^2 + p^2 + q^2) \,. \tag{4.13}$$

The constant c_1 is set to 0.36 to ensure that the energy spectrum obeys the Kolmogorov inertial range scaling at infinite Reynolds number,[1] and the frequency μ_k is defined as[35]

$$\mu_k = \frac{1}{\sqrt{2}\pi}\sqrt{\int_0^k k'^4 R(k')dk'} \,. \tag{4.14}$$

The triangle under the integral symbols in Eqs. (4.8) and (4.9) indicates an integration over all the possible closed triads composed by the wave vectors $\boldsymbol{k}$, $\boldsymbol{p}$ and $\boldsymbol{q}$ (i.e., $\boldsymbol{k}+\boldsymbol{p}+\boldsymbol{q}=0$) for each wave vector $\boldsymbol{k}$, and the coefficients x, y and z are the cosines of its interior angles

$$x = \frac{\boldsymbol{p}\cdot\boldsymbol{q}}{pq} = \frac{k^2-p^2-q^2}{2pq} , \tag{4.15}$$

$$y = \frac{\boldsymbol{k}\cdot\boldsymbol{q}}{kq} = \frac{p^2-k^2-q^2}{2kq} , \tag{4.16}$$

$$z = \frac{\boldsymbol{k}\cdot\boldsymbol{p}}{kp} = \frac{q^2-k^2-p^2}{2kp} . \tag{4.17}$$

4.2.3 EDQNM Model for the Scalar Correlation Spectrum

The scalar correlation spectrum $B^{\alpha\beta}(\boldsymbol{k},\boldsymbol{p})$ is the Fourier transform of the two-point scalar correlation $B^{\alpha\beta}(\boldsymbol{x}_1,\boldsymbol{x}_2)$, where α and β can denote species A or B. Under the homogeneous isotropic assumption, the expression for $B^{\alpha\beta}(\boldsymbol{k},\boldsymbol{p})$ can be simplified to

$$B^{\alpha\beta}(\boldsymbol{k},\boldsymbol{p}) = \frac{2\pi^2 E_B^{\alpha\beta}(k)}{k^2}\hat{\delta}(\boldsymbol{k}+\boldsymbol{p}) . \tag{4.18}$$

Scalar correlations $\langle\phi_\alpha\phi_\beta\rangle$ are related to the scalar spectrum by

$$\langle\phi_\alpha\phi_\beta\rangle = \int_0^\infty E_B^{\alpha\beta}(k)\, dk . \tag{4.19}$$

The final EDQNM equation for scalar spectrum $E_B^{\alpha\beta}(k)$ is[45]

$$\left[\frac{\partial}{\partial t} + (\mathcal{D}_\alpha+\mathcal{D}_\beta)k^2 + 2\lambda_\phi(k)\right] E_B^{\alpha\beta}(k) = T^{\alpha\beta}(k), \tag{4.20}$$

where

$$\lambda_\phi(k) = \frac{1}{2}\int\int_\triangle \Theta_M^{kpq} M_1 E_u(p)\, dpdq , \tag{4.21}$$

$$T^{\alpha\beta}(k) = \int\int_\triangle \Theta_M^{kpq} M_2 E_u(p) E_B^{\alpha\beta}(q) dpdq , \tag{4.22}$$

$$\Theta_M^{kpq} = \frac{1-e^{-\mu_M^{kpq} t}}{\mu_M^{kpq}} , \tag{4.23}$$

$$\mu_M^{kpq} = c_2\mu_k + c_3(\mu_p+\mu_q) + \nu(k^2+p^2+q^2) , \tag{4.24}$$

$$M_1 = \frac{3N^2 q}{2p^3 k}\,, \quad M_2 = \frac{3N^2 k}{2p^3 q}\,, \tag{4.25}$$

$$N^2 = \frac{1}{4}(k+p+q)(k+p-q)(k+q-p)(p+q-k)\,. \tag{4.26}$$

The constants c_2 and c_3 are set to 0.36.

4.3 Langevin Model

The Langevin model proposed here is based on a discrete representation of the three-dimensional wave vector space in spherical shells of radius $k_n = k_0\lambda^{n-1}$, where $n = 1,2,...,N+1$, and λ is the inter-shell ratio. We choose a logarithmic shell distribution so that the model can span a broad range of scales with even moderate values of N. The Langevin models are stochastic differential equations (SDEs) for real variables $u_n(t)$ and $\phi_n^\alpha(t)$, which stand for the fluctuations associated with shell n. They are defined such that an ensemble of their realizations satisfies

$$\langle u_n(t)u_m(t)\rangle = \delta_{nm}E_u(k_n,t)\,, \tag{4.27}$$

$$\langle \phi_n^\alpha(t)\phi_m^\beta(t)\rangle = \delta_{nm}E_B^{\alpha\beta}(k_n,t)\,. \tag{4.28}$$

where $E_u(k,t)$ and $E_B^{\alpha\beta}(k,t)$ develop in accordance with the EDQNM model [Eqs. (4.8) and (4.20), respectively]. Here, $E_u(k_n,t)$ and $E_B^{\alpha\beta}(k_n,t)$ refer to the energy variance and scalar covariance contained within the finite shell, or equivalently they are the integrals of the respective spectra, $E_u(k,t)$ and $E_B^{\alpha\beta}(k,t)$, over the shell. (Note that we distinguish between the energy and scalar spectra and the equivalent energy variance and scalar covariance by the argument.)

4.3.1 Langevin Equation for the Velocity

The velocity in each shell satisfies an Ornstein-Uhlenbeck process

$$du_n(t) + \lambda_u(k_n)u_n(t)dt = r_0(k_n)dW_n^{[0]}(t) \,, \tag{4.29}$$

where $dW_n^{[0]}(t)$ is a vector-valued Wiener process increment which satisfies

$$\langle dW_n^{[0]}(t)dW_m^{[0]}(s)\rangle = \delta_{nm}\delta(t-s)dsdt \,. \tag{4.30}$$

Multiplying both sides of Eq. (4.29) by $u_n(t)$ and averaging based on Ito calculus[21], we obtain

$$\left[\frac{\partial}{\partial t} + 2\lambda_u(k_n)\right] E_u(k_n) = r_0^2(k_n) \,, \tag{4.31}$$

Comparing this equation with Eq. (4.8), $r_0^2(k_n)$ is determined to be

$$r_0^2(k_n) = \int\int_{\triangle} \Theta_R^{k_n pq} V_1 E_u(p)E_u(q)dpdq \,. \tag{4.32}$$

However, Eq. (4.8) depicts a decaying energy spectrum, while our study uses a statistically stationary turbulent flow, which leads to the following modified definition of $r_0(k_n)$

$$r_0^2(k_n) = 2\lambda_u(k_n)E_u(k_n) \,. \tag{4.33}$$

Here $E_u(k)$ is supplied from the stationary energy spectrum from the DNS, thus eliminating any error associated with the prediction of the energy spectrum.

4.3.2 Stochastic Shell Mixing Model (SSMM)

We propose two similar SDEs for the spectral coefficients of the fluctuating scalar concentrations

$$d\phi_n^A(t) + \left[\mathcal{D}_A k_n^2 + \lambda_\phi(k_n)\right]\phi_n^A(t)dt = r_1(k_n)dW_n^{[1]}(t) \,, \tag{4.34}$$

$$d\phi_n^B(t) + \left[\mathcal{D}_B k_n^2 + \lambda_\phi(k_n)\right]\phi_n^B(t)dt = r_2(k_n)dW_n^{[1]}(t) + r_3(k_n)dW_n^{[2]}(t) \,, \tag{4.35}$$

where $dW_n^{[0]}(t)$, $dW_n^{[1]}(t)$ and $dW_n^{[2]}(t)$ are mutually independent Wiener process increments, i.e., $\langle dW_n^{[i]}(t) dW_n^{[j]}(t) \rangle = 0$ for $i \neq j$. Again, by means of Ito calculus, we can get the explicit expressions for $r_1(k_n)$–$r_3(k_n)$ summarized below[44]

$$r_1^2(k_n) = T^{AA}(k_n) \, , \tag{4.36}$$

$$r_1(k_n) r_2(k_n) = T^{AB}(k_n) \, , \tag{4.37}$$

$$r_3^2(k_n) = T^{BB}(k_n) - r_2^2(k_n) \, . \tag{4.38}$$

4.3.3 Bounded Stochastic Shell Mixing Model (BSSMM)

A common weakness shared by almost all Monte-Carlo based mixing algorithms for scalars is their potential to violate the scalar bounds imposed by the initial and boundary conditions. The SSMM model proposed above suffers from the same shortcoming. This is evident in Fig. 4.1 (b), which shows the PDF for scalar A at $t^* = 0$ and $t^* = 0.6$ (details of the initialization of the model are given in Section 4.5), where $t^* = t/T$, and T is the large eddy turn over time. Notice that the SSMM prediction for the PDF at $t/T = 0.6$ (line with dots) extends beyond both bounds (indicated by the vertical lines). The PDF from the DNS (details of DNS are given in Section 4.4), in contrast, does not violate the bounds, as shown in Fig. 4.1 (a). The issue can be seen more clearly in Fig. 4.2, which shows the extrema of the scalar concentrations as a function of time. The extrema predicted by the SSMM model go well outside the bounds over the first eddy turnover time, and then remain relatively constant thereafter, whereas the extrema for the DNS are decaying to zero with time. The level of these violations of the bounds could not be tolerated in a reacting system, where they would imply excess reactant or negative concentrations.

The problem arises from the random terms, which are an indispensable component of the model because they ensure the PDF relaxes to a Gaussian shape at long times. Advec-

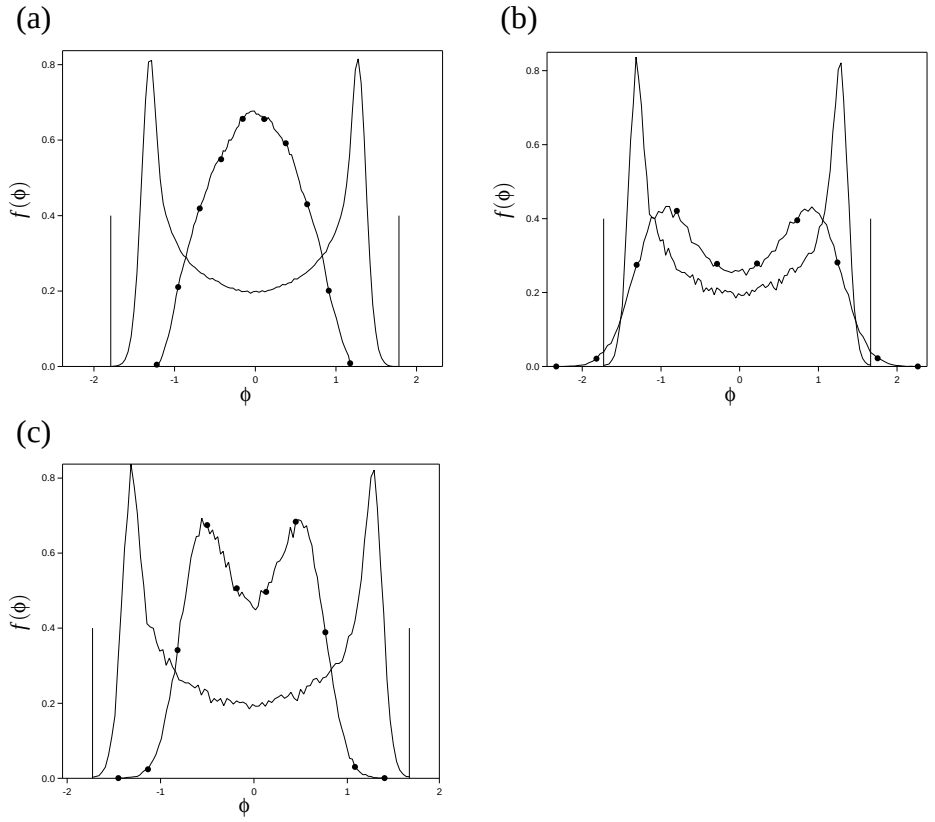

Figure 4.1: A comparison of the PDF of scalar A at $t^* = 0$ (solid lines in all three plots) and $t^* = 0.6$ (lines with dots in all three plots). Plot (a) is from DNS, (b) is from the SSMM, (c) is from the BSSMM. In all plots, the vertical lines indicate the initial bounds of scalar A, which are the same as in plot (b) and (c), but slightly different in plot (a) due to the mismatch between DNS and the model initializations.

tion by the Navier-Stokes velocity is conservative, which implies the scalar concentration of a Lagrangian fluid particle should not be affected by advection. While the modeling of advection in the SSMM conserves the scalar variance *on average* (i.e., when averaged over the population of particles), it does not conserve the concentration for each particle. As a consequence, particle concentrations can wander outside the bounds imposed by the initial and boundary conditions.

Restoring the conservation principle on a per particle basis would eliminate the problem with the bounds. To achieve this goal, we introduce an additional "zeroth" mode to

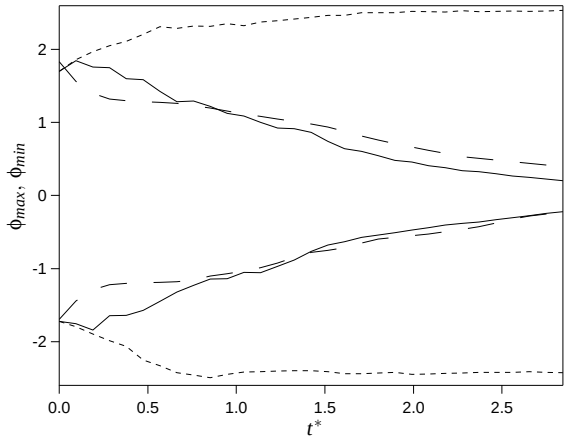

Figure 4.2: Comparison of the extrema of scalar A from DNS, SSMM and BSSMM. Solid lines represent the results from DNS, dotted lines are from SSMM, dashed lines are from BSSMM. The initial scalar spectrum peaks at $k_s = 2$ with $Sc_A = 1$.

the shells, ϕ_0^α. The zeroth mode is designed to capture the residual scalar advection that violates the conservation principle. Including the zeroth mode in the definition of the scalar concentration for a particle yields

$$\phi_\alpha(t) = \sum_{n=1}^{N} \phi_n^\alpha(t) + \phi_0^\alpha = \sum_{n=0}^{N} \phi_n^\alpha(t) \,, \tag{4.39}$$

where the zeroth modes for scalars A and B, respectively satisfy

$$d\phi_0^A(t) = -\omega_A \phi_A(t) dt + \sum_{n=1}^{N} \left[\lambda_\phi(k_n) \phi_n^A(t) dt - r_1(k_n) dW_n^{[1]}(t) \right] \,, \tag{4.40}$$

$$d\phi_0^B(t) = -\omega_B \phi_B(t) dt + \sum_{n=1}^{N} \Big[\lambda_\phi(k_n) \phi_n^B(t) dt - r_2(k_n) dW_n^{[1]}(t) - r_3(k_n) dW_n^{[2]}(t) \Big] \,. \tag{4.41}$$

ω_A and ω_B are coefficients with units of inverse time that are defined below. Incorporating the governing equations for the scalars [Eqs. (4.34) and (4.35)], we can derive an

expression for the resulting change in the scalar fluctuation

$$d\phi_A(t) = -\omega_A\phi_A(t)dt - \sum_{n=1}^{N} \mathcal{D}_A k_n^2 \phi_n^A(t)dt \ , \tag{4.42}$$

$$d\phi_B(t) = -\omega_B\phi_B(t)dt - \sum_{n=1}^{N} \mathcal{D}_B k_n^2 \phi_n^B(t)dt \ . \tag{4.43}$$

Multiplying by $2\phi_A(t)$ on both sides of Eq. (4.42) and taking the ensemble average yields

$$\frac{d\langle\phi_A^2\rangle}{dt} = -\chi_A - 2\omega_A\langle\phi_A^2\rangle - 2\sum_{n=1}^{N} \mathcal{D}_A k_n^2 \langle\phi_0^A\phi_n^A\rangle \ , \tag{4.44}$$

where $\chi_A = 2\sum_{n=1}^{N} \mathcal{D}_A k_n^2 E_B^{AA}(k_n)$ is the dissipation rate of scalar A. The above equation is derived assuming the scalar concentration in each shell is independent of the others. The exact equation for the scalar variance in isotropic turbulence is

$$\frac{d\langle\phi_A^2\rangle}{dt} = -\chi_A \ . \tag{4.45}$$

Comparing Eqs. (4.44) and (4.45) allows us to determine the coefficient ω_A for consistency

$$\omega_A = -\mathcal{D}_A \frac{\sum_{n=1}^{N} k_n^2 \langle\phi_0^A\phi_n^A\rangle}{\langle\phi_A^2\rangle} \ . \tag{4.46}$$

Applying the same procedure to scalar B yields

$$\omega_B = -\mathcal{D}_B \frac{\sum_{n=1}^{N} k_n^2 \langle\phi_0^B\phi_n^B\rangle}{\langle\phi_B^2\rangle} \ . \tag{4.47}$$

The additional term we added to the zeroth mode governing equations [first term on the RHS of Eqs. (4.40) and (4.41)] has a form similar to the classical interaction by exchange with the mean (IEM) model proposed by Villermaux and Devillon[41]. In that model, the frequencies ω_A and ω_B are prescribed in terms of the turbulence frequency $C_\phi\varepsilon/K$, where K is the turbulent kinetic energy, ε is the energy dissipation rate and C_ϕ is a model parameter to be specified which is usually set to 2. With the SSMM, these terms compensate for the residual (non-conservative) advected scalar, stored in the zeroth mode, which originates from the random terms. In that sense the model is fully prescribed, with no unspecified

coefficients. Moreover, unlike IEM, the SSMM relaxes the PDF to a Gaussian distribution at long times.

The performance of the BSSMM model is shown in Figs. 4.1(c) and 4.2. As may be seen, the addition of the zeroth mode has greatly reduced the occurrence of scalar concentrations outside of the bounds. Moreover, the extrema predicted by the BSSMM model decay to zero in reasonable agreement with the DNS. Note that at early times, the BSSMM model still yields a slight violation of the bounds (particularly the lower bound). The violation at early times is due to the way in which the PDF has been initialized. No attempt was made to control the initial conditional scalar dissipation rate, and hence at short times the scalar can still violate the bounds. Nevertheless, the benefits of the zeroth mode at longer times are clear, and hence hereafter all model calculations will be done with the BSSMM model.

It should be noted that other tests of the bounds exist for multiple scalars. McDermott and Pope[28] introduced the "joint boundedness" concept, which states for conserved passive scalars with equal diffusivities, the convex hull of all compositions $\phi_\alpha(t)$ cannot expand with time, i.e., the convex hull at time t_2 must be a subset (contained within) the convex hull at time t_1 for any $t_2 > t_1$. The test is not applicable to this study for two reasons: (i) under the specific initial conditions we used, the "convex hull" in the ϕ_A–ϕ_B phase space corresponds to a straight line that cannot be evaluated by this criterion; and (ii) the scalar diffusivities in the test we ran were not equal, and so the guarantees are not applicable. As part of future work, we would like to consider a more general initial condition to more completely apply the McDermott and Pope test.

4.3.4 Numerical Implementation

The SDEs [Eq. (4.29), (4.34), (4.35), (4.40) and (4.41)] for the velocity and scalars are advanced for an ensemble of realizations. Each realization is referred to as a 'particle' indexed by integer $m = 1, 2, \cdots, M$, where M is the total number of realizations. It is convenient to introduce an additional index to represent the particle number, i.e., $\phi^{\alpha}_{m,n}(t)$ indicates the scalar concentration in the n^{th} shell of the m^{th} particle at time t. Each particle obeys the same governing equation, although each realization is independent.

We update the SDEs using a $3/2$-order scheme.[4] Using Eq. (4.34) to illustrate the approach, the numerical update takes the form

$$\phi^{A}_{m,n}(t+\triangle t) = \phi^{A}_{m,n}(t) - \left[\mathcal{D}_A k_n^2 + \lambda_\phi(k_n)\right]\left[\frac{1}{3}\phi'^{A}_{m,n}(t) + \frac{2}{3}\phi''^{A}_{m,n}(t)\right]\triangle t + r_1(k_n) N_1[0,1]\sqrt{\triangle t}, \tag{4.48}$$

where

$$\phi'^{A}_{m,n}(t) = \phi^{A}_{m,n}(t) - \frac{1}{2}\left[\mathcal{D}_A k_n^2 + \lambda_\phi(k_n)\right]\phi^{A}_{m,n}(t)\triangle t\,, \tag{4.49}$$

$$\phi''^{A}_{m,n}(t) = \phi'^{A}_{m,n}(t) + \frac{3}{2} r_1(k_n)\left\{\frac{1}{2}\left[N_1[0,1] + \frac{1}{\sqrt{3}} N_2[0,1]\right]\right\}\sqrt{\triangle t}\,. \tag{4.50}$$

and $N_1[0,1]$ and $N_2[0,1]$ are two independent standard normal random numbers (zero mean and unit variance).

Particle statistics are obtained by summing over the wavenumbers

$$u_m(t) = \sum_{n=1}^{N} u_{m,n}(t)\,, \tag{4.51}$$

$$\phi^{\alpha}_{m}(t) = \sum_{n=0}^{N} \phi^{\alpha}_{m,n}(t)\,, \tag{4.52}$$

which can be considered as a single representation of the fine-grained PDF.[33] Spectral

expectations are approximated by the ensemble averages as follows

$$E_u(k_n) = \frac{1}{M}\sum_{m=1}^{M} u_{m,n}^2(t) \tag{4.53}$$

$$E_B^{\alpha\beta}(k_n) = \frac{1}{M}\sum_{m=1}^{M} \phi_{m,n}^{\alpha}(t)\phi_{m,n}^{\beta}(t)\,. \tag{4.54}$$

which approach the expectations in the limit $M \to \infty$. As demonstrated by Xia et al.[44], the 'particle' and 'spectral' representations of the variance are consistent.

4.4 DNS Study of Mixing

As mentioned in Section 4.1, an inherent assumption made in deriving the SSMM is that the rate of mixing depends upon the scalar spectrum, but not its PDF. The assumption originates from the EDQNM theory, which does not consider the PDF of the scalar field(s) in advancing the spectrum.[18,19,27,39,40] In this section, we test this assumption using DNS.

The DNS is of isotropic turbulence within a periodic cube of length 2π with 128^3 grid points. The fluctuating velocity and pressure fields are obtained by solving Eqs. (4.3) and (4.4) using a pseudospectral fluid code that was recently developed in our group.[3] The isotropic turbulence is made stationary by forcing the first two wavenumbers in a manner similar to Eswaran and Pope[8]. The velocity field was updated for 20 eddy turnover times to establish a stationary turbulence state. The energy spectrum was obtained by averaging the instantaneous spectrum over those 20 large eddy turnover times. The resulting velocity statistics are summarized in Table 4.1.

Once the turbulence has achieved a stationary state, we introduce two fluctuating scalars A and B that are evolved according to Eq. (4.5). The scalar fields are updated using the second-order finite difference scheme of Kurganov and Tadmor[24] that guarantees the scalars obey the bounds imposed by the initial and boundary conditions. A pseu-

Table 4.1: Parameters used in DNS calculations (dimensional parameters are in arbitrary units). Note that u' is the turbulence intensity, $L = \frac{\pi}{2u'^2}\int_0^\infty \frac{E(k)}{k}dk$ is the integral length scale, $T = \frac{L}{u'}$ is the large eddy turnover time, ν is fluid kinetic viscosity, ε is dissipation rate, η is the Kolmogorov length scale, $Re_L = \frac{u'L}{\nu}$ is Reynolds number based on integral length scale, R_λ is the Reynolds number based on the Taylor microscale, and L_ϕ is the integral length scale of the scalar fields.

u'	L	T	ν	ε	η	Re_L	R_λ	$L_\phi(k_s=2)$	$L_\phi(k_s=9)$
0.71	1.5	2.1	0.015	0.21	0.064	73	35	0.6	0.3

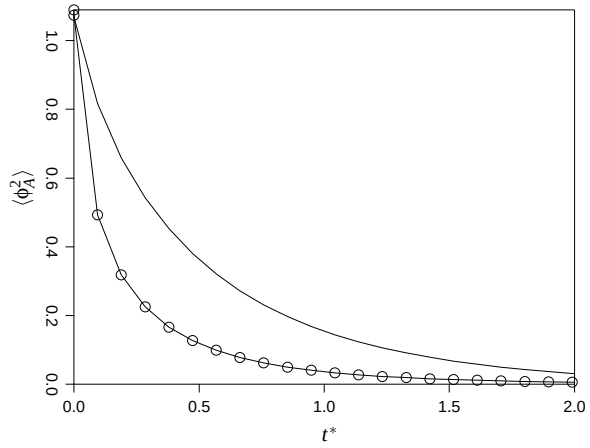

Figure 4.3: Comparison of scalar variance for cases I (solid line) and II (solid line with circles) as a function of dimensionless time, $t^* \equiv t/T$.

dospectral calculation of the scalar fields will not obey the bounds[26] without introducing other nonlinear mappings.[30] The mean concentration of both scalars are set to zero, i.e., $\langle\phi_A\rangle = \langle\phi_B\rangle = 0$. We are interested in controlling both the initial scalar spectrum and its PDF. Scalars A and B are initialized identically and hence are perfectly correlated—they differ only in their mass diffusivities, or equivalently their Schmidt numbers, where Sc_A and Sc_B are 1 and $\frac{1}{4}$ respectively, allowing us to investigate the effects of differential diffusion.[2,37,39,40] Applying the initialization procedure developed by Eswaran and Pope[7], it is possible to independently manipulate the initial scalar spectrum and its PDF. Using this procedure we produced four separate cases. In cases I and II, the scalars are initial-

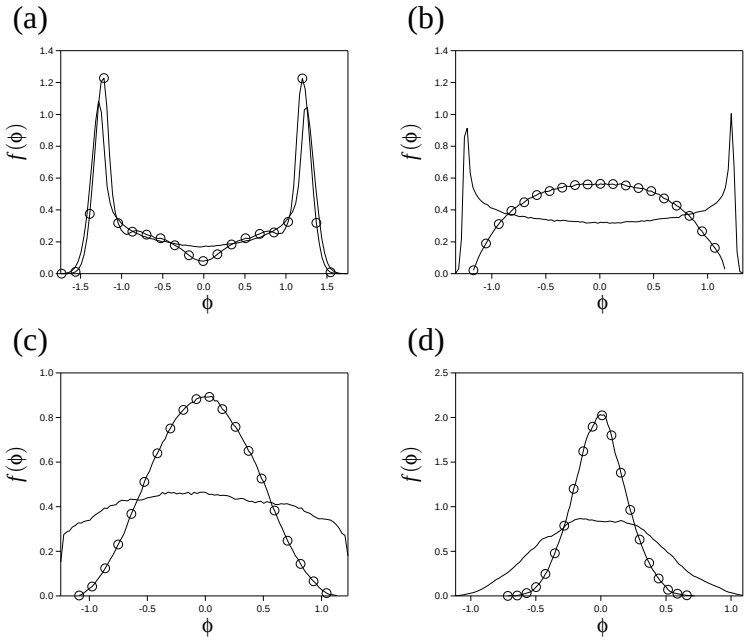

Figure 4.4: Comparison of evolution of the scalar PDFs for cases I and II at times: (a) $t^* = 0$, (b) $t^* = 0.19$, (c) $t^* = 0.38$, (d) $t^* = 0.95$. The initial PDFs for the two cases are nearly identical, but the scalar spectra are peaked at $k_s = 2$ (solid line) and $k_s = 9$ (line with circles), respectively.

ized with PDFs that are nearly double delta functions, but the scalar spectra are peaked at wavenumbers 2 and 9, respectively. The comparison of these two cases will capture the dependence of the mixing on the scalar spectrum. Cases III and IV involve scalars that have nearly identical spectra, but the PDF of case III is a double delta function and case IV is Gaussian. The comparison of these two cases will capture the dependence of mixing on the PDF.

Figure 4.3 shows a comparison of the evolution of the scalar variances for cases I and II as a function of dimensionless time $t^* \equiv t/T$. It is apparent that the variance for case II, initialized with the peak in the spectrum at higher wavenumber (smaller scale), decays more quickly than case I. The result is consistent with the classical experiment of Warhaft and Lumley[43], which showed the same in wind tunnel measurements of temperature fluctuations, as well as the DNS by Eswaran and Pope[7]. The evolution of the PDF in time is

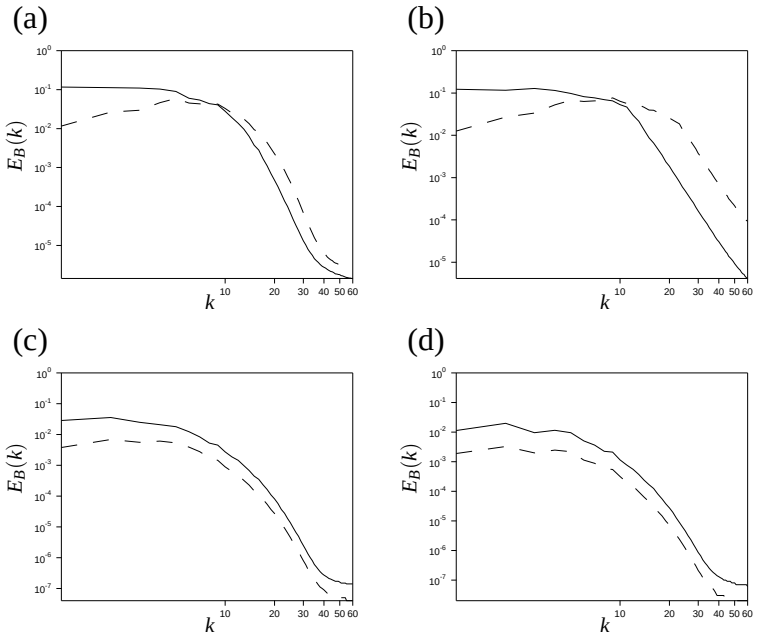

Figure 4.5: Comparison of scalar spectra for cases I and II at times: (a) $t^* = 0$, (b) $t^* = 0.1$, (c) $t^* = 0.95$, (d) $t^* = 1.4$. Solid and lines represent the scalar field with $k_s = 2$ and the dashed lines are for $k_s = 9$.

shown in figure 4.4. Consistent with the variance, we observe that the PDF undergoes a more rapid transformation to a near Gaussian shape for case II. It is interesting to note that the PDF shape changes for the two cases are similar, and so moving the peak in the initial spectrum mainly changes the time scale for those transformations, but not the transformations themselves.

The evolution of the two scalar spectra in time are shown in Fig. 4.5. It is apparent that, while initially the spectral shapes are quite different, they evolve into a self-similar shape after roughly one eddy turnover time. This is seen more clearly in Fig. 4.6, which shows the two spectra at time $t^* = 1.6$ normalized by their instantaneous variance. Aside from the difference in variance the two spectra are nearly identical. The fact that the spectra relax into a self-similar shape implies the effect of the initial scalar spectrum ultimately decays away and the subsequent self-similar decay law scales with the large eddy turnover time of the energy spectrum.

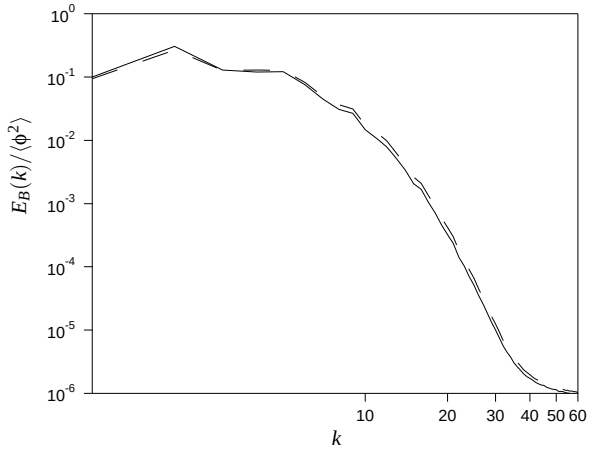

Figure 4.6: Scalar spectrum normalized by its variance for cases I and II at $t^* = 1.6$. Solid line represents the scalar field with $k_s = 2$ and the dashed line is for $k_s = 9$.

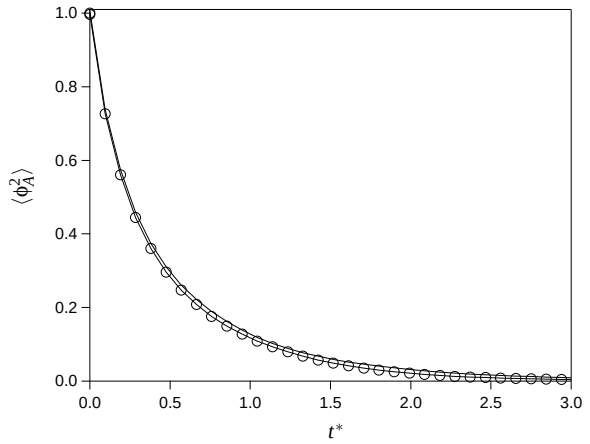

Figure 4.7: Comparison of the evolution of the scalar variance for cases III and IV. Solid line represents the scalar field initialized with a double-delta PDF and the solid line with circles represents scalar field initialized with a Gaussian PDF.

The equivalent results for cases III and IV are shown in Figs. 4.7 and 4.8. Despite the fact that the initial PDFs are completely different, we see the rate of decay of the scalar variances is nearly identical. Apparently the scalar spectrum is primarily controlling this rate. The PDFs initially are very different; however, over time they evolve into nearly the same Gaussian shape. The spectra, which were initialized nearly identically, remain so

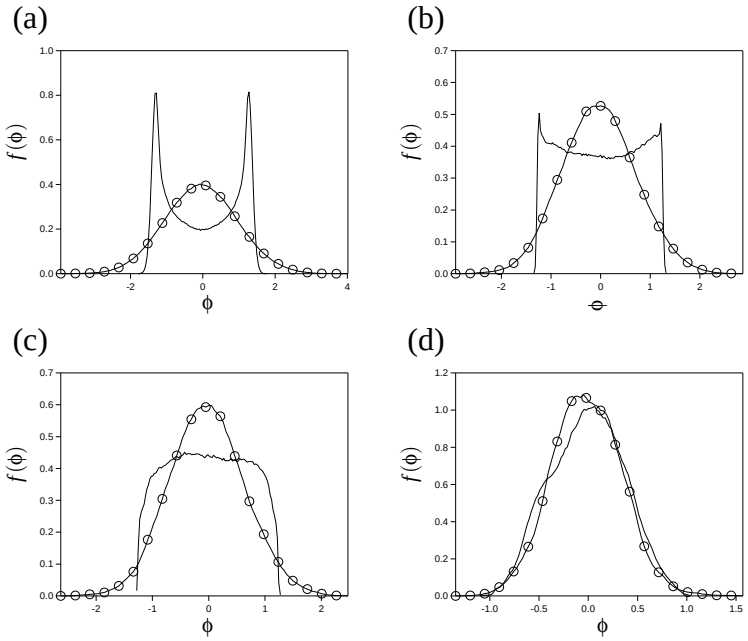

Figure 4.8: Comparison of the scalar PDF for cases III and IV at times: (a) $t^* = 0$, (b) $t^* = 0.19$, (c) $t^* = 0.28$, (d) $t^* = 0.95$. Solid lines represent the scalar field initialized with a double-delta PDF and the solid lines with circles represent scalar field initialized with a Gaussian PDF.

throughout the decay process (see Fig. 4.9). The results of the study support the assumption made in deriving the SSMM that the mixing rate is predominantly controlled by the scalar spectrum, at the low value of the Reynolds number considered in this study.

4.5 Model Comparisons

In this section, we compare the predictions of the bounded SSMM model to the DNS on two scalar fields whose initial spectra peak at $k_s = 2$ (i.e., case III in Section 4.4) and $k_s = 9$ (i.e., Case II in Section 4.4). The inputs to the model are the stationary turbulent kinetic energy spectrum, and the initial scalar spectra and PDFs. To eliminate any errors associated with the EDQNM prediction of the turbulent kinetic energy spectrum, particularly over the forced wavenumbers, we substitute the spectrum obtained from the DNS for

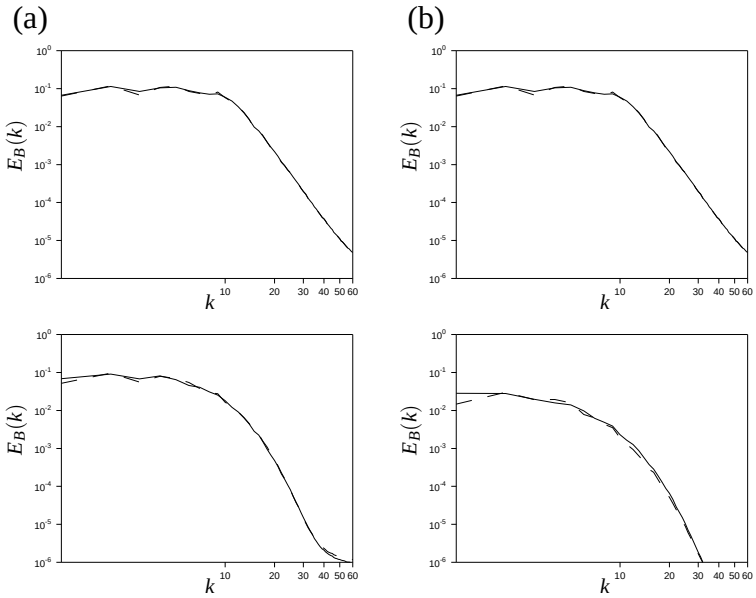

Figure 4.9: Comparison of the scalar spectra for cases III and IV at times: (a) $t^* = 0$, (b) $t^* = 0.19$, (c) $t^* = 0.28$, (d) $t^* = 0.95$. Solid lines represent the scalar field initialized with a double-delta PDF and the solid lines with circles represent scalar field initialized with a Gaussian PDF.

$E_u(k_n)$.

To initialize the scalar concentrations, we must determine $\phi^A_{m,n}(0)$ such that

$$\frac{1}{M}\sum_{m=1}^{M}\left[\phi^A_{m,n}(0)\right]^2 = E_B^{AA}(k_n)\ , \tag{4.55}$$

and the PDF of

$$\phi_A(0) = \sum_{n=1}^{N}\phi^A_{m,n}(0) \tag{4.56}$$

matches the initial PDF of scalar A [note that scalars A and B are initialized to be exactly the same, hence we focus the discussion on the initialization of scalar A with the understanding $\phi^B_{m,n}(0) = \phi^A_{m,n}(0)$].

The algorithm to generate the desired initial condition is mainly based on the "acceptance/rejection" method by von Neumann[42], which is a commonly used technique to generate observations from a distribution, especially when the form of the distribution

makes sampling difficult. Instead of sampling directly from the target distribution, an instrumental distribution which is easier to sample is used, and the samples drawn are probabilistically accepted or rejected.

The procedure to determine $\phi^A_{m,n}(0)$ is outlined below:

1. Generate a set of ψ^A_n with variance consistent with $E^{AA}_B(k_n)$ from DNS for each $n = 1, 2, \cdots, N$, i.e.,

$$\psi^A_n = \sqrt{E^{AA}_B(k_n)}\zeta_n \,. \tag{4.57}$$

   where ζ_1, $\zeta_2, \cdots, \zeta_N$ are independent standard Gaussian random variables with zero mean and unit variance, i.e., $N(0,1)$.

2. Calculate the particle based scalar fluctuation $\psi_A = \sum_{n=1}^{N} \psi^A_n$. Note that the PDF of ψ_A, $g(\psi_A)$, is Gaussian since ψ_A is a linear combination of independent Gaussian random variables.

3. Generate a uniformly distributed random variable $u \sim U(0,1)$.

4. If $u \leq \frac{f(\psi_A)}{Cg(\psi_A)}$, accept by setting $\phi^A_{m,n}(0) = \phi^B_{m,n}(0) = \psi^A_n$; otherwise reject (discard) ψ^A_n and return to step 1. Here $f(\psi_A)$ denotes the target PDF and $g(\psi_A)$ represents the known instrumental distribution. The constant C is defined as sup $\frac{f(\psi_A)}{g(\psi_A)}$.

5. Repeat the above steps until M samples of the distribution have been completed.

In the above example the two scalars are initialized to be exactly the same, however this need not be the case with the above initialization procedure. The number of total samples of the instrumental distribution required to generate the desired number of samples with the target distribution depends on the value of C. The larger C is, the more unlikely the acceptance criterion becomes, and hence the larger number of samples required for each acceptance. Since the target distribution (here a "double-delta" distribution) is being

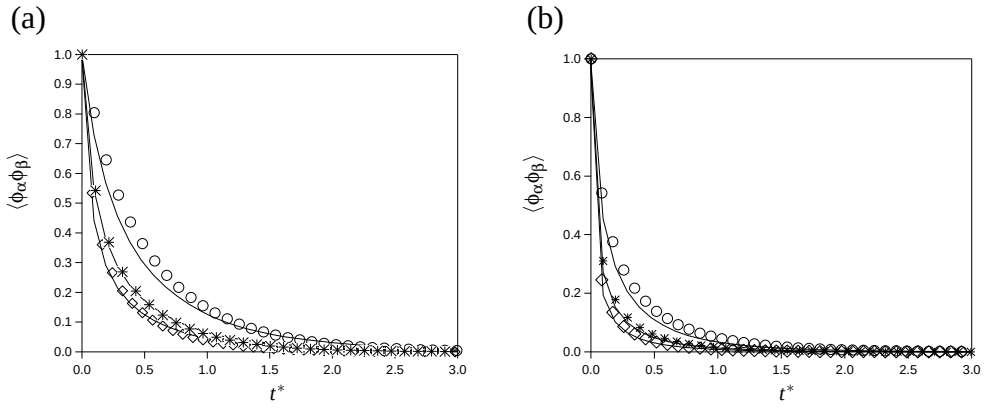

Figure 4.10: Comparison of the scalar variances and covariance for (a) $k_s = 2$ and (b) $k_s = 9$. Lines are the DNS results and symbols are the SSMM predictions for: $\langle\phi_A^2\rangle$ (circles), $\langle\phi_B^2\rangle$ (diamonds) and $\langle\phi_A\phi_B\rangle$ (stars).

generated based on sampling from a Gaussian instrument, the value of C is quite large [$C \sim O(10^3)$]. This leads to a long computation time required to initialize the scalar field. Even though the "acceptance/rejection" method is adequate for generating the desired spectrum and PDF, it eventually will be desirable to seek a more efficient initialization algorithm.

We advance the particle concentrations using the numerical algorithm described in Section 4.3.4. Fig. 4.10 shows a comparison of the DNS and model predictions for the single-point auto- and cross-correlations of the scalar fluctuations, i.e., $\langle\phi_\alpha\phi_\beta\rangle$, as a function of time for both fields with $k_s = 2$ and $k_s = 9$. The agreement between the model and DNS is very good for all three curves in both figures, supporting our claim that the SSMM captures the effects due to variations in the molecular diffusivity, initial length scale of the scalar, and differential diffusion.

A comparison of the spectral predictions of the SSMM with the DNS are shown in Fig. 4.11 and Fig. 4.12. While there are some discrepancies, the overall agreement is very good. Moreover, the moderately large discrepancies at high wavenumbers are mainly due to the finite difference scheme used in the DNS, which we believe is responsible for

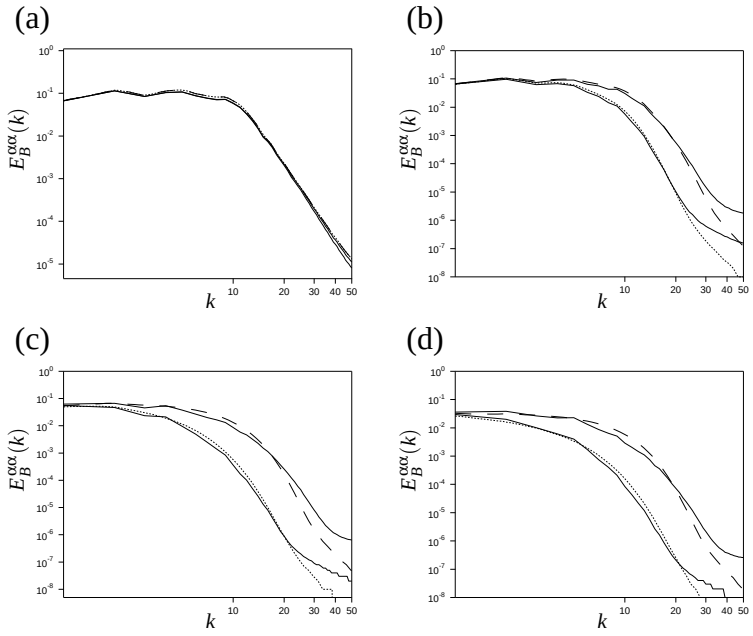

Figure 4.11: Comparison of the scalar autocorrelation spectra for $k_s = 2$ at times: (a) $t^* = 0$, (b) $t^* = 0.09$, (c) $t^* = 0.38$, (d) $t^* = 0.76$. Solid lines are the DNS results; dashed and dotted lines are the SSMM prediction for $E_B^{AA}(k)$ and $E_B^{BB}(k)$, respectively.

the flattening of the spectrum at high wavenumbers. There is clear evidence from the agreement of the cross correlation spectrum that the model is capturing the effects due to differential diffusion. For example, the model predicts that the effects due to differential diffusion begin at high wavenumbers (small scales) and evolves towards the lower wavenumbers in time due to the transfer processes. This is consistent with the generally accepted view of differential diffusion.[20,31,36,46,47] The comparisons of the model spectral predictions with DNS for $k_s = 9$ are shown in Figs. 4.13 and 4.14. It is evident that the model captures the faster mixing of the scalar in good agreement with the DNS.

Figures 4.15 and 4.16 show a comparison of the model prediction and DNS for the time evolution of the PDF of scalars A and B, respectively. The first thing to note is that the modified PDF model satisfies the bounds, confirming the approach we have taken in introducing the zeroth mode to account for the residual advection resulting from the

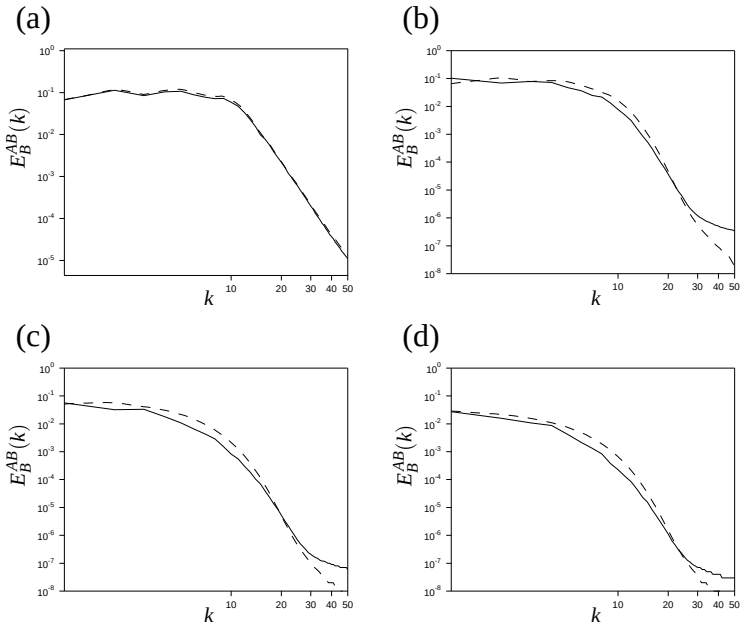

Figure 4.12: Comparison of the scalar cross-correlation spectra for $k_s = 2$ at times: (a) $t^* = 0$, (b) $t^* = 0.09$, (c) $t^* = 0.38$, (d) $t^* = 0.76$. Solid lines are the DNS results and dashed lines are the SSMM prediction for $E_B^{AB}(k)$.

random terms (see Section 4.3.3). We see that the model captures much of the shape changes in the PDFs. The main discrepancy between the model and DNS lies in the rate the PDF changes from "bimodal" to "unimodal". In both cases, this transition occurs more rapidly in the DNS than the model predicts. Apparently the modeled drift of the particle concentrations towards the center of the PDF is a bit too slow. This may be related to distribution of dissipation rates, which are known to be approximately log normal, but are predicted to be chi-squared by the SSMM. This is inherent to the use of a Langevin formulation to advance the scalar concentrations. Nevertheless, the model captures the effect of the molecular diffusivities, as can be seen in the differences in the evolution of scalars A and B. Figures 4.17 and 4.18 show the corresponding PDFs for $k_s = 9$. We again see the model is able to capture the effect of the reduced length scale for the scalar on the mixing process. In summary, the model captures a substantial portion of the dynamics in good accord with the DNS.

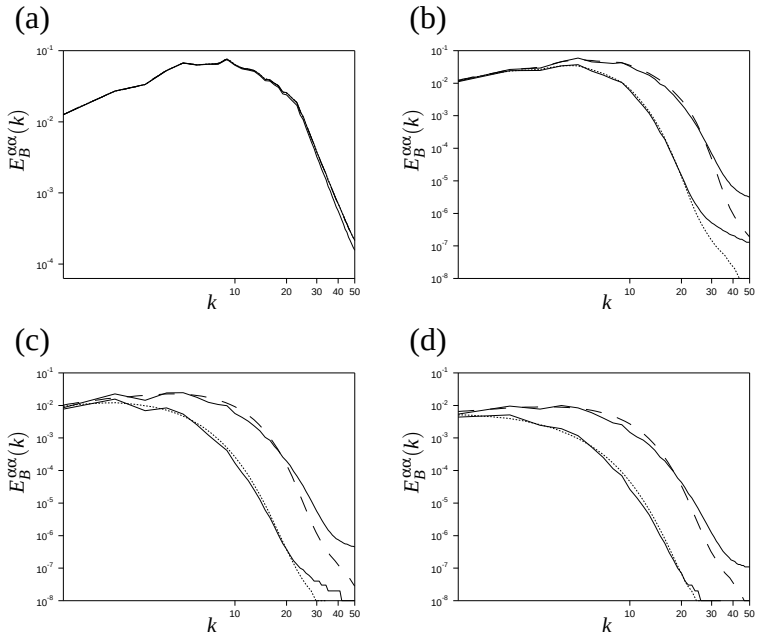

Figure 4.13: Comparison of the scalar autocorrelation spectra for $k_s = 9$ at times: (a) $t^* = 0$, (b) $t^* = 0.09$, (c) $t^* = 0.38$, (d) $t^* = 0.76$. Solid lines are the DNS results; dashed and dotted lines are the SSMM prediction for $E_B^{AA}(k)$ and $E_B^{BB}(k)$, respectively.

4.6 CONCLUSIONS

We have developed a modified form of the stochastic shell mixing model (SSMM) that takes into consideration the bounds of the scalar. The model uses a Monte Carlo scheme to advance scalar concentrations of notional particles that are subdivided into wavenumber shells. In this manner, the model inherently carries information about the scalar spectrum (distribution by shell) and PDF (distribution by particle). A unique aspect of the model is that it explicitly and separately accounts for advection by the fluid velocity and scalar dissipation. Because dissipation is computed explicitly, the model can account for molecular effects associated with the scalar diffusivity, including differential diffusion. An inherent weakness of Monte Carlo algorithms for the scalar is they typically do not obey the scalar bounds. The native form of this model suffers from the same shortcoming. We eliminate

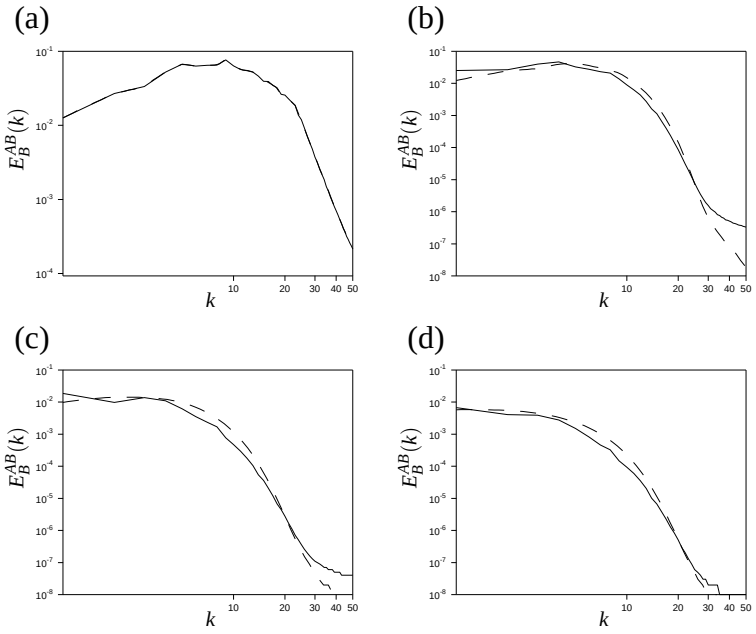

Figure 4.14: Comparison of the scalar cross-correlation spectra for $k_s = 9$ at times: (a) $t^* = 0$, (b) $t^* = 0.09$, (c) $t^* = 0.38$, (d) $t^* = 0.76$. Solid lines are the DNS results and dashed lines are the SSMM prediction for $E_B^{AB}(k)$.

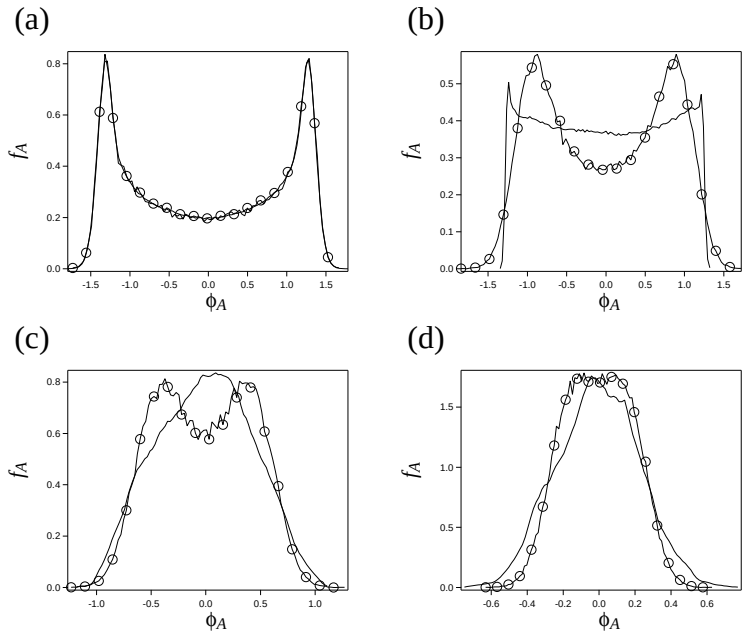

Figure 4.15: Evolution of the PDF for scalar A with $k_s = 2$ at times: (a) $t^* = 0$, (b) $t^* = 0.19$, (c) $t^* = 0.76$, (d) $t^* = 1.6$. Solid lines are the DNS results and lines with circles are the SSMM model.

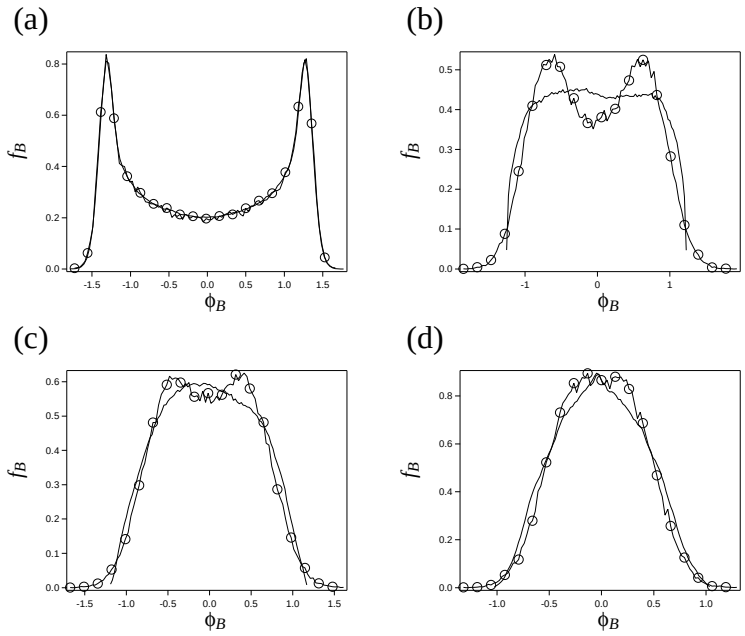

Figure 4.16: Evolution of the PDF for scalar B with $k_s = 2$ at times: (a) $t^* = 0$, (b) $t^* = 0.19$, (c) $t^* = 0.76$, (d) $t^* = 1.6$. Solid lines are the DNS results and lines with circles are the SSMM model.

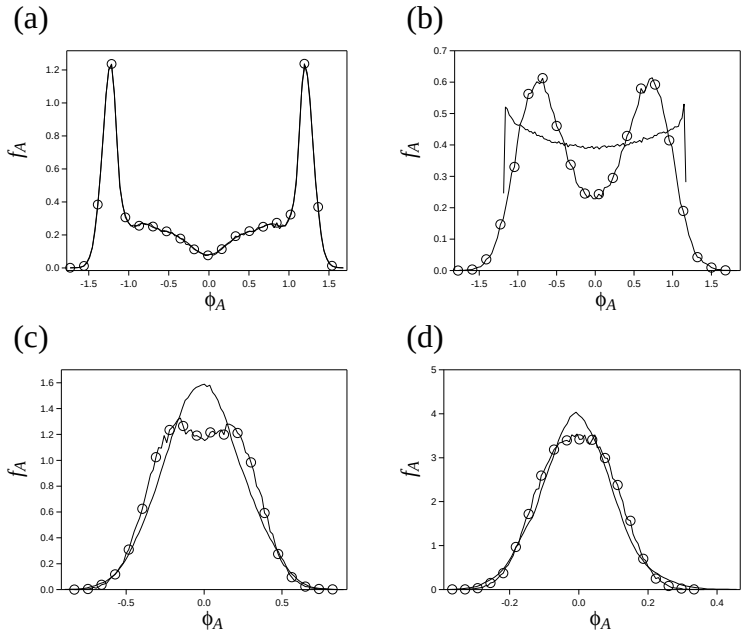

Figure 4.17: Evolution of the PDF for scalar A with $k_s = 9$ at times: (a) $t^* = 0$, (b) $t^* = 0.19$, (c) $t^* = 0.76$, (d) $t^* = 1.6$. Solid lines are the DNS results and lines with circles are the SSMM model.

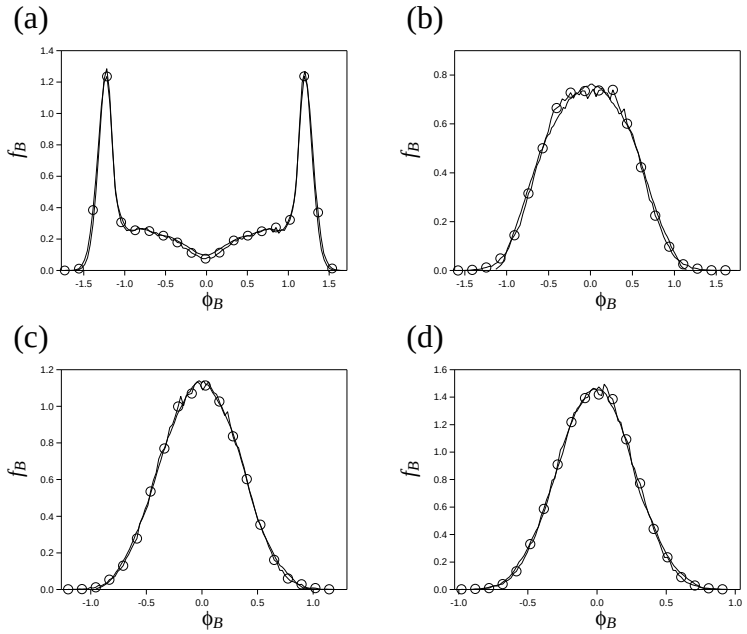

Figure 4.18: Evolution of the PDF for scalar B with $k_s = 9$ at times: (a) $t^* = 0$, (b) $t^* = 0.09$, (c) $t^* = 0.19$, (d) $t^* = 0.38$. Solid lines are the DNS results and lines with circles are the SSMM model.

this problem by introducing an additional "zeroth" mode for the scalar. This zeroth mode is used to precisely subtract off the residual advection resulting from the random terms so that the model is precisely conservative for each particle, eliminating the problem with the bounds. The zeroth mode has no means for dissipation, hence we also introduce a decay term similar in form to the mixing term in the IEM model.[6] The coefficients are chosen so that the rate of decay of the scalar variances equal the original decay rates in the absence of the zeroth mode. The resulting model is therefore self consistent to second order, and bounded.

An inherent assumption in the model is that mixing is controlled by the scalar spectrum and not its PDF. We test this conjecture using DNS of scalars that have been initialized in pairs so as to match the spectra, but not the PDF and vice versa. The results of the study confirm the conjecture, lending further support to the model. However, since the DNS study here is made at a relatively low Reynolds number ($R_\lambda = 35$), the results may depend

more strongly on this parameter. As part of the future work, we will run DNS at higher Reynolds number to investigate how sensitive the results are to this parameter.

We then make detailed comparisons between the SSMM predictions and the DNS. Overall the results are in very good agreement. The model captures the effects of differential diffusion to the single-point statistics and the spectra. However, the model does consistently over predict the time required for the initially bimodal PDF to relax to a unimodal (near Gaussian) shape. Apparently the implied drift of the scalar fluctuation towards zero is too slow in the model. Nevertheless, the overall performance of the model is quite good and provides an important basis for future mixing models. The next step in the advancement of the model will be to consider an inhomogeneous scalar field. This will be the topic of a future paper.

ACKNOWLEDGEMENTS

The authors are grateful to Dr. T. Vaithianathan for technical discussions and for the work in his thesis that forms the basis of the SSMM. We also acknowledge Mr. Yang Liu for several theoretical contributions he made in the early stages of this work. This study was supported by the National Science Foundation under grant CTS-0121573.

REFERENCES

[1] J. C. Andre and M. Lesieur. Influence of helicity on the evolution of isotropic turbulence at high Reynolds number. *J. Fluid Mech.*, 81:187, 1977.

[2] C. J. Brownell and L. K. Su. Planar laser imaging of differential molecular diffusion in gas phase turbulent jets. *Phys. Fluids*, 20(3):035109, 2008.

[3] K. A. Brucker, J. C. Isaza, T. Vaithianathan, and L. R. Collins. Efficient algorithm for simulating homogeneous turbulent shear flow without remeshing. *J. Comp. Phys.*, 225:20–32, 2007.

[4] C.-C. Chang. Numerical solutions of stochastic differential equations with constant diffusion coefficients. *Math. Comput.*, 49:523–542, 1987.

[5] S. Corrsin. On the spectrum of isotropic temperature fluctuations in isotropic turbulence. *J. Appl. Phys.*, 22:469–473, 1951.

[6] Cesar Dopazo. Probability density function approach for a turbulent axisymmetric heated jet. Centerline evolution. *Phys. Fluids*, 18:397–404, 1975.

[7] V. Eswaran and S. B. Pope. Direct numerical simulations of the turbulent mixing of a passive scalar. *Phys. Fluids*, 31:506–520, 1988.

[8] V. Eswaran and S. B. Pope. An examination of forcing in direct numerical simulations of turbulence. *Comput. Fluids*, 16:257–278, 1988.

[9] R. O. Fox. The Fokker-Planck closure for turbulent molecular mixing: Passive scalars. *Phys. Fluids A*, 4:1230–1244, 1992.

[10] R. O. Fox. Improved Fokker-Planck model for the joint scalar, scalar gradient PDF. *Phys. Fluids A*, 6:334–348, 1994.

[11] R. O. Fox. The Lagrangian spectral relaxation model of the scalar dissipation in homogeneous turbulence. *Phys. Fluids*, 9:2364–2386, 1997.

[12] R. O. Fox. The Lagrangian spectral relaxation model for differential diffusion in homogeneous turbulence. *Phys. Fluids*, 11:1550–1571, 1999.

[13] R. O. Fox. *Computational models for turbulent reacting flows*. Cambridge University Press, New York, 2003.

[14] R. O. Fox and P. K. Yeung. Improved Lagrangian mixing models for passive scalars in isotropic turbulence. *Phys. Fluids*, 15:961–985, 2003.

[15] F. Gao and E. E. O'Brien. Joint probability density function of a scalar and its gradient in isotropic turbulence. *Phys. Fluids A*, 3:1625–1632, 1991.

[16] D. C. Haworth. Progress in probability density function methods for turbulent reacting flows. *Prog. Energy Combust. Sci.*, 36(2):168–259, 2010.

[17] S. Heinz. *Statistical Mechanics of Turbulent Flows*. Springer-Verlag, 2003.

[18] S. Herr, L.-P. Wang, and L. R. Collins. EDQNM model of a passive scalar with a uniform mean gradient. *Phys. Fluids*, 8:1588–1608, 1996.

[19] J. R. Herring, D. Schertzer, M. Lesieur, G. R. Newman, J. P. Chollet, and M. Larcheveque. A comparitive assessment of spectral closures as applied to passive scalar diffusion. *J. Fluid Mech.*, 124:411–438, 1982.

[20] A. R. Kerstein, M. A. Cremer, and P. A. McMurtry. Scaling properties of differential molecular effects in turbulence. *Phys. Fluids*, 7:1999, 1995.

[21] Fema C. Klebaner. *Introduction to stochastic calculus with applications*. Imperial College Press, 2005.

[22] A. N. Kolmogorov. The local structure of turbulence in an incompressible viscous fluid for very large Reynolds numbers. *Dokl. Akad. Nauk. SSSR*, 30:299–303, 1941.

[23] Ying-Yan Kuo and E. E. O'Brien. Two-point probability density function closure applied to a diffusive-reactive system. *Phys. Fluids*, 24(2):194–201, 1981.

[24] A. Kurganov and E. Tadmor. New high-resolution central schemes for nonlinear conservation laws and convection-diffusion equations. *J. Comput. Phys.*, 160:241–282, 2000.

[25] V. R. Kuznetsov and V. A. Sabel'nikov. *Turbulence and Combustion*. Hemisphere, 1990.

[26] A. D. Leonard and J. C. Hill. Direct numerical simulation of turbulent flows with chemical reaction. *J. Sci. Computing*, 3:25, 1988.

[27] M. Lesieur. *Turbulence in fluids, stochastic and numerical modeling*. M. Nijhoff, Boston, 1987.

[28] R. McDermott and S. B. Pope. *J. Comput. Phys.*, 226:947C–993, 2007.

[29] R. E. Meyers and E. E. O'Brien. The joint PDF of a scalar and its gradient at a point in a turbulent flow. *Combust. Sci. Technol.*, 26:123, 1981.

[30] E. G. Moody and L. R. Collins. Effect of mixing on nucleation and growth of titania particles. *Aerosol Sci. Tech.*, 37:403–424, 2003.

[31] Vebjorn Nilsen and George Kosàly. Differential diffusing scalars in turbulence. *Phys. Fluids*, 9:3386–3397, 1997.

[32] A. M. Obukhov. Structure of the temperature field in turbulent flows. *Izv. Akad. Nauk SSSR, Geogmagn and Geophys. Ser.*, 13:58–69, 1949.

[33] S. B. Pope. PDF methods for turbulent reactive flows. *Prog. Energy Combust. Sci.*, 11:119–192, 1985.

[34] S. B. Pope. Lagrangian PDF methods for turbulent flows. *Annu. Rev. Fluid Mech.*, 26:23–63, 1994.

[35] A. Pouquet, M. Lesieur, J. C. Andre, and C. Basdevant. Evolution of high Reynolds number two-dimensional turbulence. *J. Fluid Mech.*, 72:305–319, 1975.

[36] J. R. Saylor and K. R. Sreenivasan. Differential diffusion in low Reynolds number water jets. *Phys. Fluids*, 10:1135–1146, 1998.

[37] L. L. Smith, R. W. Dibble, L. Talbot, R. S. Barlow, and C. D. Carter. Laser raman scattering measurements of differential molecular diffusion in nonreacting turbulent jets of H_2 / CO_2 mixing with air. *Phys. Fluids*, 7:1455–1466, 1995.

[38] K. R. Sreenivasan. On local isotropy of passive scalar in turbulent shear flows. *Proc. R. Soc. London Ser. A*, 434:165, 1991.

[39] M. Ulitsky and L. R. Collins. On constructing realizable, conservative mixed scalar equations using the eddy damped quasi-normal markovian theory. *J. Fluid Mech.*, 412:303–329, 2000.

[40] M. Ulitsky, T. Vaithianathan, and L. R. Collins. A spectral study of differential diffusion of passive scalars in isotropic turbulence. *J. Fluid Mech.*, 460:1–38, 2002.

[41] J. Villermaux and J. C. Devillon. *In Proc. Second Int. Symp. On Chemical Reaction Engineering*, pages 1–13, 1972.

[42] J. von Neumann. *Various Techniques Used in Connection with Random Digits*, volume 12 of *Applied Mathematics Series*. 1951. U. S. National Bureau of Standards.

[43] Z. Warhaft and J. L. Lumley. An experimental study of the decay of temperature fluctuations in grid generated turbulence. *J. Fluid Mech.*, 88:659–684, 1978.

[44] Yanjun Xia, Yang Liu, T. Vaithianathan, and Lance R. Collins. Eddy damped quasi normal Markovian theory for chemically reactive scalars in isotropic turbulence. *Phys. Fluids*, 22(4):045103, 2010.

[45] Yanjun Xia, T. Vaithianathan, and Lance R. Collins. Stochastic shell model for turbulent mixing of multiple scalars with mean gradients and differential diffusion. *Flow, Turbul. Combust.*, 2010. in press.

[46] P. K. Yeung. Multi-scalar triadic interactions in differential diffusion with and without mean scalar gradients. *J. Fluid Mech.*, 321:235, 1996.

[47] P. K. Yeung. Correlations and conditional statistics in differential diffusion: Scalars with uniform mean gradients. *Phys. Fluids*, 10:2621–2635, 1998.

[48] P. K. Yeung. Lagrangian characteristics of turbulence and scalar transport in direct numerical simulations. *J. Fluid Mech.*, 427:241–274, 2001.

CHAPTER 5

SUMMARY AND FUTURE WORK

The PDF method provides an excellent modeling strategy to study the complexity of turbulent mixing of inert or reacting scalars. However, molecular diffusion, a very important phenomenon which is the fundamental mechanism for scalars to mix, has to be modeled in the PDF framework. An inaccurate description of molecular diffusion can severely undermine the performance of the PDF methodology. To properly model molecular mixing, a full spectrum of length (and time) scales needs to be provided. This thesis is all about how to realize this idea. An EDQNM spectral model is chosen as a backbone based on its good performance on studying of turbulence. The ultimate goal is to combine the strengths of the spectral model and the PDF method to provide a better description of complicated turbulent mixing/reacting systems. The modeling process focuses on three different aspects as summarized below:

5.1 EDQNM Model for Reactive Flows

In Chapter 2, an EDQNM model for two initially unpremixed reactants undergoing an isothermal, bimolecular reaction with constant reaction rates in homogeneous isotropic turbulent flow is developed. The model predictions are accessed by comparing with direct numerical simulations (DNS). Overall, the EDQNM model is able to capture the mixing rates and reaction rates reasonably well. An excellent agreement is achieved for the mean concentrations of both the reactants and the product. Higher-order statistics, such as the second-order scalar auto- and cross- correlations, are in overall good agreements with DNS as well. However, the time scale for reactant-product and product-product correlations is not well predicted.

A parametric study is also made to investigate the effects of different dimensionless parameters such as Reynolds number, Schmidt number and Damköhler number on differential diffusion. It is observed that the effect of differential diffusion decreases with increasing Reynolds numbers, but it does not vanish even at very high Reynolds numbers. Damköhler numbers play a different role in differential diffusion with regard to the reactants and the product. The statistics involving pure reactants decrease with increasing Damköhler numbers, however, the statistics related to product species increase with increasing Damköhler numbers. It suggests that differential diffusion may be more important with intermediate species in fast-rate chemistry.

The study of the evolution of scalar correlation spectra reveals that differential diffusion is initiated at large wavenumbers (i.e., small scales) and moves to lower wavenumbers through an inverse cascade. A close check of the spectra shows that the product species is formed at a smaller scale than the reactants. This suggests that EDQNM model has sufficient flexibilities to account for the complex dynamics of mixing and chemical reaction, even with the discrepancies in predicting the time scales for the product.

Collectively the results suggest that the EDQNM model, being able to inherently represents all the scales present in a turbulent reacting system, has a distinct advantage over single-point mixing models. If a PDF mixing model can provide spectral information at the same time, a better description of turbulent mixing is expected. This is indeed the fundamental idea behind some recent attempts in the literature to bring PDF and spectral models together[1,2,5], as well as the ultimate goal of the work in this thesis. Currently the model is restricted to a simple reaction, however, the restrictions can be relaxed since the approach is systematic.

5.2 Stochastic Shell Mixing Model for Scalar Fields with Uniform Mean Gradients

In Chapter 2, the realizable EDQNM model for a single scalar with a uniform mean scalar gradient in homogeneous turbulent flow[4] is first extended to multiple scalars, then a shell model in the form of Langevin equation is derived over the full spectrum for scalar fields. By design this shell model is consistent with EDQNM model. The drift and diffusion terms in the Langevin equations of velocity and scalars within each shell are carefully calibrated so that the ensemble averages of velocity variance, scalar fluxes and scalar-scalar correlations precisely match the EDQNM predictions. The motivation of the development of this stochastic shell mixing model (SSMM) is that the sum of each realization over the shells supplies a model for the fine-grained velocity-scalar joint PDF. It has been shown that the results from the SSMM are able to reproduce the EDQNM predictions to within statistical errors due to finite size of the ensemble. A comparison of Lagrangian correlation functions involving the scalar concentrations, scalar dissipation rate and velocity fluctuations along particle paths with the DNS results by Yeung[7] is shown. Overall the results are in good qualitative agreement, despite a discontinuity in the slope of the correlation functions at $t = 0$, which is due to the nature of Wiener processes adopted in the model equations. However, the resulting errors are important only at small times.

The development of the stochastic shell model is an important step towards a new mixing model for the PDF method. The spectral information is embedded in the distributions across the shells, and a fine-grained joint PDF can be extracted by summing all the realizations over the shells. Differential diffusion is taken into account at a level equivalent to EDQNM theory. The nature of the Langevin model ensures the relaxation toward a Gaussian from any initial scalar distributions in the long run. However, violation of the

bounds of the scalars raises a challenge for all stochastic models, including this one.

5.3 Bounded Stochastic Shell Mixing Models

A stochastic shell mixing model for turbulent mixing of multiple scalars with distinct diffusivities is derived. A Monte Carlo scheme is used to advance the scalar concentrations and velocities of each notional particle which carry a spectral distribution across themselves. Thus both spectral information and fine-grained joint PDFs are inherently expressed. However, an inevitable weakness of Monte Carlo algorithms for scalars is that the bounds are not obeyed. An additional "zeroth" mode is introduced for the scalars, which precisely subtracts off the residual advection rendered by the random terms in the governing Langevin equations while reproducing the decay rate by introducing a decay term similar to the expression of IEM model. The resulting model is therefore bounded and consistent to second order. Detailed comparisons between the bounded SSMM predictions and DNS data are given respectively for two scalar fields with different scalar length scales. An overall good agreement has been achieved except that the model predicts a lower rate for the initially bimodal PDF to relax to a unimodal shape than the DNS. The bounded SSMM model shows the capability of capturing the effects of differential diffusion to scalar spectra and therefore the statistics. Hence it provides an important basis for future mixing models.

A DNS study of the dependence of scalar mixing on the initial spectral distribution and PDF has also been performed. Since there is an inherent assumption in the SSMM model that mixing depends on scalar spectra instead of its PDF. This conjecture is tested by comparing the DNS results which have been initialized with the same spectra but different PDFs, and vice versa. The assumption has been validated by the results of this DNS study

(at a low Reynolds number), confirming the underlying basis of the SSMM model.

5.4 Future Work

A test of the underlying assumption of the new stochastic shell mixing model should be made by DNS at higher Reynolds numbers, as mentioned in Chapter 4. And a new initial condition (i.e., scalar *A* and scalar *B* are not linearly dependent initially) is to be generated for BSSMM to check the joint boundedness (the shrinking of the convex hull in the ϕ_A–ϕ_B phase space) when *A* and *B* have equal molecular diffusivities.

Besides, although the violation of the bounds has been solved by introducing an additional zeroth mode for isotropic homogeneous fields, it remains open for the inhomogeneous system. Further extension of the SSMM needs to be done on more realistic problems, such as mixing in a scalar fields with varying mean gradients, or general three-dimensional system. As a result, the boundedness problems need to be taken care of in the corresponding statistically equivalent stochastic models.

Reaction, on the other side, poses another challenge. The study within this thesis focused only on simple reactions while realistic combustion involves more complicated chemical reactions. When it is applied to more complicated chemistry, simplifications have to be found for treating the coupling between mixing and chemical reaction so the model is meaningful both theoretically and computationally to practical applications.

Another issue is since the stochastic model employs Monte-Carlo particles to perform the calculation, the computational cost and accuracy have to be balanced, especially when it is extended to a three-dimensional practical problem. For example, the number of particles used in a three-dimensional realistic CFD calculation is usually significantly less than

the one used in this work ($100,000$ particles used in calculations performed in Chapter 3 and 4) and can induce significant statistical errors. One possible way to partially overcome this problem is to use a more accurate estimation of spectrum at each local grid point by using variance reduction[3].

Spectral information about velocity and scalar fields are not always readily available in CFD codes. How to construct the spectral information based on the known quantities such as turbulent kinetic energy and dissipation rate has yet to be explored. The better the spectrum represents the real flow, the better chances for the model to be successful. A good starting point could be the model spectrum proposed by Pope[6].

REFERENCES

[1] R. O. Fox. The Langrangian spectral relaxation model of the scalar dissipation in homogeneous turbulence. *Phys. Fluids*, 9:2364–2386, 1997.

[2] S. Frankel, T.-L. Jiang, and P. Givi. Modeling of isotropic reacting turbulence by a hybrid mapping-edqnm closure. *AIChE J.*, 38:535–543, 1992.

[3] S. G. Henderson. *Handbook of Simulation*. Elsevier, 2006.

[4] S. Herr, L.-P. Wang, and L. R. Collins. EDQNM model of a passive scalar with a uniform mean gradient. *Phys. Fluids*, 8:1588–1608, 1996.

[5] T.-L. Jiang and E. E. O'Brien. Schmidt, Damkohler and Reynolds number effects on second-order reactions in isotropic turbulence. *Chem. Eng. Comm.*, 106:185–206, 1991.

[6] S. B. Pope. *Turbulent Flows*. Cambridge University Press, 2000.

[7] P. K. Yeung. Lagrangian characteristics of turbulence and scalar transport in direct numerical simulations. *J. Fluid Mech.*, 427:241–274, 2001.